Arabidopsis thaliana ROP GTPase activating proteins: At the crossroad of cell division and cell expansion

Dissertation

der Mathematisch-Naturwissenschaftlichen Fakultät

der Eberhard Karls Universität Tübingen

zur Erlangung des Grades eines

Doktors der Naturwissenschaften

(Dr. rer. nat.)

vorgelegt von

Dorothee Stöckle

aus Nürtingen

Tübingen

2015

Tag der mündlichen Qualifikation:	25.09.2015
Dekan:	Prof. Dr. Wolfgang Rosenstiel
1. Berichterstatter:	Dr. Sabine Müller
2. Berichterstatter:	Prof. Dr. Gerd Jürgens

In Gedenken an meinen Vater

I Danksagung

Die vorliegende Arbeit wurde am Zentrum für Molekularbiologie der Pflanzen (ZMBP) der Eberhard Karls Universität Tübingen am Lehrstuhl für Entwicklungsgenetik unter der Leitung von Dr. Sabine Müller angefertigt.
Bei Dir Sabine möchte ich mich dafür bedanken, dass Du mir die Möglichkeit gegeben hast bei Dir zu promovieren und mich geduldig in die Molekularbiologie eingeführt hast.
Gerd, Dir danke ich dafür, dass Du die Zweitkorrektur übernommen hast und deiner unermüdlichen Art mir „good luck“ zu wünschen. ☺

Liebe EntGen, ich könnte mich jetzt bei jedem namentlich Bedanken, und zum Ausdruck bringen, was ich von jedem Einzelnen gelernt habe und stets eine unvergessliche Erinnerung beifügen. Da ich hier kein Danksagungs-Ranking erstellen will, möchte ich es so ausdrücken: Ich durfte von Euch allen sehr viel lernen und es gab sehr viele tolle Momente, die ich hier gar nicht alle aufzählen kann! Ihr und damit meine ich jeden einzelnen von Euch, seid in den letzten Jahre zu einer Art Familie geworden, und dafür möchte ich Euch Danken!
Zwei Perlen hingegen möchte ich noch separat erwähnen. Caterina Brancato und Brigitte Schneck. Caterina Dir danke ich die für Deine stets hohe Protoplastentransformations-effizienz, und dass Du auch mal eine Probe mehr angenommen hast als du eigentlich musstest. Brigitte, ein klarer Dank geht auch an Dich, für Deinen unermüdlichen im Kampf gegen unser „schmutziges Geschirr“.
Des Weiteren möchte ich mich bei unserem Gärtner-Team bedanken, welches in den verschiedensten Situation behilflich war.

Table of Contents

1 Zusammenfassung / Summary

1.1 Zusammenfassung

Zellteilung ist ein grundlegender Prozess in lebenden Organismen. In Eukaryoten sind die meisten Zellteilungsmechanismen konserviert. Bei höheren Pflanzen entwickelte sich eine spezielle Art der Zellteilung. Pflanzenzellen sind von einer Zellwand umgeben, die sowohl die Form der Zelle sowie deren Position im Gewebe bestimmt. Daher ist die molekulare Kontrolle über die Positionierung der neuen Zellwand während der Zellteilung, und über die Ausrichtung der Zellestreckung von besonderer Bedeutung in der pflanzlichen Entwicklung. Das pflanzenspezifische Präprophaseband, eine Zytoskelettanordnung am Zellkortex, beschreibt die Position der Zellteilungsebene zu Beginn der Mitose und zeigt somit auch die exakte, zukünftige Insertionsstelle der Zellplatte an. Die Zellplatte entsteht durch Vesikelfusion in der Zellteilungsebene und expandiert vom Inneren der Zelle nach außen zur parentalen Plasmamembran, geführt von der zweiten pflanzenspezifischen Zytoskelettanordnung, dem Phragmoplasten. Die Fusion der Zellplatte mit der parentalen Plasmamembran erfolgt exakt an der, vom Präprohaseband vorhergesagten, kortikalen Zellteilungsseite. Da das Präprophaseband am Ende der Prophase disassembliert, ist es wichtig, die positionelle Information des Präprophasebandes zu erhalten. In der Modellpflanze *Arabidopsis thaliana* (*A. thaliana*) gibt zwei Mitglieder der Kinesin-12 Klasse von Motorproteinen, die PHRAGMOPLAST ORIENTING KINESINS (POK) 1 und 2, die die positionelle Information des Präprophasebandes während der gesamten Mitose und Zytokinese aufrechterhalten. Der Ausfall dieser beiden Proteine führt zu einer Fehlpositionierung neu synthetisierter Zellwände. Dies bedeutet, dass POK1 und POK2 eine wichtige Funktion bei der Zellteilung übernehmen. Zum besseren Verständnis der POK Funktion und ihrer Rolle in der Zellteilung ist es wichtig, einen Blick auf das Netzwerk von interagierenden Proteinen zu werfen. Bis jetzt sind die Proteine TANGLED (TAN) und RanGAP1 als Interaktionspartner von POK1 bekannt. Sie lokalisieren während der Zellteilung ebenso wie POK1 an der kortikalen Zellteilungsseite. Zwei weitere, bisher nicht charakterisierte

Proteine wurden als POK1-Interaktionspartner in Hefe-Zwei-Hybrid-Experimenten identifiziert.

In der vorliegenden Studie werden die beiden neu identifizierten Interaktionspartner von POK1 charakterisiert und im den Kontext der Zellteilung und Zellexpansion untersucht. Beide identifizierten Proteine sind GTPase-aktivierende Proteine (GAPs), von nun an bezeichnet als PHGAP1 und PHGAP2. Sie gehören zu einer kleinen Unterfamilie von pflanzlichen Rho of Plants (ROP) GTPase-aktivierenden Proteine (GAPs), gekennzeichnet durch eine Pleckstrin-Homologie (PH) Domäne. Die Untersuchungen von PHGAP1 und PHGAP2 ergaben, dass beide Proteine eine redundante Funktion aufweisen und mit POK1 an der kortikalen Zellteilungsebene ko-lokalisieren. Darüber hinaus tragen PHGAP1 und PHGAP2 zum korrekten Einbau der Zellplatte in die parentale Zellwand bei, da Embryonen der *phgap1/phgap2*-Knockdown-Mutanten Fehlpositionierung von Zellwänden aufweisen. Jedoch ist der zugrundeliegende Mechanismus noch nicht aufgeklärt. Außerdem, spielen diese beiden Proteine eine wichtige Rolle in der Entwicklung von Blattepidermiszellen in *A. thaliana*. Die Zellformen der Blattepidermiszellen von *phgap1 phgap2* Knockdown Mutanten zeigen starke Veränderungen. Dies deutet auf eine Fehlregulierung der ROP-Aktivität, durch PHGAP1 und PHGAP2 hin. Die Hauptaufgabe von ROPs in Blattepidermiszellen ist die Etablierung von polarem Zellwachstum durch Induktion des Aktin-Filament-Netzwerks und die Initiierung von Mikrotubuli-Bündelungen. Diese Ergebnisse lassen darauf schließen, dass PHGAP1 und PHGAP2 durch Inaktivierung bestimmter ROPs eine essentielle Rolle für die Regulation des Zytoskeletts in unterschiedlichen Entwicklungsstadien spielen.

1.2 Summary

Cell division is a fundamental process in every living organism. Therefore it is important to investigate this mechanism. Higher plants developed a separate kind of cell division since the cells are not motile unlike mammal or yeast cells. Land plants have to overcome the rigidity of the cellulosic cell wall. Plants developed specific cytoskeletal arrays, the preprophase band and the phragmoplast. The preprophase band predicts the insertion site of the future, partitioning new wall, the cell plate. The cell plate is formed by vesicle fusion, initiated in the center of the cell and expands towards the parental plasma membrane, where the preprophase band originally predicted the insertion sites. The cell plate formation is facilitated by the plant specific cytoskeletal array, the phragmoplast. Since the preprophase band disappears at the end of prophase it is important to maintain the positional information it provides. In the model plant *Arabidopsis thaliana* (*A. thaliana*) two members of the kinesin-12 class motor proteins, PHRAGMOPLAST ORIENTING KINESIN (POK) 1 and 2 preserve this information while localizing at the former position of the preprophase band throughout mitosis and cytokinesis. The absence of these two proteins results in mis-positioned cell walls indicating that POK1 and POK2 carry out an important function in cell wall positioning during cell division. For better understanding of POK function and its role in plant cell division, it is essential to have a closer look at the network of interacting proteins. So far, TANGLED and RANGAP1 are known as interaction partners of POK1 and present the identity of the CDZ.

In this study two novel interaction partners of POK1 were characterized and investigated in the context of cell division and cell shape establishment. Both identified proteins are Rho of plant (ROP)-GTPase activating proteins (GAPs), designated PHGAP1 and PHGAP2. They belong to a small subfamily of Rho of plant GTPase activating proteins (ROPGAPs) characterized by a Pleckstrin Homology (PH) domain. Both PHGAP1 and PHGAP2, co-localize with POK1 at the cortical division site. The *phgap1 phgap2* double mutant embryo analysis suggests that both proteins are functionally redundant and contribute to the correct insertion of the new cell wall. In addition to their function in cell

division, they play a major role in pavement cell establishment. *phgap1 phgap2* knockdown mutants display a severely altered pavement cell shape suggesting that regulation of ROPs, by PHGAP, is important for polar pavement cell growth, which is achieved by inducing actin filament network or microtubule bundling. This study suggests that PHGAP1 and PHGAP2 regulate the cytoskeleton by inactivating certain ROPs during different developmental stages.

1 Introduction

Higher plants consist of different cell types fulfilling diverse functions in specialized tissues. During plant development the fundamental processes of cell division and cell expansion play an important role for the determination of cell shape and the morphology of the plant. In contrast to mammals or yeast, plant cells are not motile owing to their cellulosic cell walls. In consequence, the position where the future cell division will take place and the site where cell expansion occurs, need to be regulated in order to maintain cell shape. The selection of the division plane takes place before mitosis and is crucial for correct positioning of the new cell wall between the daughter cells. Tubulin and actin are common key players forming specific cytoskeletal arrays to accomplish cell division and cell expansion. In land plants there are two plant specific cytoskeletal arrays, the preprophase band and the phragmoplast that assist the plant specific mode of cell division (Figure 1).

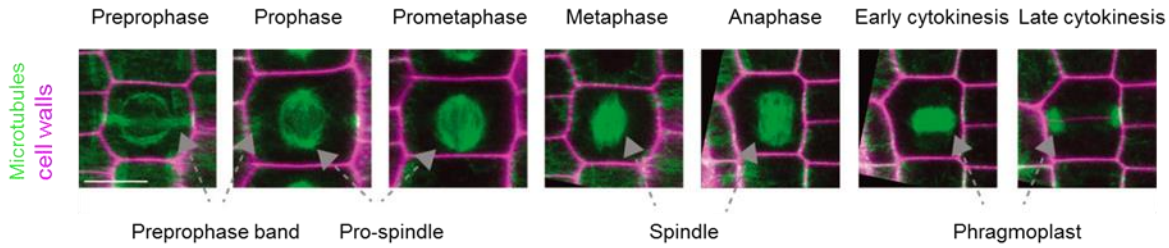

Figure: 1 Overview of microtubule reorganization during plant cell division. Mitotic cell cycle stages are depicted in a chronological order. Microtubules are visualized by GFP-MBD fusion proteins (green) and cell walls by propidium iodide staining (magenta). Images are maximum projection of GFP-MBD z-stacks merged with single plane images of propidium iodide. The figure is taken from a recent review on plant cell division (Lipka et al., 2015)

Microtubules are formed by tubulin (Inoue and Salmon, 1995) heterodimers consisting of α-tubulin and β-tubulin. These heterodimers join in a “head-to-tail” manner and are the basic modules of protofilaments. Thirteen of these protofilaments join laterally to assemble the microtubule. Microtubules are polar filaments with a highly dynamic plus end, which exposes the β-tubulin of the tubulin heterodimer towards the cytosol, and the less dynamic minus end which is terminated by an α-tubulin. In general, both microtubule

ends may polymerize however in vivo, minus ends are often bound to nucleation sites, preventing polymerization.

The plus end cycles between guanosin triphosphate (GTP) and guanosin diphosphate (GDP) (Berry and Shelanski, 1972; Jacobs et al., 1974). When the GTP bound β-tubulin cap is completely hydrolyzed it comes to a depolymerization process, called catastrophe, which takes place until new GTP bound tubulin heterodimers are bound. Then a new polymerization cycle, also named rescue, begins. This alternating growing and shrinking process is called dynamic instability (Mitchison and Kirschner, 1984). A third tubulin, γ-tubulin, is involved in the nucleation of the microtubule similar to other eukaryotes. However, plants are lacking the canonical microtubule organizing centers such as centrosomes or spindle pole bodies as known from animals and fungi. Plant microtubule nucleation is organized by a conserved protein complex including γ tubulin and additional complex proteins. Together they form the ring shaped γ-tubulin ring complex (γ-TuRC) which is located dispersed throughout the plant cell cortex, along existing microtubules and associated with chromatin (Pastuglia et al., 2006).

The function of the other prominent cytoskeleton protein, namely actin, is not completely clear in plant cell division. Like tubulin, actin is a very dynamic protein. The monomeric or globular (G-) actin is the basic module of filamentous (F-) actin. F-actin assembly takes place accompanied by ATP hydrolysis. ATP-bound G-actin is added at the plus/barbed end whereas the depolymerization of ADP bound G-actin takes place at the minus/pointed end (Korn et al., 1987). The nucleation of F-actin is mainly driven by the ACTIN RELATED PROTEIN-2/3 (ARP2/3) complex and by formins (Mathur, 2005; Blanchoin and Michelot, 2012). Nucleation of branched F-actin is only mediated by the ARP2/3 complex (Mullins et al., 1998; Rouiller et al., 2008). Spontaneous nucleation is prevented by PROFILIN (Hussey et al., 2006). Mutations in actin or its associated proteins do not impair cell division, indicating that they are not essential for cell division. However, drug induced actin depolymerization results in obliquely positioned new cell walls (Kojo et al., 2013). From prometaphase to anaphase, F-actin is diminished from the so-called actin depleted zone which forms at the site that was occupied by the preprophase band. Thus, the actin depleted zone serves as a negative marker of the cell plate insertion site.

The actin depleted zone was first identified in *Trandescantia virginiana* stamen hair cells (Cleary et al., 1992). Notably, this actin depleted zone is bordered by actin enrichments designated twin peaks (Sano et al., 2005). Yet it is not clear what the function of the actin depleted zone might be and how its assembly and maintenance are regulated.

2.1 The preprophase band and the phragmoplast control the position where cytokinesis takes place

The preprophase band predicts the division plane in almost every cell type at the entry of mitosis. This belt-like structure appears at the transition of the G2- to the M-phase (Pickett-Heaps and Northcote, 1966), delineating the periphery of the future division plane. The preprophase band formation requires a multifunctional protein complex consisting of the heterotrimeric protein phosphatase 2A (PP2A) complex with its regulatory subunit FASS/TONNEAU (TON) 2and TON1a and TON1b, two closely related proteins, and members of the TON1 RECRUITING MOTIF (TRM) protein family (Camilleri et al., 2002; Azimzadeh et al., 2008; Spinner et al., 2010; Kirik et al., 2012; Spinner et al., 2013).

The preprophase band, made of microtubules and actin, disassembles at the end of the prophase. Maintenance of the positional information where division will take place is accomplished by marker proteins, which are recruited to the preprophase band during prophase. The important proteins in this process are PHRAGMOPLAST ORIENTING KINESINS (POK) 1, a member of the kinesin-12 class motor proteins (Lipka et al., 2014), the microtubule associated protein TANGLED (TAN) (Walker et al., 2007) and the Ran regulatory protein RANGAP1 (Xu et al., 2008). These proteins establish the cortical division zone (CDZ) and define the site of cell plate fusion, the cortical division site (CDS), later in cytokinesis.

The absence of the proteins, that are either responsible for preprophase band formation or for the CDZ establishment, result in abnormally inserted cell plates (Smith et al., 1996; Muller et al., 2006; Walker et al., 2007; Spinner et al., 2013).

After spindle formation and chromosome segregation, the phragmoplast assembles from the remnants of the spindle apparatus. The phragmoplast consists of antiparallel microtubules and actin filaments which facilitate the formation and expansion of the cell plate from Golgi derived vesicles. The phragmoplast expands centrifugally from the interior of the cell towards the periphery to the cortex where the CDS is defined. A recent report showed that myosin VIII plays a role in phragmoplast extension in moss and tobacco (Wu and Bezanilla, 2014). Myosin VIII links phragmoplast microtubules to the cortical division site via F-actin filaments during phragmoplast expansion. The authors proposed that F-actin may interact with the microtubules bridging the cell cortex and the phragmoplast. After reaching the parental cell wall, the cell plate fuses to the parental cell wall. (Figure1 and Figure2).

2.1.1 Contribution of POK and TAN to phragmoplast guidance

It is known that POK1 and POK2 are required for maintenance of the cortical division site. Mutations in *POK1* and *POK2* lead to miss oriented cell walls (Lipka et al., 2014). POKs were initially identified as interaction partners of TAN (Muller et al., 2006). POK1 and TAN are recruited to the preprophase band during prophase. When POK1 becomes immobilized in metaphase, TAN is tethered to POK1 since TAN localization is abolished in *pok1 pok2* double mutants (Lipka et al., 2014). In early cytokinesis the initial broad TAN ring undergoes narrowing by a yet unknown mechanism, which likely results in the accurate position of the CDS (Walker et al., 2007). The exact mechanism of phragmoplast guidance and the way the cell plate fuses to the parental cell wall is still unclear.

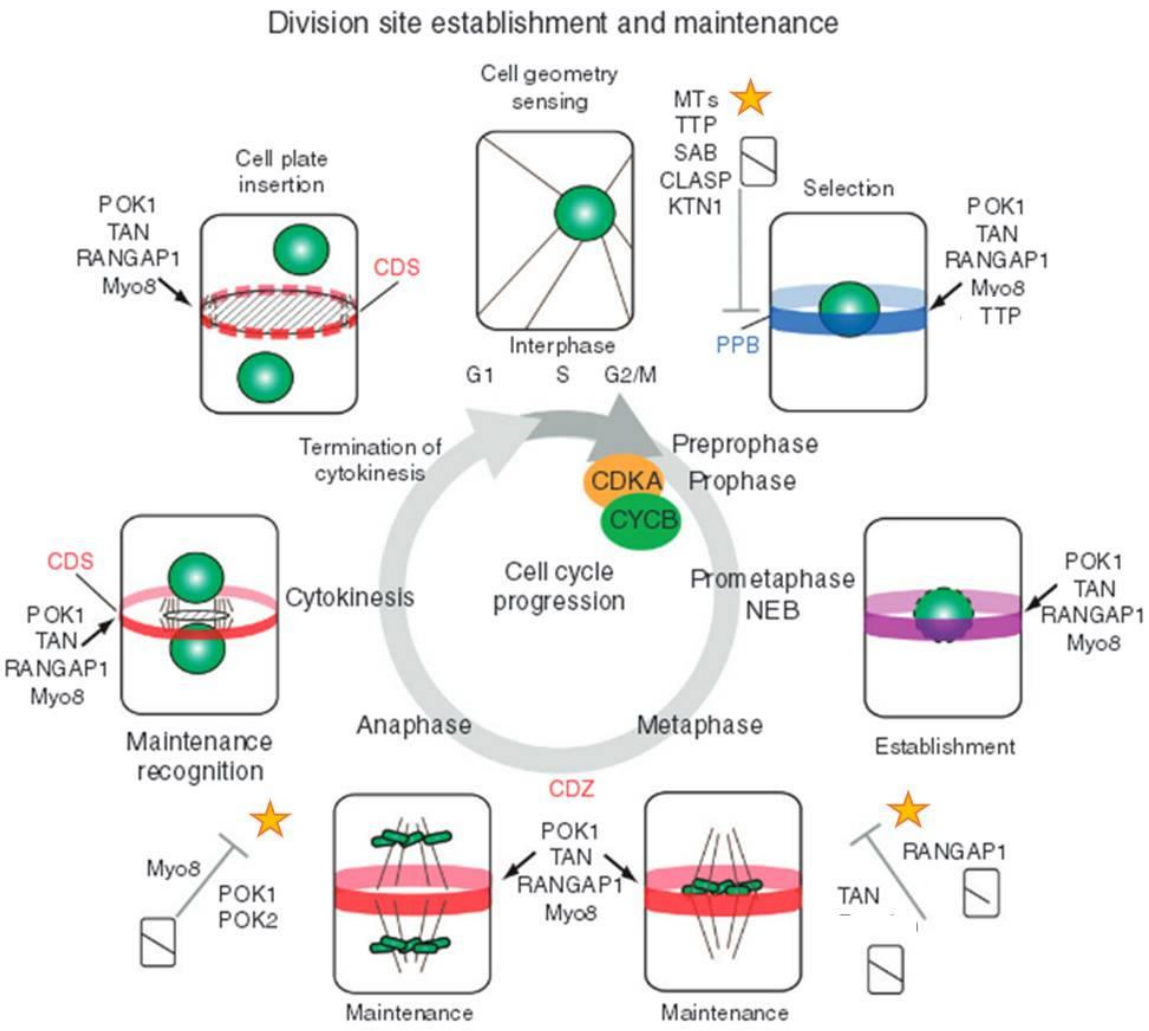

Figure: 2 Overview of plant cell division with focus on the preprophase band (PPB), cortical division zone (CDZ) and the cortical division site (CDS). When the cell is entering mitosis, the nucleus (green) migrates to the center and the PPB (blue) assembles by the help of the TTP (TON1/TRM/PP2a) complex. Microtubule associated proteins (MAPs, SABRE (SAB), CLASP, MICROTUBULE ORGANIZATION (MOR) 1 and KATANIN (KTN) 1) co-localize with the PPB controlling its position. In preprophase – PHRAGMOPLAST ORIENTING KINESIN (POK) 1, TANGLED (TAN), RANGAP1 and myosin (Myo) 8 are recruited to the PPB. They serve as markers (red ring) for the cortical division zone (CDZ) and the cortical division site (CDS) because they mark the position of the disassembled PPB until cell plate insertion. From anaphase to early cytokinesis, the CDZ undergoes narrowing to form the CDS which predicts the exact position of the cell plate insertion. Yellow asterisks indicate alterations in cell plate insertion in the absence of the indicated proteins. Adapted from Lipka et al., 2015.

2.2 Regulation of cell expansion and cell shape formation in plants

Since plant cells are encased by cell walls, which define the plant cell shape, it is crucial to regulate cell expansion in order to acquire the appropriate cell shape. As in cell division, the cytoskeleton plays a critical role in cell expansion and cell shape formation. The actin network promotes directional growth by providing tracks for vesicles containing cell wall materials. Polar tip growth of pollen tubes, root hairs and trichomes relies on accelerated vesicle trafficking. Vesicles derived from the Golgi apparatus, migrate to a defined region at the apex, fuse with the plasma membrane and release their vesicle content for integration to the cell wall. Another prominent examples for polarized growth are leaf epidermal cells, also known as pavement cells displaying their characteristic jigsaw puzzle shape. In both processes, pollen tube growth and pavement cell establishment, small GTPases play a regulatory role (Fu et al., 2002; Fu et al., 2005; Hwang et al., 2008; Yang, 2008).

Small GTPases are conserved and versatile molecular switches found throughout biological kingdoms. These small G-proteins are divided into the five subfamilies Ras, Rab, Ran, Arf and Rho GTPases. These are important in signal transduction pathways (Bourne et al., 1990). Small GTPases cycle between an active GTP-bound form and an inactive GDP-bound form (Wittinghofer and Pal, 1991). The regulation of small GTPase activity is carried out by guanine nucleotide exchange factors (GEFs) which trigger the activation (Bos et al., 2007), and GTPase activating proteins (GAPs) stimulating the intrinsic GTPase activity to accelerate the hydrolysis of GTP to GDP (Bourne et al., 1990). In their active GTP-bound form small GTPases influence cellular processes such as the organization and dynamics of the cytoskeleton and vesicle trafficking by interacting with their effector proteins. There is a family of small GTPase in plants which consists of 11 isoforms, designated Rac-like GTPases or Rho-related GTPases from plants (RAC/ROPs) (Vernoud et al., 2003). These GTPases are most similar to the mammalian Rho/Rac family of small GTPases based on the amino acid identity (Li et al., 1998). Most of them are ubiquitously expressed, but ROP1, ROP3 and ROP5 are expressed in pollen (Li et al., 1998) based on microarray data from the genevestigator database (Hruz et al.,

2008) (Figure 3). ROP1 for example plays a crucial role in the control pollen tube growth (Lin and Yang, 1997; Kost et al., 1999). ROP1 is locally active at the pollen tube apex and mediates the balances between elongation and diameter of the pollen tube cap by controlling counteracting pathways (Gu et al., 2005; Hwang et al., 2010). The *A. thaliana* receptor like kinase PRK2 promotes ROP1 activation via physical interaction with RopGEF1. It was shown that constitutively active (CA)-RopGEF1 complements the dominant negative (DN)-PRK2 germination defects which suggests that this PRK2 - RopGEF1 - ROP1 pathway controls polarized pollen tube growth (Chang et al., 2013). Active GTP bound ROP1 interacts with the effectors ROP interactive CRIB domain (RIC) 3 and RIC4. Both, RIC3 and RIC4 are responsible for actin dynamics in the pollen tube and facilitates exocytosis (Lee et al., 2008). The RIC4 pathway induces F-actin filament networking formation, which results in vesicle migration and accumulation at the apex where the vesicles release their cell wall content in order to fuse with the plasma membrane while the RIC3 dependent Ca^{2+} signaling promotes F-Actin disassembly (Gu et al., 2005). For ROP1 inactivation the GAP Rho Enhancer 1 (REN1) is essential (Hwang et al., 2008). The prevention of lateral expansion of active ROP1 seems to be mediated by REN1 and RhoGAP1 (Hwang et al., 2010) (Figure 4B).

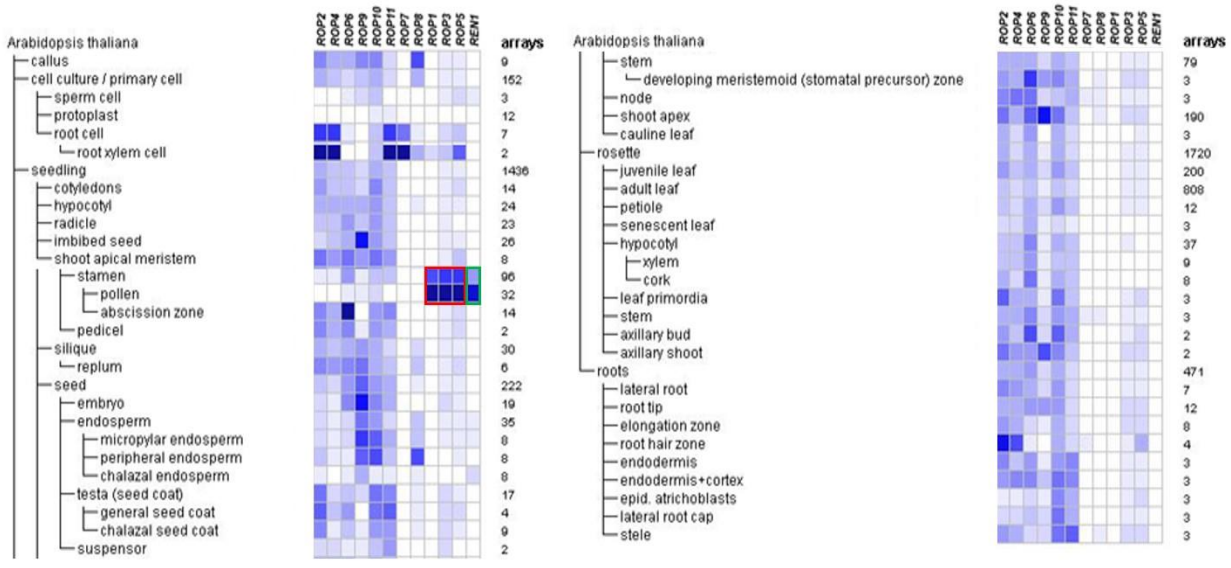

Figure 3: Overview of micro array expression data of plant specific Rho GTPases (genevestigator, https://genevestigator.com/gv/) in different *A. thaliana* tissues. Specific pollen tube expression of *ROP1*, *ROP3* and *ROP5* are boxed in red while the pollen specific GTPase activating protein REN1 is boxed in green.

In pavement cells the polarity establishment is mediated by the redundantly acting ROP2/ROP4 and ROP6. The establishment of the pavement cell shape requires a interplay of active ROP2/ROP4 and ROP6 in order to coordinate indented cell growth (Figure 4A). Activated ROP2 induces actin filament network formation via binding to RIC4, which is responsible for lobe building, with concurrent inhibition of RIC1, an effector protein of ROP6. In contrast, ROP6 recruits RIC1 which activates KATANIN, a microtubule severing protein, controlling microtubule bundling and thereby constituting the necks. Furthermore, overexpression of RIC1 leads to increased bundling of microtubules and inhibits the ROP2-RIC4 interaction (Fu et al., 2005; Fu et al., 2009; Xu et al., 2010; Lin et al., 2013; Xu et al., 2014). The activation of the three ROPs involved in pavement cell establishment is regulated by auxin, the AUXIN BINDING PROTEIN1 (ABP1) and the transmembrane kinase (TMK). The ROP-GEF SPIKE1 might be viewed as a “master-regulator” of ROP activities. It was shown that it physically interacts with ROP2, ROP3, ROP4, ROP5 and ROP6 (Basu et al., 2008; Lin et al., 2012) (Figure 4 A and C).

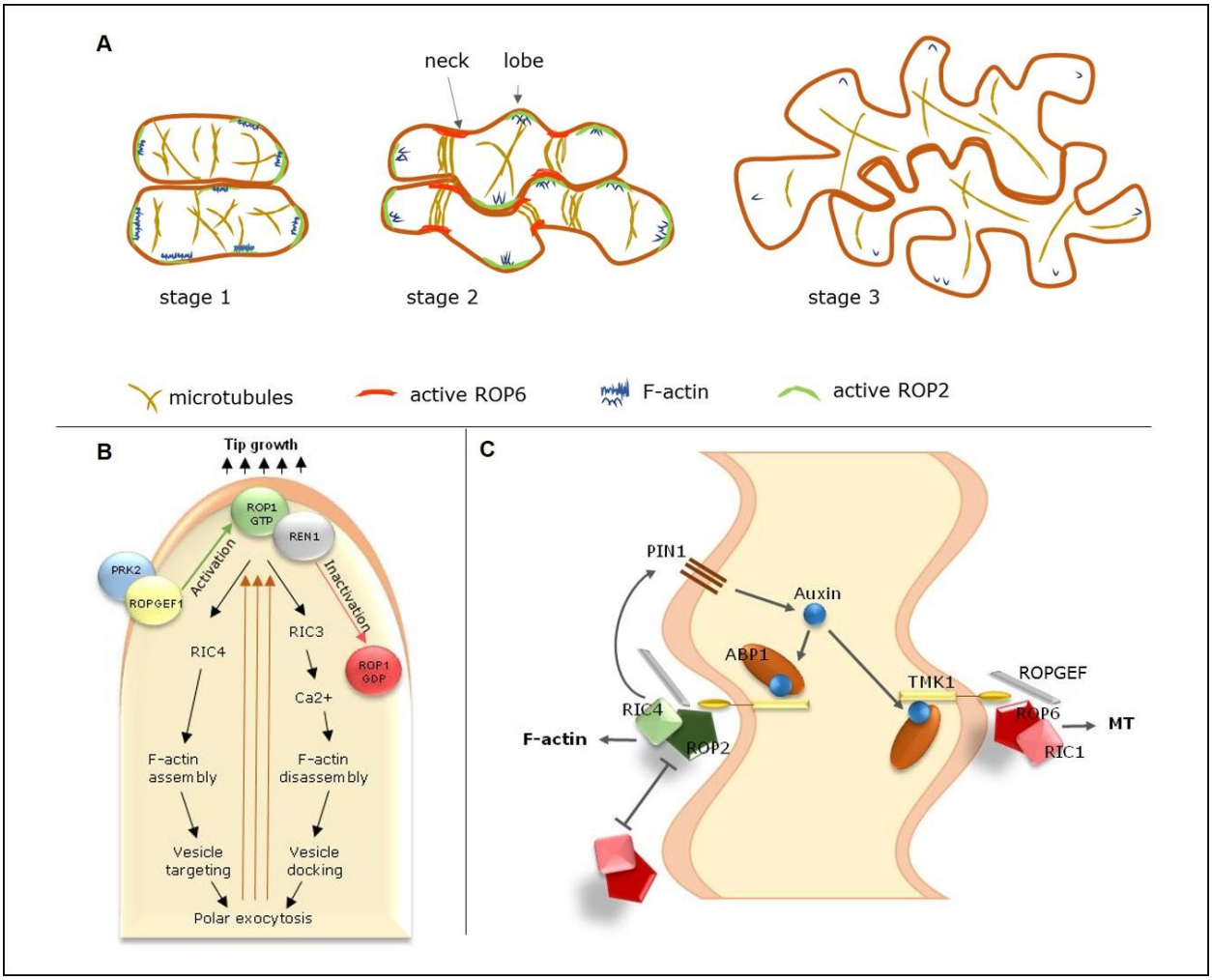

Figure 4: Models for cell expansion and cell shape formation in *A. thaliana* pollen tube and pavement cells. **(A)** The formation of the characteristic jigsaw puzzle appearance of pavement cells. **Stage 1** cells are oval to rectangular and expand in regions of active ROP2 which induces the F- actin filament network. **Stage 2** is an interplay of active ROP2 and active ROP6. While active ROP2 promotes the outgrowth of lobes ROP6 activity prevents the outgrowth by inducing microtubule bundling. In **Stage 3** the pavement cell is almost fully-grown and completely interdigitates but still secondary lobes can be formed. **(B)** Model of polarized growth in the pollen tube. ROP1 is locally activated at the plasma membrane of the pollen tube tip by PRK2 and ROPGEF1. ROP1 regulates two antagonistic pathways through the effectors RIC4 and RIC3. While RIC4 promotes F-actin assembly, RIC3-dependent Ca^{2+}signaling promotes F-actin disassembly. The outcome of the two antagonistic pathways is a highly dynamic system of F-actin regulation which facilitates polar exocytosis. Polarized exocytosis seems to cause the migration of the ROPGAP REN1 to the apex of the pollen tube which inhibits the global activity of ROP1. This leads to a restriction of active ROP1 except for the tip growing region. **(C)** Activation of ROP signaling via AUXIN BINDING PROTEIN 1 (ABP1) Transmembrane Kinase 1 (TMK1) auxin receptor complex and subsequent downstream ROPGEF. Self-activation of auxin via the ROP2-PIN1 positive feedback loop takes place upstream of ROP2 and ROP6 in the extracellular matrix. The intracellular domain of TMK1 interacts with the ROP2 and the ROP6 leading to their activation. Directly interaction takes place via ROPGEF Downstream activation of RIC1 and RIC4is followed. RIC1 which binds to microtubule and RIC4 which promotes F-actin assembly. The active ROP2/RIC4 pathway is also important for auxin maxima in the extracellular matrix by inhibiting PIN1 internalization in the lobing regions. The Models of pavement cell establishment and pollen tube growth are modified from(Craddock et al., 2012).

3. Aim of this work

Over the last decades many relevant proteins were identified and investigated in plant cell division. The kinesin 12 class proteins POK1 and POK2 were identified to be crucial for the maintenance of the CDZ/CDS during cell division. To understand POK function in its developmental context, it is essential to characterize POK interaction partners. A pair of putative ROP GTPase activating proteins (ROPGAPs), containing a Pleckstrin Homology (PH) domain, were identified. To investigate the biological relevance of the *in vitro* interaction between POK1 and the ROPGAPs, designated PHGAPs, interaction and co-localization analysis of PHGAP and POK1 fusion proteins were performed *in vivo*. Functional characterization of *PHGAPs* using genetic analysis should further elucidate the contribution of PHGAPs to plant development. The genetic analysis of PHGAPs also raised the question whether PHGAPs acted as regulators of ROP activity during cell expansion. This work is aimed to contribute to a better understanding of the molecular mechanisms that require PHGAP activity during cell division and cell expansion in plants.

4 Experimental Procedures

4.1 Plant Growth

For analyzing mutant phenotypes, localization studies, crosses and reproduction, seeds were surface sterilized and placed on ½ MS medium (Murashige and Skoog medium) followed by stratification at 4°C in the dark for at least two days. Then plants were grown in growth chambers under long day conditions (cycling 16 h light / 8 h dark) at 19°C to 22°C. For further experimentation and propagation two to three weeks old seedlings were transferred to soil.

4.2 Plant material

In this study *Arabidopsis thaliana* plants, ecotype Columbia (Col-0, wild type) were used. For mutant analysis of *PHGAP* genes, different T-DNA insertion lines (*phgap1-04D* (WiscDsLoxHs135_04D), *phgap1-3* (WiscDsLox357_G01), *phgap1-1*(SALK_152917), *phgap2-51* (SALK_083351), *phgap2-23* (SALK_131823) were obtained from the Arabidopsis biological resource center (ABRC, Ohio, US) and Nottingham Arabidopsis stock center (NASC, Nottingham, UK). All other transgenic lines in this study were created by *Agrobacterium tumefaciens (A. tumefaciens)* mediated transformation of respective plasmids (Clough and Bent, 1998).

For examining the microtubule, cytoskeleton two previously described microtubule reporter lines, *p35S:GFP-MBD* (Marc et al., 1998), *pUBN:RFP-MBD* (Lipka et al., 2014) were used.

4.3 Generation of fluorescent fusion proteins (XFP)

For localization studies cDNA of *PHGAP1* and *PHGAP2* was obtained from seedlings or flower buds and cloned into Gateway® (Inivtrogene) compatible pENTR vectors. In addition, a pENTR clone (G21877) was obtained from ABRC for *PHGAP2*. pENTR-PHGAP1 and pENTR-PHGAP2 were subsequently recombined with appropriate destination vectors *pUBN*:GFP and *pUBN*:RFP destination vectors (Grefen et al., 2010) as well as pEG104*Pro35S*:YFP destination vector (Earley et al., 2006) using LR clonase. Stable plant transformation was mediated by the *A. tumefaciens* strain GV3101. Transformants were selected on nutrient agar plates containing 0.05% phosphinotricin (Duchefa) or by spraying plants with 0.1% Basta (Bayer) (pUBN-XFP) or nutrient plates containing 50 mg/l kanamycin. Three independent *pUBN:GFP-PHGAP1* and ten independent *pUBN:GFP-PHGAP2* T1 lines were selected and propagated for further analysis. For *pEG104:YFP-GAP2* eight independent T1 lines were selected and propagated. Analysis of localization patterns were performed using confocal microscopy in the T2 generation and all lines showed comparable localization pattern and fluorescence intensity. In case of *pEG104:YFP-PHGAP1*, all lines showed very weak fluorescence indicating potential down-regulation of the transgene in seedlings.

For co-localization studies selected lines expressing RFP-PHGAP1 and RFP-PHGAP2 were crossed with YFP-POK1 lines previously characterized in Lipka et al., 2014.

Investigation of the respective GAP domains in PHGAP1 and PHGAP2 were carried out by substitution of a highly conserved catalytic arginine residue within the GAP domain by leucine. As previously shown, a conserved arginine in the GAP-Domain is essential for GAP activity (Sermon et al., 1998).The respective residues in PHGAP1 (R198L) and PHGAP2 (R203L) were mutated to leucine by site directed mutagenesis using mismatch primers in a rolling cycle PCR reaction. Respective mutations were introduced into pENTR cPHGAP1 and pENTR cPHGAP2.

For the generation of pENTR ROP2, cDNA was amplified from *pUNI* clone U09414 and cloned into pENTR3C using restriction enzymes KpnI and EcoRV. Constitutively active *carop2* and *carop4* mutants were created by site directed mutagenesis of pDONOR221cROP2 and pENTR-D-TOPOcROP4 (U17137). *ROP6* cDNA was amplified from *pGBT9:CA-ROP6* as well as from *pGBT9:DN-ROP6* provided by Shaul Yalowsky. Primers used for cloning are found in the Appendix 7.1

4.4 Analysis of pavement cell shape

The analysis of the pavement cell shape was performed ten days after germination. For each seedling one cotyledon was stained with propidium iodide (10 µg/ml, Sigma) and imaged at the Leica TCS SP2 with a 20x 0.70NA objective. Image stacks of epidermal cells were taken at z-intervals between 2µm and 4µm. ImageJ (version 1.49d NIH) was used to create maximum z-projections of image stacks. The cell shape parameters, perimeter and area were, quantified using Photoshop CS6 extended version. To quantify differences in pavement cell shape, the statistical analysis was focused on skeleton and circularity (Le et al., 2006; Sorek et al., 2011) .

The skeleton is a measure for cell lobes, counting the number of endpoints (x) of a cell minus two (Skeleton = x-2, Figure 5). The circularity describes the complexity of a shape and is calculated as follow: $(4\pi \text{ area})/(\text{perimeter}^2)$, where a circle has the value $(4\pi \pi r^2)/(2\pi r)^2 = 1$. That means a more complex shape has a value <1 (Figure 5).

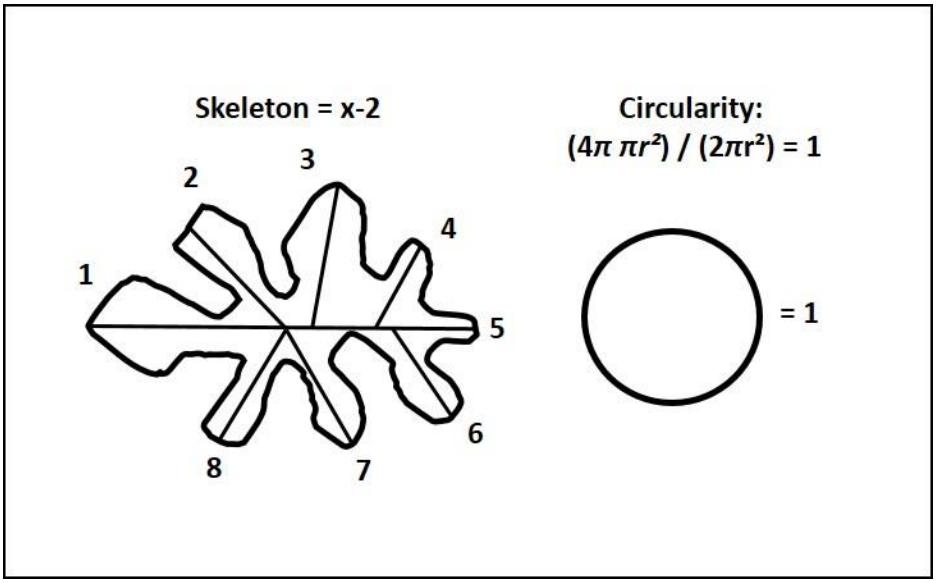

Figure 5: Illustration of the quantification methods used for cell shape analysis. Skeleton analysis is made using the following formula Skeleton = x-2. This includes counting the end points with subtraction of two. The formula named above describes the unit circle. The more the calculated value is approximates 1 the more the cell looks like a circle.

4.5 Analysis of embryos

For the analysis of fertility and embryo defects, fertilized and non-fertilized ovules were counted and subsequently mounted in chloral hydrate:glycerol:water-solution 8:3:1 (w:v:v) chloral hydrate between 10 min to 1.5 h depending on the embryonic developmental stage (Gross-Hardt et al., 2007). Differential Interfering Contrast (DIC) images were taken on a Zeiss Axiophot microscope.

4.6 Transmission analysis

Transmission defects of *phgap1* and *phgap2* were determined by reciprocal crossing of *phgap1*/+ *phgap2*/+ heterozygous plants with wild type. In the filial generation of these crosses, segregation of the respective T-DNA insertions was analyzed by PCR based genotyping (used primers, Appendix 7.2).

4.7 Pollen tube growth analysis

For analysis of the pollen, the medium (10 % sucrose, 0.5 M $CaCl_2$, 1 % H_3BO_3, 0.5 M KCl, 0.1 M $MgSO_4$, 1.5 % agarose pH7.4 (Serva), was prepared immediately before the experiment. After placing a thin layer of medium on a microscope slide, mature pollen were carefully plated on the surface of the polymerized medium and stored in humid chamber at 22 C° for about eight hours. Afterwards, images were taken at the Zeiss Axiophot.

4.8 Interaction studies using ratiometric Bimolecular Fluorescence Complementation (rBiFC)

The Gateway compatible 2 in 1 system (Grefen and Blatt, 2012) was used to test putative interactions of PHGAP1 and PHGAP2 with. In short, potential interaction partners were fused to either nYFP or cYFP on the same plasmid, each expressed under the control of a 35S promoter. In addition, the plasmid includes an internal expression control (*p35S*:RFP). Interaction strength was determined by the YFP/RFP ratio. The amplicons (primers listed in table 3) with appropriate recombination sites were cloned into either pDONOR221-P3P2 or pDONOR221-P1P4 by BP clonase. Subsequent LR clonase reaction was performed with the pBiFCt-2in1-NN destination vector.

Polyethylene glycol (PEG) mediated transfections of plasmids into A*. thaliana* root cell protoplasts were carried out by the transformation unit of the ZMBP (Schutze et al., 2009) Imaging of the protoplasts was carried out at least 22 h after transfection. Identical confocal settings were used for respective experiments to compare the interaction strength. YFP and RFP confocal images were recorded of cross sections of individual transfected protoplasts.

The analysis was performed as described in Lipka et al., 2014. YFP signal was selected with the segmented line tool in Image J. Average fluorescence signal intensity was measured for YFP and RFP in the selected region. YFP/RFP ratio was calculated in Excel 2013, Microsoft.

4.9 Water homeostasis and water transport

4.9.1 Water homeostasis

Analysis of water homeostasis of four week old *phgap1 phgap2* and wild type plants was performed according to Hwang et al., 2011. Equally sized rosette leaves from each genotype were used to determine the loss of water. Every two hours (t = 0h to t = 10h) one rosette leaf from each phenotype was weighed at room temperature (23°C). Weight loss over time was depicted as percentage of the weight at time point t = 0. (Hwang et al., 2011)

4.9.2 Water transport

Water conductance was examined according to Lie et al., 2013. Inflorescences of *phgap1 phgap2* double mutants and wild type were cut with a razor blade 2 cm beneath the oldest flower, siliques were removed and inflorescences were immediately put into blue ink (Pelikan) and were placed back into the growth chamber. The time between cutting and the time when the ink reached the first sepals was determined for each genotype.

4.10 Gene expression analysis

Gene expression analysis of *PHGAP1* and *PHGAP2* was performed by two different approaches. About 1.5 kb promoter fragments of *PHGAP1* and *PHGAP2* were amplified and subcloned into pGEM®T-easy (Promega). Using PstI restriction site flanking the promoters, *proPHGAP1* and *proPHGAP2* were cloned into the pDW137 vector containing the ß-glucuronidase (GUS) reporter gene (Blazquez et al., 1997). For generating *proPHGAP1:NLS-dTOM* and *proPHGAP2*:NLS–dTOM the promoters were amplified from respective pGEM clones using primers that contained AatII and NotI resctriction sites for cloning into pDR13 (Ripper and Groß-Hardt, unpublished). Constructs were transformed into Col-0. *proPHGAP2:NLS–dTOM* and *proPHGAP2:GUS* were generated as a part of a bachelor thesis (Lauster, 2013).

4.10.1 Histochemical ß-glucuronidase (GUS) Assay

GUS assays were performed as previously described (Hauser and Bauer, 2000; Muller et al., 2006). In short, plant material expressing *proPHGAP1:GUS* and *proPHGAP2:GUS* were fixed in 90% acetone for 20 min. After a 5 min wash in 0.1M TRIS, pH 7.5 the plant material was transferred to the GUS staining solution (1mg/ml X-Gluc,Peqlab, 37-2710, , 200 µl/ml MeOH and 100µl 10X GUS buffer (1M TRIS pH 7.5, 29 mg/ml NaCl, 6.6 mg/ml $K_3Fe(CN)_6$, 5.8 mg/ml $KFe(CN)_6$^-4) and incubated in vacuum for about 40 min. *proPHGAP1:GUS* plant material was incubated for 3 days at 37°C and *proPHGAP2:GUS* plant material was incubated for 3h to obtain visible staining. After 15 min incubation of the plant material in 0.24 M HCl, 20% MeOH at 57°C a stepwise rehydration was performed with 50%, 40%, 30% and 10% EtOH. Finally, the samples were mounted in 50% glycerol and inspected under the Leica MZFL3 binocular and the Axiophot epifluorescence microscope in the bright field mode.

4.11 Imaging

Confocal imaging was performed with a Leica SP2 microscope containing a point scanner and a Leica SP8 microscope equipped with a resonant scanner. For image acquisition at the Leica SP8, a 63x 1.2 NA water immersion objective lens and a 40x 1.10NA water immersion objective were used. Image acquisition at the SP2 was performed using the 20x 0.70 NA objective. GFP and YFP fluorescence were excited by argon/krypton lasers using the 488-nm laser line and the 514-nm laser line, respectively. RFP fluorescence was excited by the 561-nm laser line from a He/Ne laser. The collection range of the excited fluorophores varied for different experiments.

Images of the Arabidopsis siliques were taken at. DIC images of the embryos were taken at with 20x 0.5 NA.

Images of the gene expression pattern of PHGAP1 and PHGAP2 in different developmental stages were taken, in both, at Leica MZFL3 binocular and Zeiss Axiophot epifluorescence microscope in different magnifications

5 Results

5.1 POK1 and TANGLED interact *in planta*

Interaction between POK1 and TANGLED (TAN) was previously confirmed genetically and in directed yeast-two-hybrid experiments (Muller et al., 2006). Here we examined the interaction between these proteins *in planta* using ratiometric bimolecular fluorescent complementation (rBiFC) in *A. thaliana* protoplasts (Figure 6). All the proteins tested in the rBiFC studies mentioned here, including the localization controls, were driven by 35S promoter. Although both, POK1 and TAN expressions are weak, the 2in1 rBiFC is a suitable system and sensitive enough to show interaction of these low abundance proteins. YFP-TAN localization was observed in the cytoplasm (Figure 6 C), while YFP-POK1 showed a punctate localization pattern (Figure 6 D). However, the simultaneous expression of nYFP-POK1 and cYFP-TAN complemented YFP signal was predominantly detected at the cell cortex (Figure 6 A). In some instances YFP fluorescence showed a localization pattern similar to microtubules (Figure 6 F). The quantification of the relative fluorescence intensity of nYFP-POK1$_{1683\text{-}2066}$ / cYFP-TAN showed significant differences compared to the negative control nYFP-ROP2 / cYFP-TAN (Figure 6 B and G).

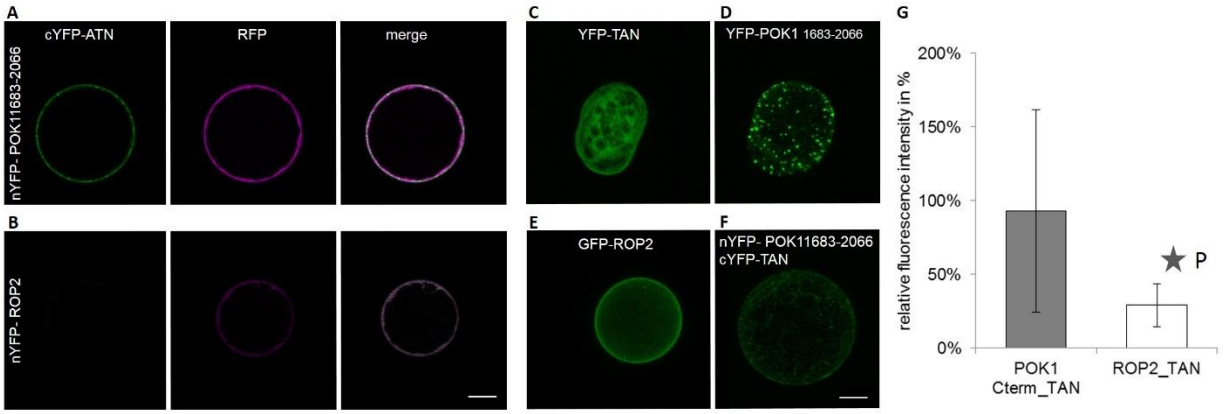

Figure 6: rBiFC interaction assay of POK1 and TAN. **(A, B)** Confocal images of *A. thaliana* protoplast co-expressing nYFP-POK1$_{1683\text{-}2066}$ and cYFP-TAN **(A)** or nYFP-ROP2 and cYFP-TAN **(B)** as negative controls. The YFP fluorescence due to the YFP POK1$_{1683\text{-}2066}$ and cYFP-TAN interaction was measured in comparison to the non-interacting nYFP-ROP2 and cYFP-TAN control. RFP, expressed from the same plasmid, was used as an internal control. **(C-F)** Localization pattern of TAN-YFP, YFPPOK1$_{1683\text{-}2066}$, GFP-ROP2 and nYFPPOK1$_{1683\text{-}2066}$ cYFP-TAN. Images are Z-projections of image stacks with z-intervals of 1

µm. Bar = 10 µm. **(G)** Quantification of the relative fluorescence intensity of the interaction partners and the control by using the YFP/RFP ratio. Data represents mean intensity of each used construct ($n \geq 26$ protoplasts). Each protoplast represents an independent transformation event. The YFP/RFP ratio of the interacting partners POK1 and TAN differs significantly ($p < 0.0001$) from the non-interacting control ROP2 and TAN.

5.2 PHGAP1 and PHGAP2 are novel interactors of POK1

In a yeast-two-hybrid screen for interactors of POK1 and POK2, two closely related proteins, designated PHGAP1 and PHGAP2 were identified (Sabine Müller, unpublished). *PHGAP1* and *PHGAP2* belong to a small subfamily of three putative *ROP-GAP* genes (Figure 7 A). A phylogenetic tree was constructed using the amino acid sequences of proteins sharing a conserved ROP GTPase activating (GAP) domain (Figure 7B). PHGAP1, PHGAP2 as well as the pollen tube specific REN1 (Hwang et al., 2008) share conserved protein domain organization and form a cluster. These three potential ROPGAPs are characterized by a Pleckstrin Homology (PH) domain at the N-termini, followed by a conserved GTPase activating (GAP) domain and coiled coil domains at the C-termini. Furthermore, they possess consensus binding motives for 14-3-3 proteins ([RK]-x-(2,3)-[ST]-x-P). PHGAP1 and PHGAP2 share more than 70% sequence identity while REN1 is more distantly related. The other ROPGAP subfamily members feature a Cdc42- and Rac-interactive binding (CRIB) domain (Figure 7 A).

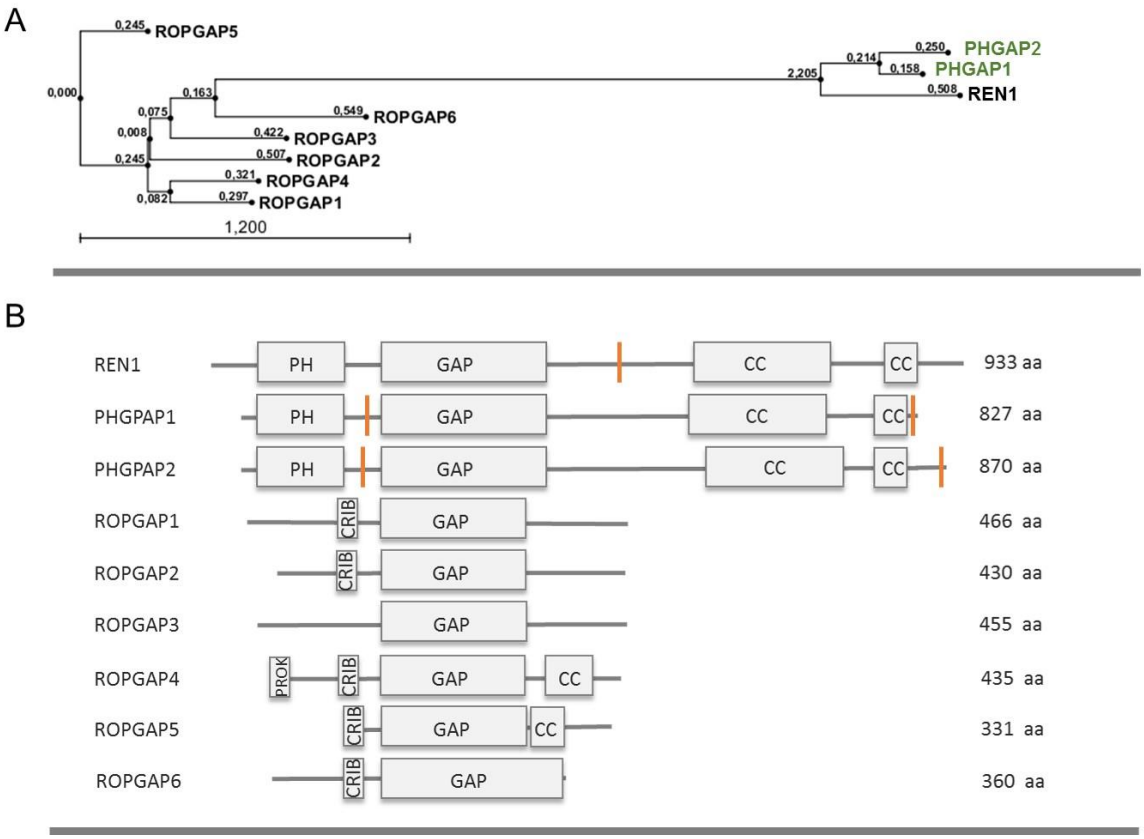

Figure 7: Phylogenetic tree and protein domain structure of *A. thaliana* ROPGAP proteins. **(A)** The phylogenetic tree illustrates the relationships of *A. thaliana* ROPGAPs. PHGAP1 and PHGAP2 are depicted in green. Phylogenetic tree was created in CLC main workbench using neighborhood joining. **(B)** Overview of ROPGAP protein domain structure. Orange lines depict 14-3-3 binding motives. Protein domain prediction was generated using online prediction tools (predictprotein (https://www.predictprotein.org/), UniPROT (http://www.uniprot.org/), Pole informatique Lyonnais (https://prabi.ibcp.fr/htm/index.php) and paircoil2 (http://paircoil2.csail.mit.edu/)).

The interaction between POK1$_{1683\text{-}2066}$ and PHGAP2 the 2in1 rBiFC was confirmed by in *A. thalinana* protoplasts. An interaction of POK1$_{1683\text{-}2066}$ and PHGAP2 could be observed (Figure 8 A) and was at least as strong as the previously characterized interaction of POK and TAN (Figure 6 A). Comparable average signal intensities were measured for interactions of POK1$_{1683\text{-}2066}$ with either TAN or PHGAP2. The n/cYFP localization pattern of the POK1$_{1683\text{-}2066}$ and PHGAP2 interaction (Figure 8 E) was more similar to the aggregation pattern of GFP-POK1$_{1683\text{-}2066}$ fusion protein (Figure 8 C) than to the cytoplasmic localization pattern of RFP-PHGAP2 fusion protein (Figure 8 D). These observations *in planta* support the initially observed interaction between POK1 and PHGAPs.

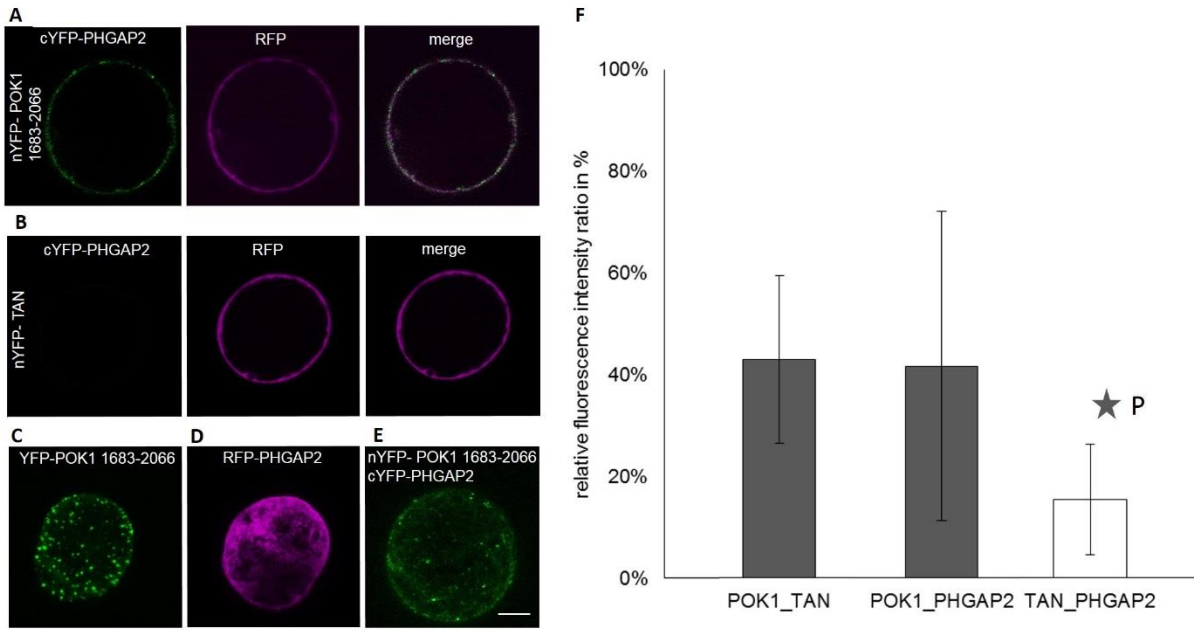

Figure 8: rBiFC Interaction Assay of POK1 and PHGAP2 expressed under the control of 35S promoter. **(A, B)** Confocal images of *A. thaliana* protoplast co-expressing nYFP-POK1$_{1683\text{-}2066}$ and cYFP-PHGAP2 **(A)** or nYFP-TAN and cYFP-PHGAP2 **(B)** as negative control. The YFP fluorescence due to the nYFP/POK1$_{1683\text{-}2066}$ and cYFP-PHGAP2 interaction, was measured and compared to fluorescence of nYFP-TAN cYFP-PHGAP2 control as well as the YFP POK1$_{1683\text{-}2066}$ cYFP-TAN positive control. RFP, expressed from the same plasmid, was used as an internal control. **(C-E)** Localization patterns of YFP-POK*1*$_{1683\text{-}2066}$, RFP-PHGAP2 and nYFP-POK1$_{1683\text{-}2066}$ expressed together with cYFP-PHGAP2. Images are Z-projections of image stacks with Z-intervals of 1 µm. PHGAP2 Bar = 10µm. Images were taken at confocal microscope. **(F)** Quantification of the relative fluorescence YFP intensity of the interaction partners and the control by using the YFP/RFP ratio. Data are means of $n \geq 29$ protoplasts for each construct. Each protoplast represents an independent transformation event. The YFP/RFP ratio of the interacting partners POK1 and TAN, POK1 and PHGAP2 is highly different ($p < 0.0001$) from the non-interacting control TAN and PHGAP2.

5.3 Gene Expression of *PHGAP1* and *PHGAP2* in *A. thaliana* is restricted to young tissues and organs

In order to examine the gene expression pattern of the two novel POK1 interactors, *promotor:GUS* studies of *PHGAP1* and *PHGAP2* as well as *promoter:NLS-dTom* gene expression of *PHGAP1* and *PHGAP2* were carried out. These experiments showed that *PHGAP1* and *PHGAP2* share substantial overlap of expression in some tissues, while they are complementarily expressed in others. For instance, in roots *PHGAP1* is only expressed in the epidermal and cortex layers, while *PHGAP*2 expression is found in the vasculature of the root (Figure 9 D and H). In leaf primordia and young leaves both, *PHGAP1* and *PHGAP2,* are expressed (Figure 9 A and E), but only *PHGAP2* is strongly expressed in stomata (Figure 9 F). In the reproductive organs, GUS-activity was observed in ovules for *PHGAP1* in sporophytic tissue adjacent to the micropylar pole. *PHGAP2* was expressed in the whole ovule (Figure 9 C and G).

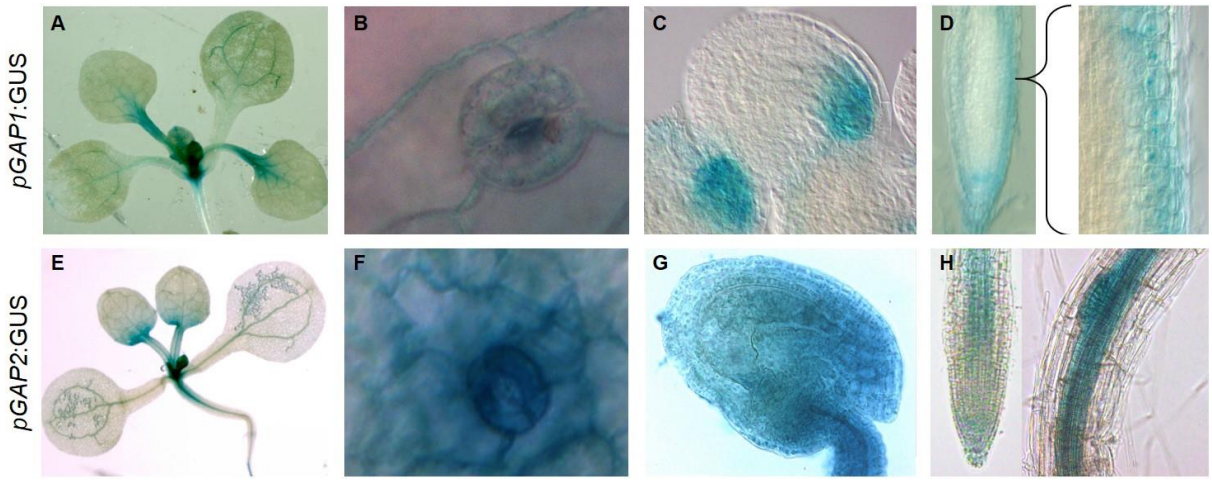

Figure 9: Bright-field images of histochemical GUS staining showing gene expression of *PHGAP1* and *PHGAP2* in different *A. thaliana* tissues. **(A, E)** Gene expression of *PHGAP1* and *PHGAP2* in young leaves and the shoot apical meristem of three weeks old seedling. **(B, F)** Low *pPHGAP1*:GUS expression was observed in stomata in contrast to the strong *pPHGAP2*:GUS expression. **(C, G)** *PHGAP* expression in ovules. **(D, H)** Expression of *pPHGAP1*:GUS and *pPHGAP2*:GUS in the root.

Furthermore, *PHGAP1* and *PHGAP2* gene expression patterns were confirmed by promoter-fusion to a nuclear localized fluorescent protein di-Tomato (dTom). Interestingly, expression of *PHGAP1* in stomata was observed (Figure 10 B). The expression patterns of both genes were confirmed in expanding pavement cells of young leaves (Figure 10 C and F) and in roots (Figure 10 A and D).

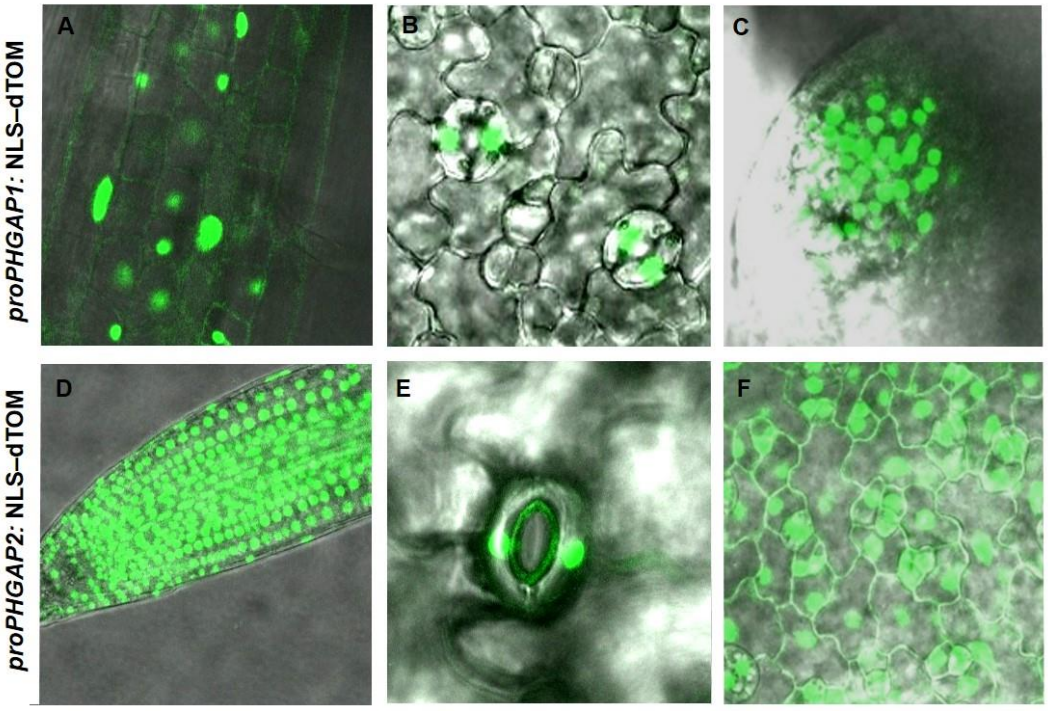

Figure 10: Gene expression pattern of *PHGAP1* and *PHGAP2* in different *A. thaliana* tissues using the fluorescent reporter dTomato (dTom). **(A)** *PHGPAP1* expression in the epidermal layer above the root elongation zone. (**B)** *pPHGAP1* gene expression in stomata of young leaves. **(C)** *pPHGAP1* gene expression in division zone of the first leaf. **(D)** Cross section of the root tip expressing *pPHGAP2*. **(E)** *pPHGAP2*:NLS-dTom signal in stomata and in expanding pavement cells. **(F)** Expression of *PHGAP2* in the leaf epidermis. Images of *pGAP1*:NLS-dTomato and *pGAP2*:NLS-dTomato images were taken four days after germination at the confocal microscope.

5.4 PHGAP1 and PHGAP2 localize in the cytosol in interphase and are recruited to the cortical division site in cytokinetic cells in *A. thaliana*

To investigate the localization pattern of PHGAP1 and PHGAP2 GFP fusions were constructed with *PHGAP1* and *PHGAP2* cDNA expressed from the *A. thaliana* ubiquitin 10 promotor (Grefen et al., 2010). The fusion proteins showed cytoplasmic localization in all cells and a distinct ring-shaped pattern in a subset of cells in *A. thaliana* root meristem (Figure 11 A and B). The ring-shaped localization was reminiscent of the POK1 localization pattern (Lipka et al., 2014).

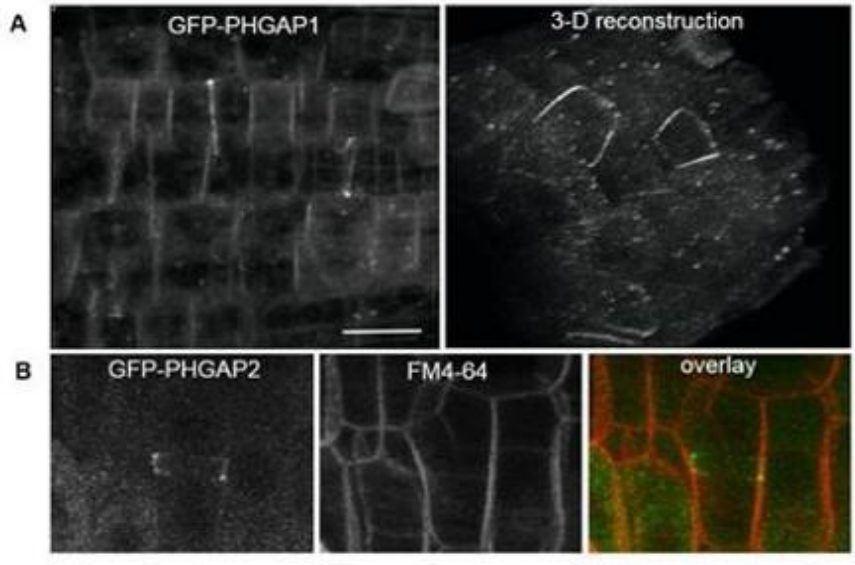

Figure 11: Confocal images of *A. thaliana* roots expressing GFP-PHGAP1 or GFP-PHGAP2. Images were taken at the epidermal layer of the root at confocal microscope. **(A)** *pUBN:GFP-PHGAP1* expressed at the epidermal layer of the root as maximum projection of a Z-stack and 3-D reconstruction. (**B)** GFP-PHGAP2 is also expressed at the epidermal layer of the root as maximum projection of a Z-stack. Counter stain of the plasma membrane by using FM4-64 dye. Bar = 20 µm

To determine the cell cycle phase of cells with the ring-shaped GFP-PHGAP1 and GFP-PHGAP2 localization, the microtubule reporter line RFP-MBD was crossed into plants expressing *pUBN:GFP-cPHGAP1* and *pUBN:GFP-cPHGAP2.* In prophase of meristematic root cells, no GFP-PHGAP1 signal was observed at the CDZ (Figure 12.A). At the transition from ana- to telophase accumulation of GFP-PHGAP1 became apparent at the cortical division zone suggesting that recruitment of PHGAP1 occurred only late in

mitosis (Figure 12 B). After the cell plate had attached to the parental cell wall, PHGAP1 localization extends to the newly made cell wall (Figure 12 C). Localization of PHGAP2 needs still to be evaluated during the cell cycle.

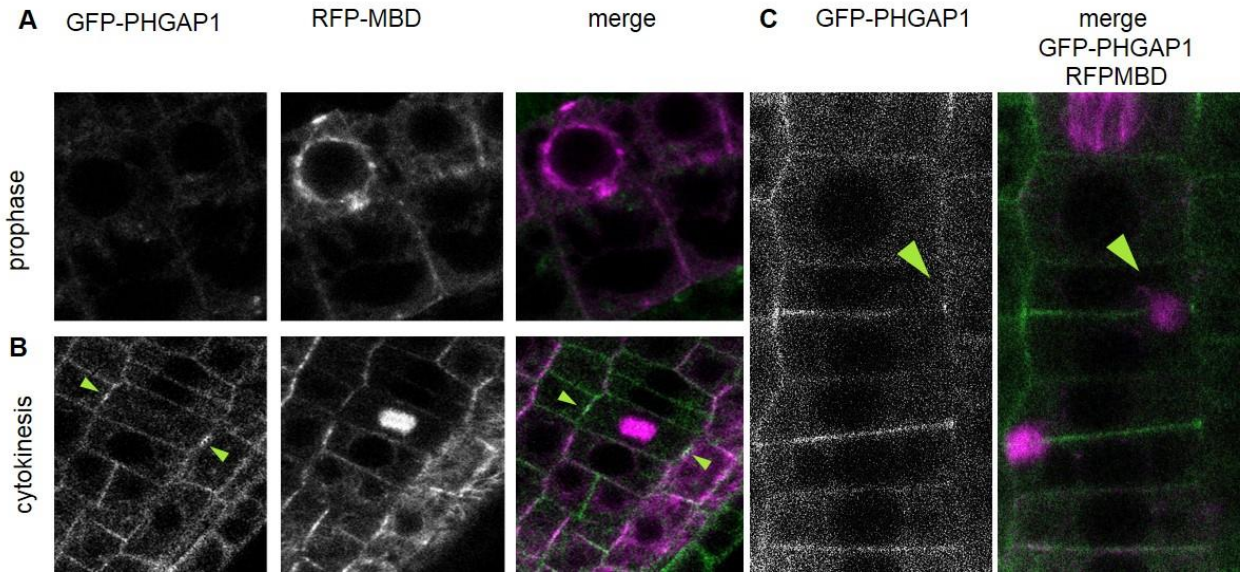

Figure12: Spatiotemporal localization pattern of GFP-PHGAP1 ring, in the cell cycle. *A. thaliana* root epidermis cells co-expressing GFP-PHGAP1 and RFP-MBD were imaged. RFP-MBD was used as a marker to identify the cell cycle stages. **(A)** In prophase, GFP-PHGAP1 was still localized in the cytoplasm and no accumulation of GFP-PHGAP1 was observed at a distinct region of the cell wall. **(B)** In early cytokines GFP-PHGAP1 is enriched at the flanks of the cell in one line with the expanding phragmoplast (arrow heads). **(C)** Co-expression of PHGAP1 and RFP-MBD show that PHGAP1 does not localize to the newly built cell wall until the phragmoplast reaches the parental cell wall (arrow heads).

5.5 PHGAP1 and POK1 co-localize at the cortical division zone

YFP-POK1 is recruited to the PPB during prophase and remains at the CDZ throughout mitosis (Lipka et al., 2014). For co-localization analysis, YFP-POK1-expressing plants were crossed with transgenic plants expressing *pUBN:*RFP-cPHGAP1. Indeed both, RFP-PHGAP1 and YFP-POK1, were co-located at the cortical division site, most likely during cytokinesis (Figure 13). Therefore, the co-localization of RFP-PHGAP1 and YFP-POK1, at the cortical division site further confirm the previously observed interaction in Y2H and rBiFC experiments.

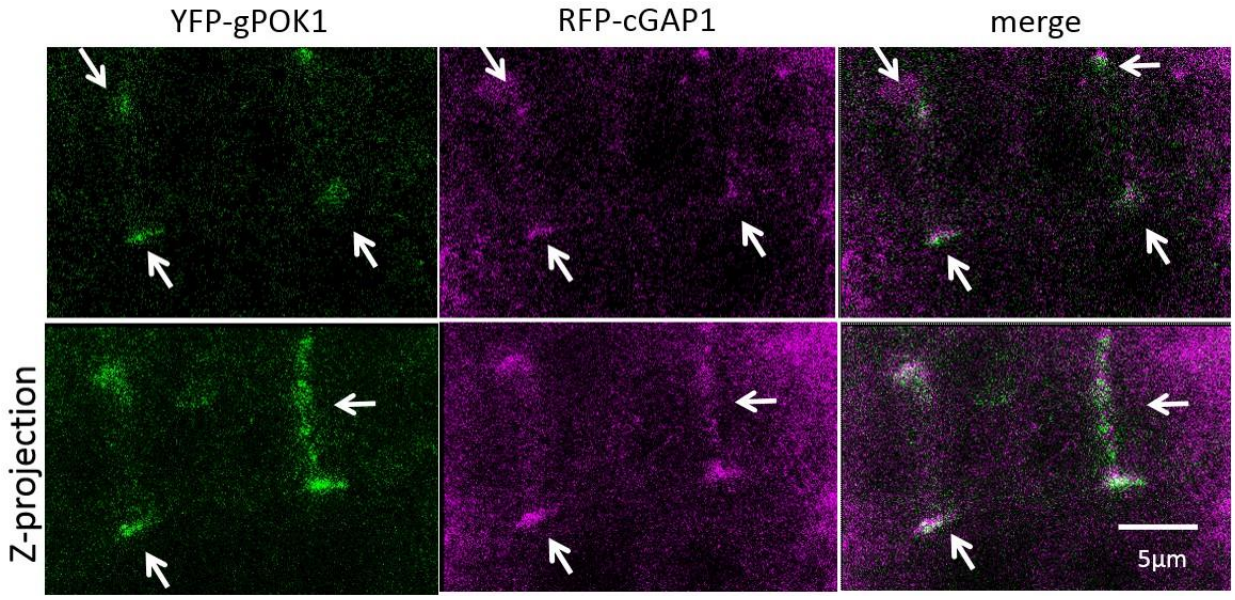

Figure13: Co-localization of RFP-PHGAP1 and YFP-gPOK1 in *A. thaliana* root epidermis cells. The upper panel shows a transverse section through two cytokinetic cells expressing YFP-gPOK1 and RFP-GAP with an accumulation at the flanks (arrows). Lower panels: The Z-projection of cells depicted in upper panels, clearly show the co-localization (arrows) of RFP-PHGAP1 and YFP-gPOK1. Images were taken at confocal microscope. Bar = 5 µm

5.6 Functional Characterization of *PHGAPs* using mutant analysis

5.6.1 *phgap* single mutants

In order to investigate the function of *PHGAPs* during plant development, several, available T-DNA insertion mutants were examined. Positions of T-DNA insertions were determined by PCR-based genotyping and sequencing (Figure 14 A). The following *phgap1* and *phgap2* alleles were characterized: *phgap1-1*, *phgap1-3*, *phgap1-04D, phgap1-09H* and *phgap2-23*, *phgap2-51* (Appendix 7.2, Genotyping Primer). None of the mutant alleles showed any phenotype. Therefore, semi-quantitative RT-PCR was performed with the respective T-DNA insertion lines to examine the transcript level. Transcript levels were not completely abolished, but were vastly reduced in the mutant alleles, *phgap1-3*, *phgap1-04D phgap2-23* and *phgap2-51* (Figure 14 B and C). The

absence of single mutant phenotypes and the high similarity of *PHGAP1* and *PHGAP2* suggest functional redundancy, and therefore, double mutants were generated.

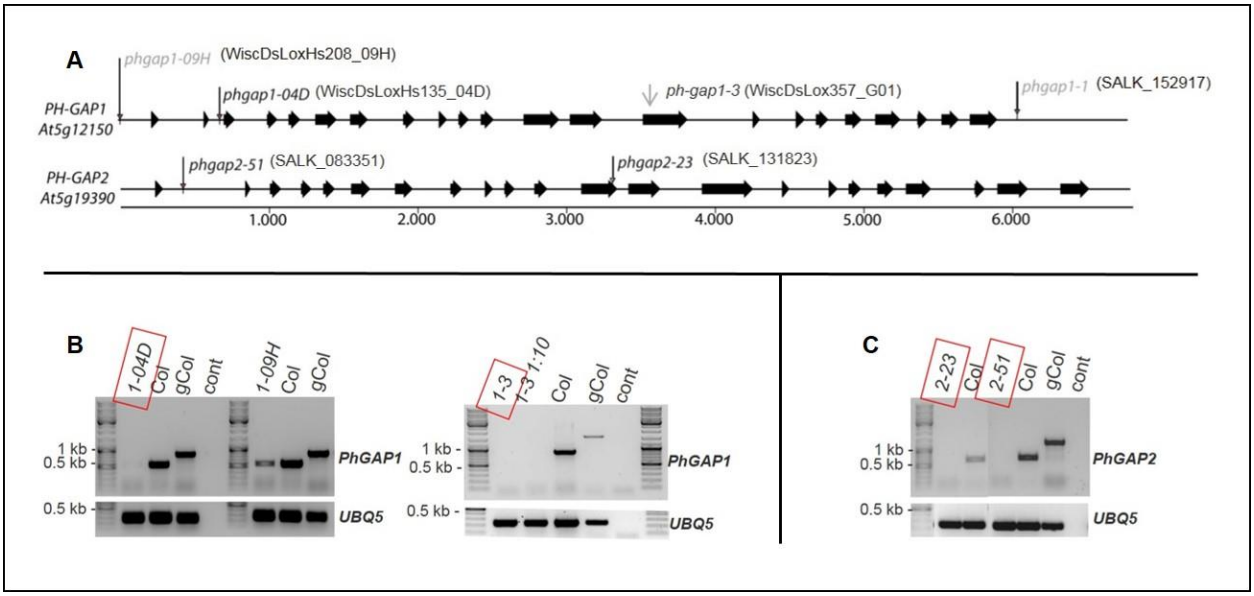

Figure 14: Gene structure of *PHGAP* genes positions of different T-DNA insertions and RT-PCR analysis. **(A)** Intron and exon organization of PHGAP1 and PHGAP2 including the position of T-DNA insertions. **(B and C)** Semi-quantitative RT-PCR analysis of *PHGAP1* and *PHGAP2* transcript levels in inflorescences. The red boxed alleles indicating down regulated transcript. These lines were used for generating double mutants.

5.6.2 *phgap* double mutants

Double mutants were generated with two different allele combinations, *phgap104D* x *phgap2-51* and *phgap1-3* x *phgap2-23*. In the following, the term *phgap1 phgap2* mutant refers to the allele combination *phgap104D* x *phgap2-51* unless indicated otherwise. . Also the double mutants did not show any obvious phenotype. So a closer examination was needed to determine mutant phenotypes.

5.6.3 phgap1 phgap2 shows defects in embryogenesis

The interaction with the mitosis specific kinesin-12 protein POK1 suggested that PHGAP1 and PHGAP2 might also play a role in cell division or at least in cytokinesis. Mutations in *POKs* lead to severe phenotypes in roots, but comparable phenotypes were not observed for *phgap1 phgap2* double mutants. One reason might be functional redundancy with other ROPGAPs which are also ubiquitously expressed (Figure 15).

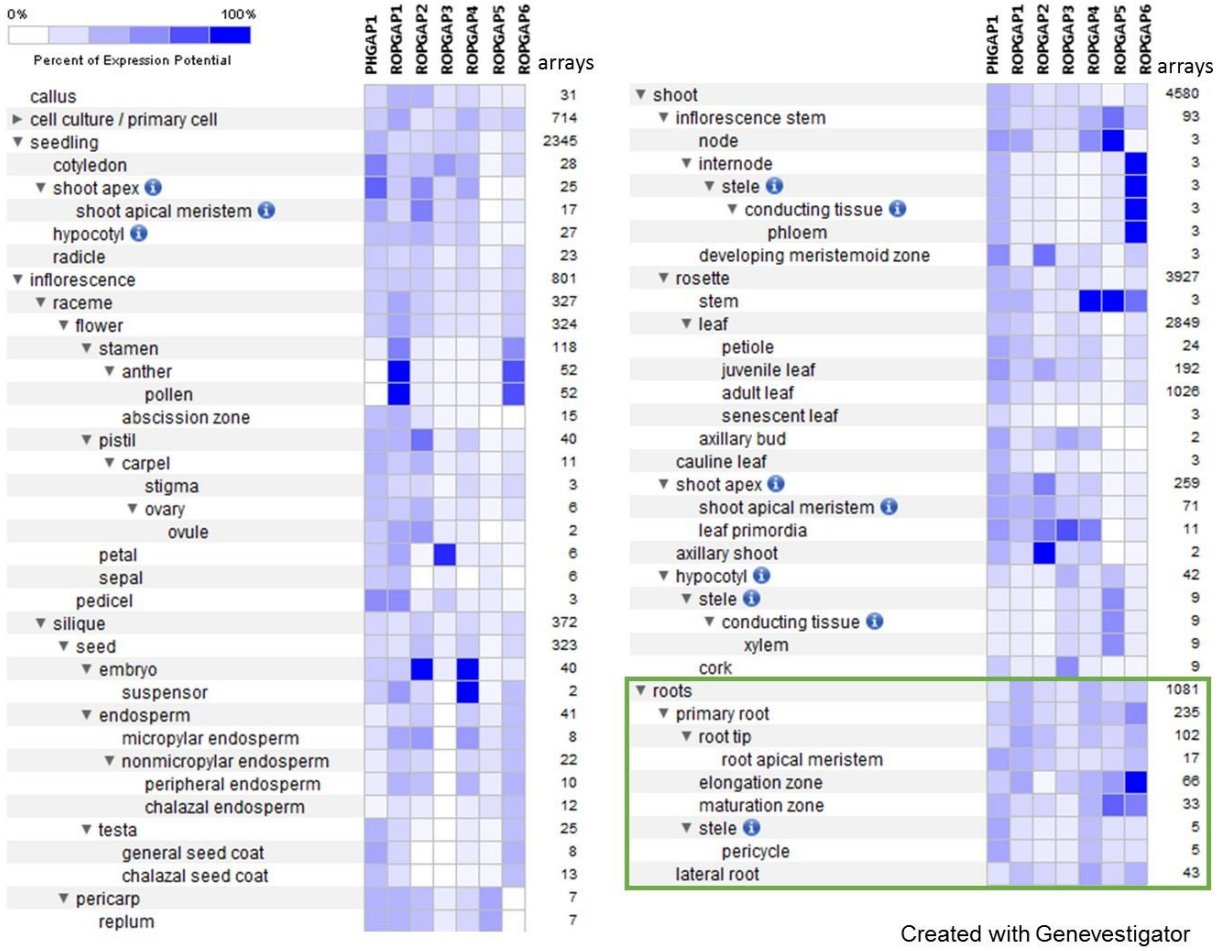

Figure 15: Overview of ROPGAP expression pattern of GAPs in different tissues of *A. thaliana* except for PHGAP2. The color intensity describes the expression potential in the different tissues. The number of tested arrays is shown beside the colored columns of the expression probability the expression of ROPGAP in roots is green boxed.

However, in addition to the regular cell division pattern in roots, also embryo development requires spatial control over cell division. Indeed, embryo development is also affected in *pok1 pok2* mutants (Muller et al.,,2006). Therefore, *phgap1 phgap2* double mutant embryos were examined. Wild type early embryo development is characterized by an almost invariant pattern of divisions. Several *phgap1 phgap2* mutants were analyzed for embryo defects. Wild type was compared to a *phgap2* (*phgap2-23*) single mutant and to two allele combination of *phgap1 phgap2* double mutants (*phgap1-3 phgap2-23* and *phgap1-04D phgap2-51*). Indeed, in *phgap1-04D phgap2-51* double mutants, a broad range of embryo phenotypes were observed displaying irregular cell wall positioning (Figure 16). Representative embryo defects, range from completely aberrant cell divisions (Figure 16 F and I) to abnormalities just in the apical part (Figure 16 E). Oblique inserted cell plates (Figure 16 G and J), additional longitudinal cell division in the hypophysis (H) as well as embryos with retarded growth and swollen cells were observed (Figure 16 G and K). The defects were most recognizable until the early heart stage, but occurred at low frequencies (Table1). The *phgap1-04D phgap2-51* mutant allele combination showed, the highest frequency of defective embryos, in contrast to the *phgap2-23* single and the *phgap1-3 phgap2-23* double mutant. In order to examine if the absence of both PHGAP proteins caused the embryo defects, the genomic construct of PHGAP2 fused, N-terminally, to a GFP was crossed with the *phgap1 phgap2* double mutant. The embryo analysis of these lines revealed that the embryo defects were reduced significantly which suggests complementation by PHGAP2 (Table 1). Furthermore, these results support PHGAP involvement in cell division.

genotype	2c to globular	heart	defective/Total	percentage
wild type	5/ 568 (0,88%)	1/117 (0,85%)	6/685	0,86%
gap2-23	9/ 431 (2,08%)	0/83 (0%)	9/514	1,75%
gap1-3gap2-23	10/218 (4,59%)	4/221 (1.8%)	14/470	2.98%
gap1-04D gap2-52	20/233 (8,58%)	4/133 (3.0%)	24/366	6,56%
pGAP2_GFPgGAP2 gap1-04D gap2-52	15/ 631 (2,3 %)	3/52 (5,7%)	18/683	2,6%

Table 1: Percentage of defective embryos in different developmental stages in different genetic backgrounds. *phgap1-04D phgap2-51* mutant allele combination showed the highest amount of defective embryos compared to the *phgap2-23* single and the *phgap1-3 phgap2-23* double mutant. Expression of genomic PHGAP2 in *phgap1-04D phgap2-51* could reduce the number of defective embryos derived from irregular cell divisions.

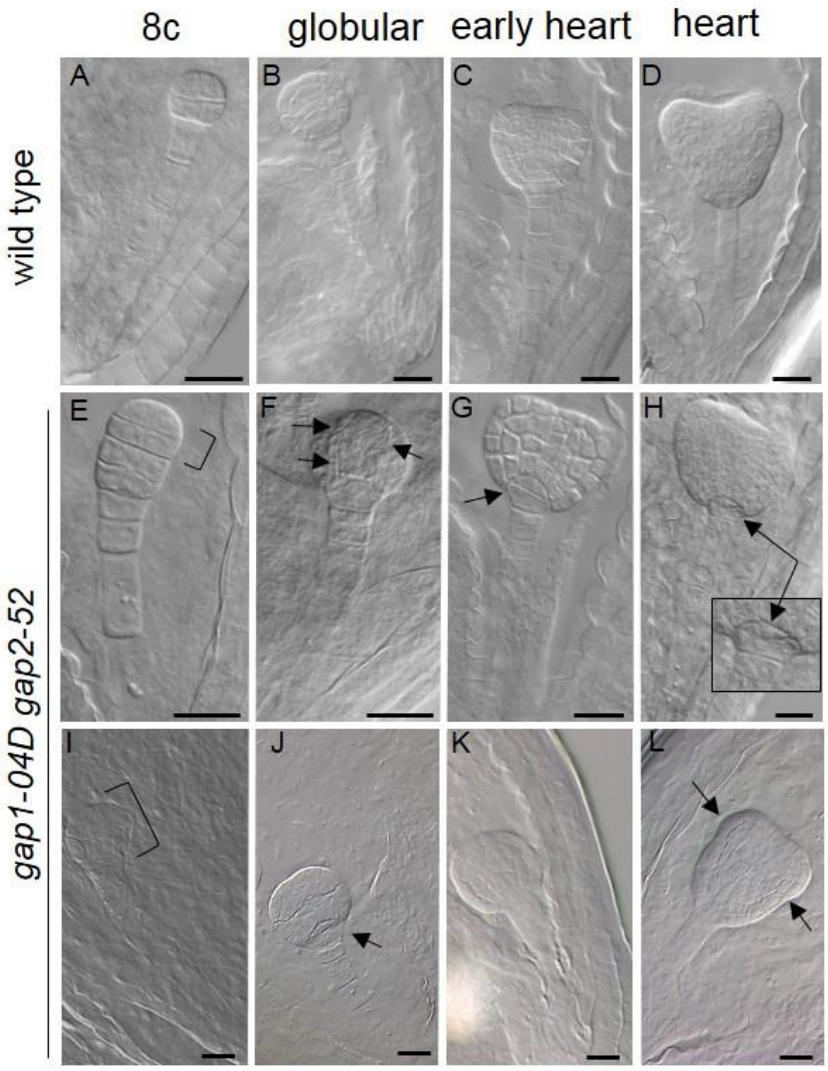

Figure 16: Overview of representative embryos defects in different developmental stages. **(A-D)** Wild type embryos are depicted from eight-cell-stage to heart stage. The panels below **(E-L)** show defective mutants in stages comparable to the wild types above. Arrows and brackets indicates altered region of the embryo. Bar = 20 µm

In addition to the embryo phenotypes, the number of fertilized ovules was obviously reduced in *phgap1 phgap2* double mutants (Figure 17 B and D). The number of ovules could be restored to the wild type numbers, by complementation using genomic PHGAP2 fused to GFP (Figure 17 C and D).

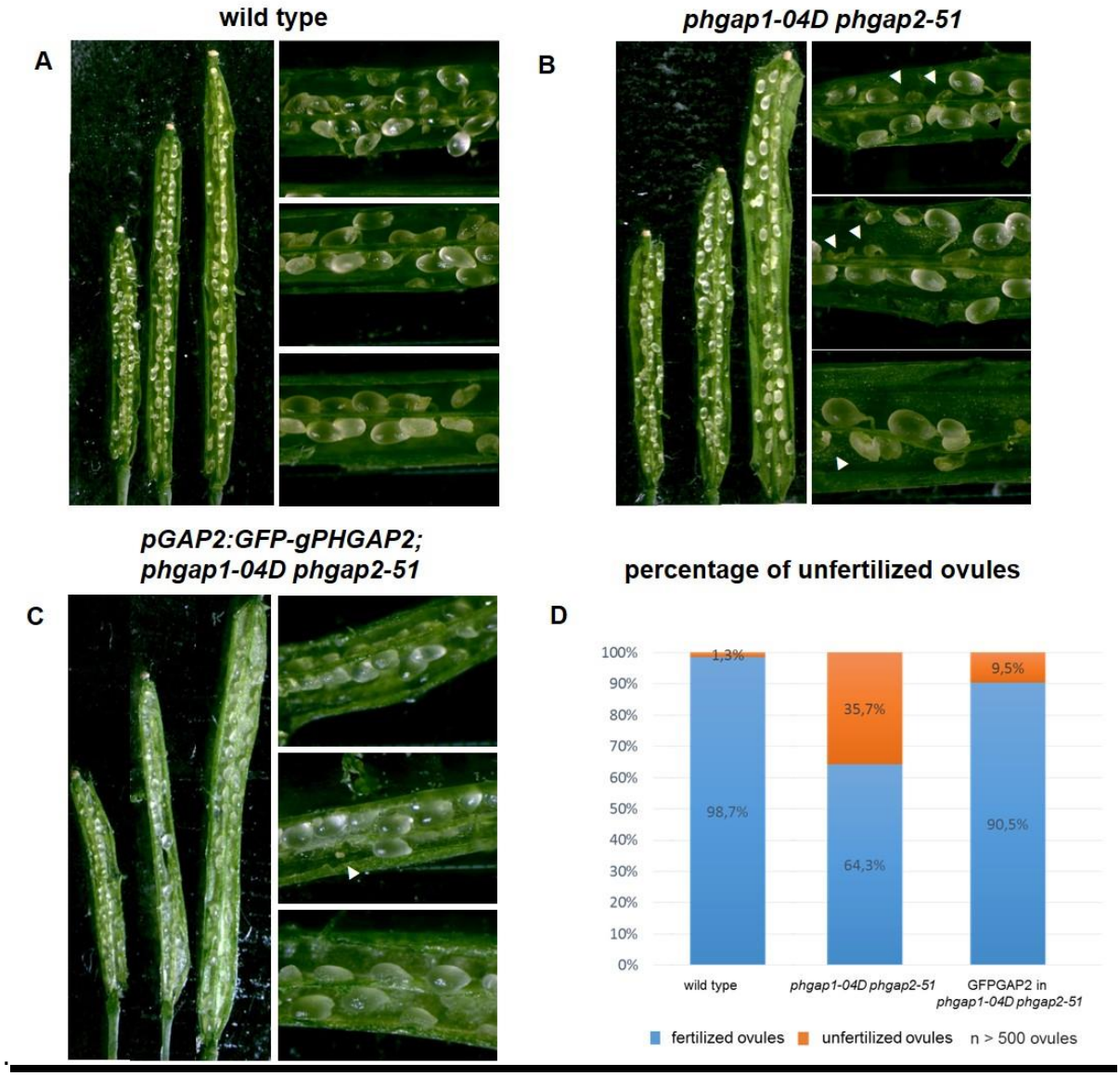

Figure 17: Overview of seed set in different stages of *A. thaliana* fruit development. **(A)** Wilde type siliques. **(B)** *phgap1-04D phgap2-51* mutant siliques. **(C)** *phgap1-04D phgap2-51* siliques expressing GFP-gPHGAP2. Unfertilized ovules are indicated by arrow heads**. (D)** Quantification of alteration in the ovules number of wild type and *phgap1-04D phgap2-51* siliques and *phgap1-04D phgap2-51* expressing *pPHGAP2:*GFP-gPHGAP2. The graph shows the differences in the fertilization rate between wild type, *phgap1 phgap2* and GFP-gPHGAP2 in the *phgap1 phgap2* background. The percentage of fertilized ovules is depicted in blue and the rate of unfertilized ovules is depicted in orange. Counted ovules n ≥ 500

5.6.4 Transmission defects of *phgap1 phgap2*

After investigating the *phgap1 phgap2* double mutant siliques and observing unfertilized ovules, it was obvious to test the transmission rate of the PHGAP1 and the PHGAP2 alleles. The transmission experiment revealed severe transmission defects through the male gametophyte. Transmission of *phgap1 and phgap2* were observed in an unexpected ratios. *phgap1* showed a transmission reduction to 15%. Similar to *phgap1, phgap2* showed a reduction of transmission to 17%, while the reciprocal transmission experiments showed approximately the expected 50 %: 50% ratio for both *phgap* alleles (Table 2).

Pollen donor	Pollen acceptor	+/-	+/+	Allele
phgap1/+ phgap2/+	**Wild type**	15.58 % n=24	84.41 % n=130	*phgap1*
		17.05 % n=29	82.90 % n=141	*phgap2*
Wild type	***phgap1/+ phgap2/+***	49.20 % n=86	50.80 % n=89	*phgap1*
		55.11 % n=97	44.89 % n=79	*phgap2*

Table 2: Transmission data of PHGAP1 and PHGAP2. In the upper part of the table transmission of PHGAP1 and PHGAP2 is shown if *phgap1/+ phgap2/+* heterozygous plant were used as pollen donor. In the lower part of the table transmission of PHGAP1 and PHGAP2 is shown if *phgap1/+ phgap2/+* heterozygous plants were used as pollen acceptor. The analysis was PCR based.

5.6.5 Pollen tube growth of *phgap1 phgap2* pollen is not altered

The observations of the embryo defects and the transmission defects led to the question how pollen is affected in the *phgap1 phgap2* mutant. Investigations of the Rho Enhancer1 (REN1), the closest relative of PHGAP1 and PHGAP2 in *A. thaliana* causes a severe pollen tube phenotype if a T-DNA is inserted in the N-terminal part of the protein (Hwang et al., 2008). Therefore, a pollen tube assay was performed. Pollen of the different *ren1* mutant alleles, *ren1-2*, *ren1-3* and a new mutant allele of REN1, the designated *ren1-4,* which has not been described yet, were used for pollen germination (Figure 18 A). The phenotype of the pollen tubes in *ren1-2* and *ren1-3* could be resembled as described by Hwang et al., 2008. It could be shown that the *ren1-4* mutant, whose T-DNA is inserted in the C-terminal part of the protein, has also a severe effect on the pollen tube growth. The phenotype of the novel *ren1-4* allele (Figure 18 B) is similar to the *ren1-1* mutant as described (Hwang et al., 2008). On the other hand the *in vitro* pollen tube growth of those *phgap1 phgap2* pollen grains that germinated is not altered compared to the wild type (Figure 1 B). However, the pollen tube assays, although performed multiple times, always showed a large portion of non-germinating pollen grains, irrespective of the genotype. Thus, it could not be determined whether pollen germination rate might be affected in *phgap1 phgap2* that might cause the observed transmission defects.

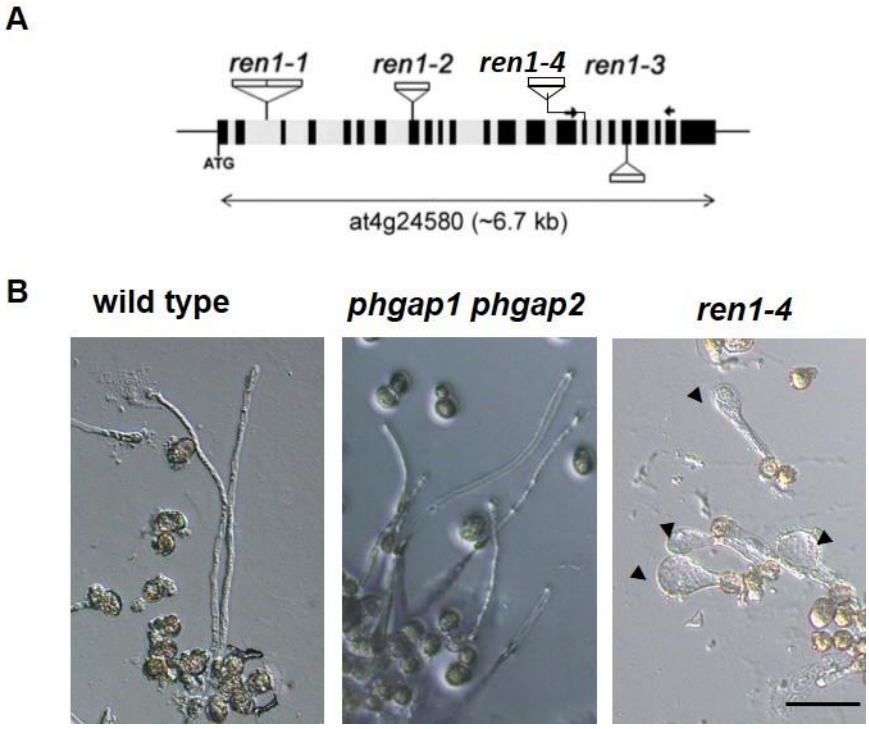

Figure 18: (A) Scheme of the exon and intron structure of the *REN1* gene containing T-DNA insertion lines (modified from Hwang et al., 2008). **(B)** Wild type, *phgap1 phgap2* and *ren1-4* pollen after 8h incubation on pollen germination medium. *ren1-4* expansions defects are indicated by arrow heads. Bar = 100 µm.

5.6.6 Expression of GFP-PHGAP2 in *ren1-4* mutants

From a previous pollen tube elongation study by Hwang and colleagues (2008) it is known that *ren1-1* mutants can be complemented by the full length CDS of REN1 driven by an LAT52 promoter. PHGAPs and REN1 are differentially expressed and are closely related. The question arose, whether PHGAP proteins might fulfil REN1 function when expressed in the pollen. Therefore, *pUBN:GFP-cPHGAP2* expressing plants were crossed with the heterozygous *ren1-4* mutant. Examination of the pollen tube growth as well as the non-germinated pollen showed expression of the GFP-PHGAP2 fusion protein, but no obvious complementation of the pollen tube elongation defects, since only a few pollen showed elongated pollen tubes (Figure 19).

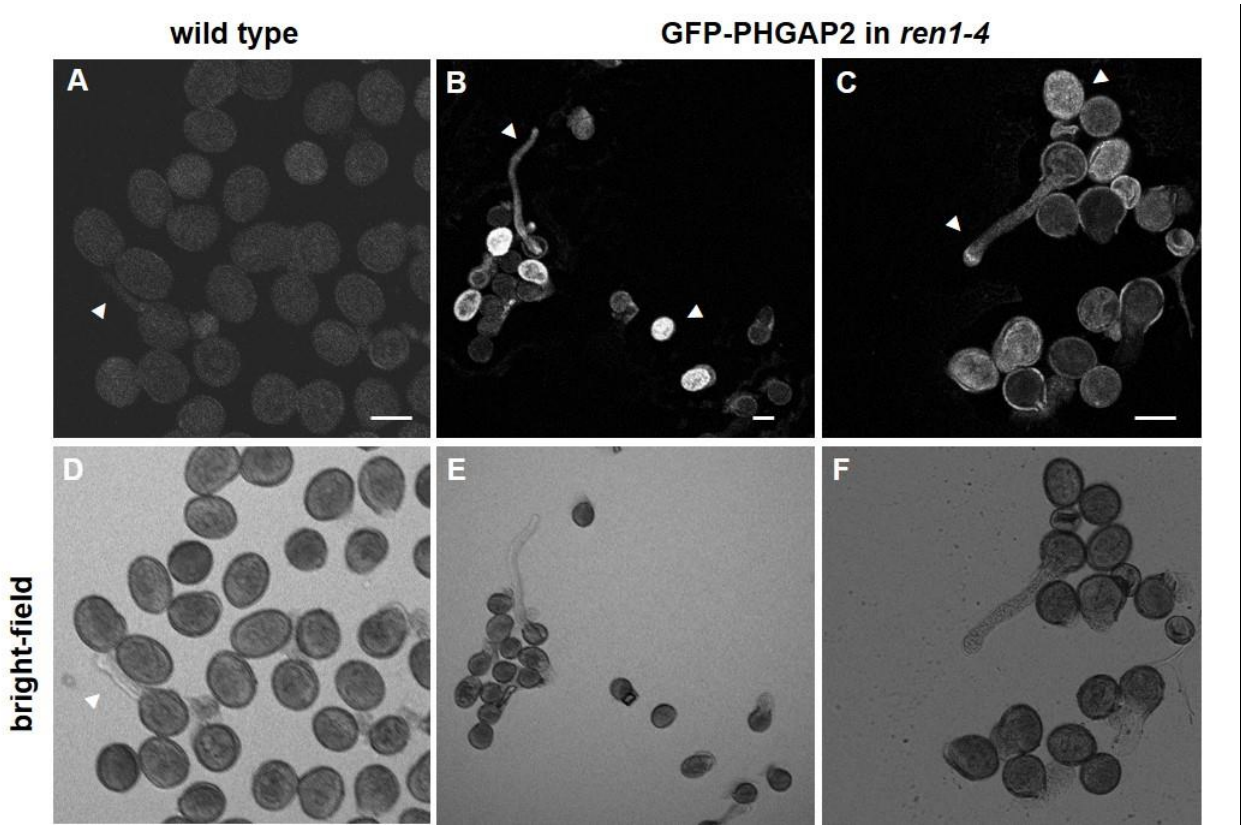

Figure 19: Expression *pUBN:GFP-PHGAP2* in *ren1-4* mutants. **(A)** Auto-fluorescence of the wild type was used as control. **(B and C)** *pUBN:GFP-PHGAP2* expressed in pollen. Arrow heads indicate expression in pollen grain and expression at the tip of pollen tube. Pollen tubes were imaged at the confocal microscope. The lower panels (**D, E and F**) are bright-field images of the fluorescent images above. Bar 20 µm

5.6.7 *phgap1 phgap2* causes severe pavement cell defects

REN1 was characterized as a functional GTPase activation protein which inhibits lateral expansion of the pollen tube by inactivation of ROP1 activity. PHGAP1 and the PHGAP2 also contain the GAP domain which suggests that they function as ROP-GAPs. We compared the gene expression patterns of the PHGAPs with gene expression patterns of publicly available ROPs. We found overlapping expression of PHGAPs with ROPs that that are essential for pavement cell establishment (Bement et al., 2005; Sorek et al., 2011). Thus, we took a closer look at the leaf morphology of *phgap1 phgap2* mutants. The macroscopic appearance of *phgap1 phgap2* mutants displays very mild mutant

phenotype. Slightly more lancet shaped leaves are recognizable compared to the wild type (Figure 20 A) and in the rosette stage a mild twisting of leaves was noticed (Figure 20 B). Indeed, in the *phgap1 phgap2* mutant the pavement cells were dramatically altered, losing the entire pavement cell complexity (Figure 20 D).

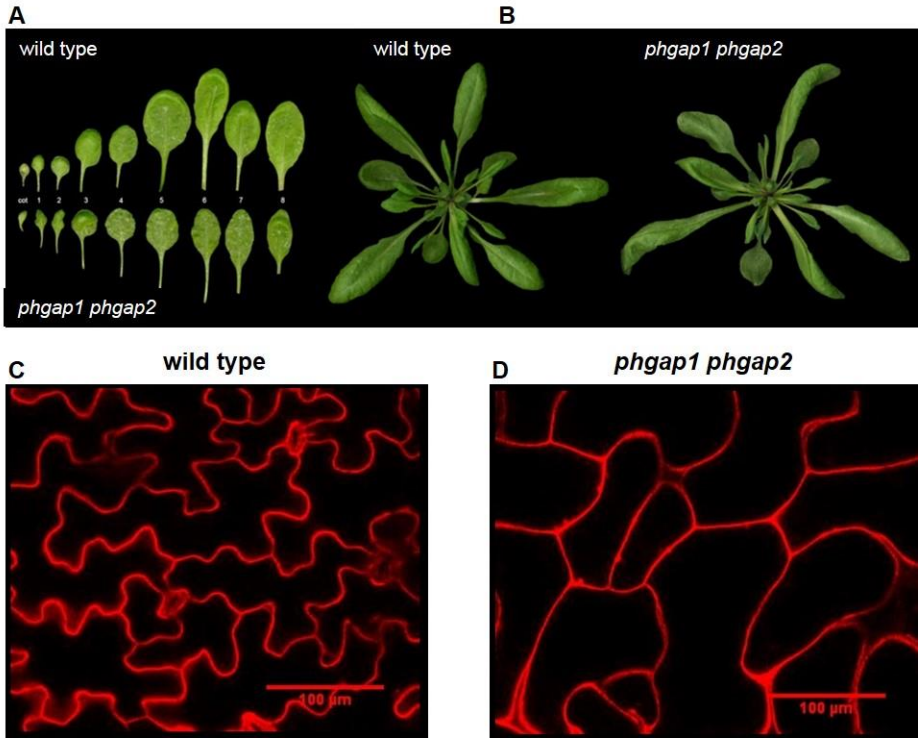

Figure 20: Comparison of *phgap1 phgap2* double mutant and wild type. **(A)** Direct comparison of the first eight leaves. Wild type is depicted in the upper panel and *phgap1 phgap2* in the lower panel. **(B)** The upper panel shows wild type and the lower panel shows the *phgap1 phgap2* mutant in rosette stage. **(C and D)** Cotyledons of ten days old seedlings were stained with propidium iodide and imaged on the abaxial side by confocal microscopy. **(C)** Wild type pavement cells. **(D)** *phgap1 phgap2* double mutant pavement cells.

The mutant pavement cell defects were characterized by quantification of the pavement cell area, the perimeter, the skeleton and the circularity. Significant differences were observed in every parameter measured in *phgap1 phgap2 mutants* compared to wild type (Figure 21).

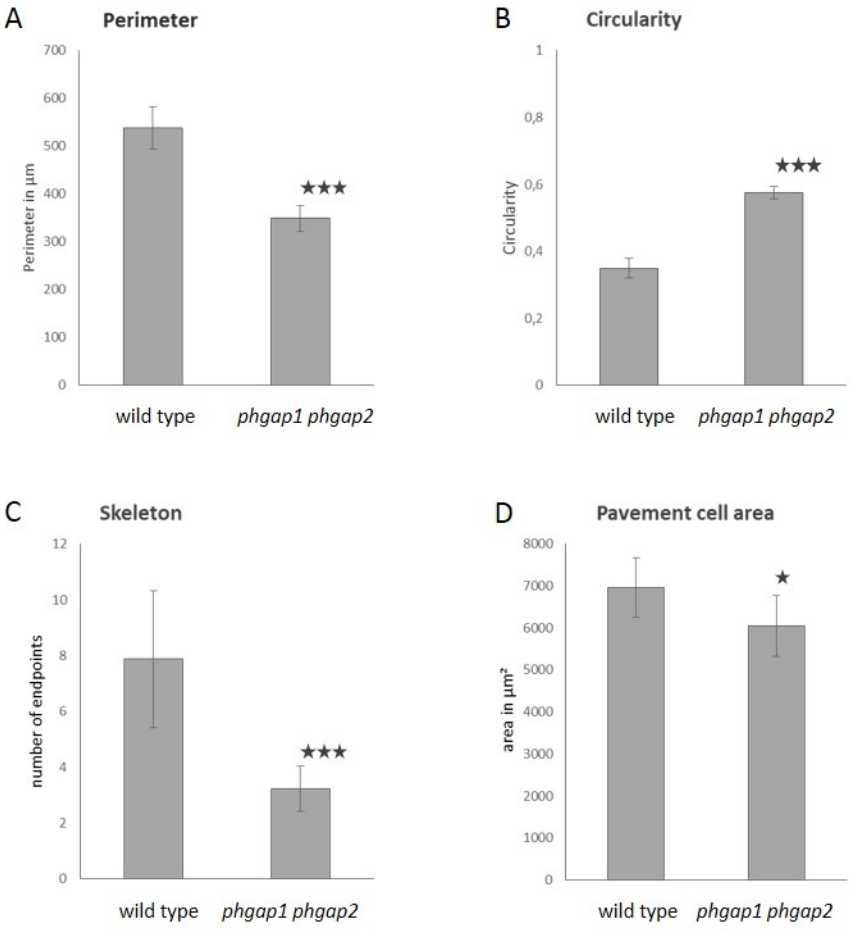

Figure 21: Quantification of the pavement cell shape parameters in *phgap1 phgap2* mutants. **(A and D)** Pavement cell area and perimeter were analyzed. **(B)** The circularity calculation was based in following formula: (4π area) / (perimeter^2). **(C)** Skeleton analyses described the diminished number of lobes in mutant pavement cells. Imaging was performed with Leica SP2, image processing accomplished with Photoshop Cs6 extended version and statistics were performed using Excel. n ≥ 500 cells.

5.6.8 Microtubule formation is altered in *phgap1 phgap2* pavement cells

After determining the pavement cells phenotype of the *phgap1 phgap2* mutant a microtubule marker was crossed into the *phgap1 phgap2* mutant, in order to investigate if the microtubule organization is affected. While in wild type, the microtubules are heavily bundled in neck regions of expanding pavement cells (Figure 22 A), in *phgap1 phgap2* mutants necks are difficult to recognize and bundling of microtubules is not evident (Figure 22 D). Analysis of the microtubule density in lobe and neck regions of the *phgap1 phgap2* mutant and the wild type, it could be shown that the microtubules in the necks of *phgap1 phgap2* were less bundled (Figure 22 H-K) indicating that microtubule organization is affected in the double mutant.

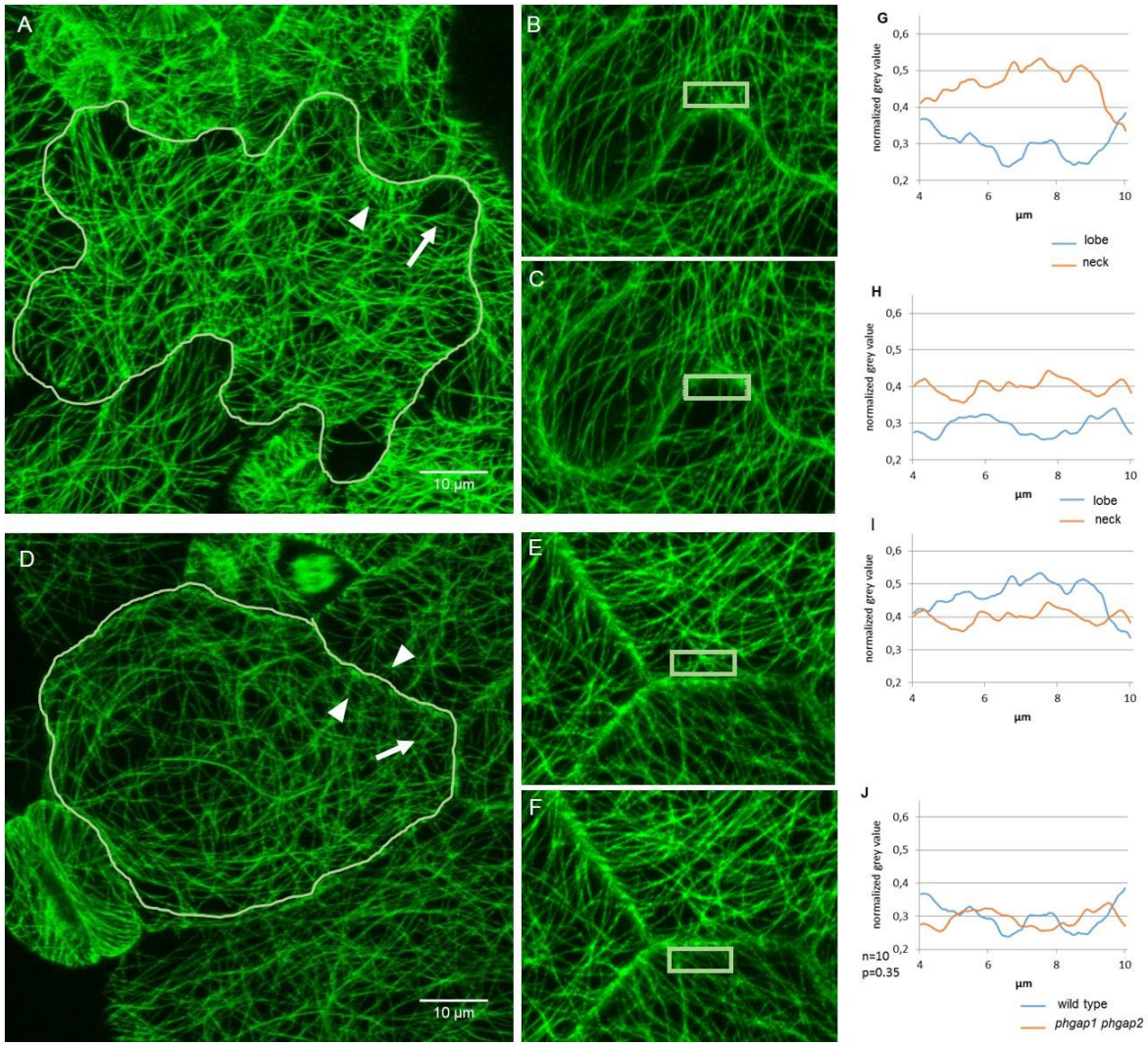

Figure 22: Microtubule distribution in pavement cells of *phgap1 phgap2* in contrast to the wild type. The regions for quantification were distinguished between lobes and necks indicated by the arrows heads (necks) and arrows (lobes). The cell shape is highlighted in light green **(A and D).** Fluorescence intensity was measured in areas indicated by light green box **(B, C, E and F)**. **(G-J)** Intensity profile of lobe and neck regions in *phgap1 phgap2* mutant and wild type. **(G)** Displays the microtubule distribution in the wild type **(H)** Displays the microtubule distribution in *phgap1 phgap2* mutant. **(I)** Distribution of wild type and *phgap1 phgap2* microtubules in lobe regions **(J)** Distribution of wild type and *phgap1 phgap2* microtubules in neck regions. Images of expanding pavement cells in stage II were taken at confocal microscope and the distribution of the microtubules were analyzed via plot profiling by using ImageJ. The graphs **(G-J)** show normalized gray values. n=10 **(G, H and I)** $p = 0.0001$ **(J)** $p = 0.35$

5.6.9 Complementation of the pavement cell phenotype

Complementation studies were essential to corroborating the functionality of PHGAP1 and PHGAP2 proteins. These experiment were performed by crossing *pUBN:GFP-cPHGAP2* into the *phgap1 phgap2* mutant background. Analysis of the *phgap1 phgap2* mutant carrying the *pUBN:GFP-cPHGAP2* showed an almost complete rescue of the pavement cell shape phenotype (Figure 23 C). Quantitative analysis supports the optical impression (Figure 23 E).

In case of *pro35s:YFP-GAP1* crossed into the *phgap1 phgap2* mutant, no statistical analysis was performed, but the phenotype suggests that the YFP-construct does rescue the pavement cell shape phenotype (Figure 23 B). To achieve full complementation further studies will be undertaken with genomic fusion proteins.

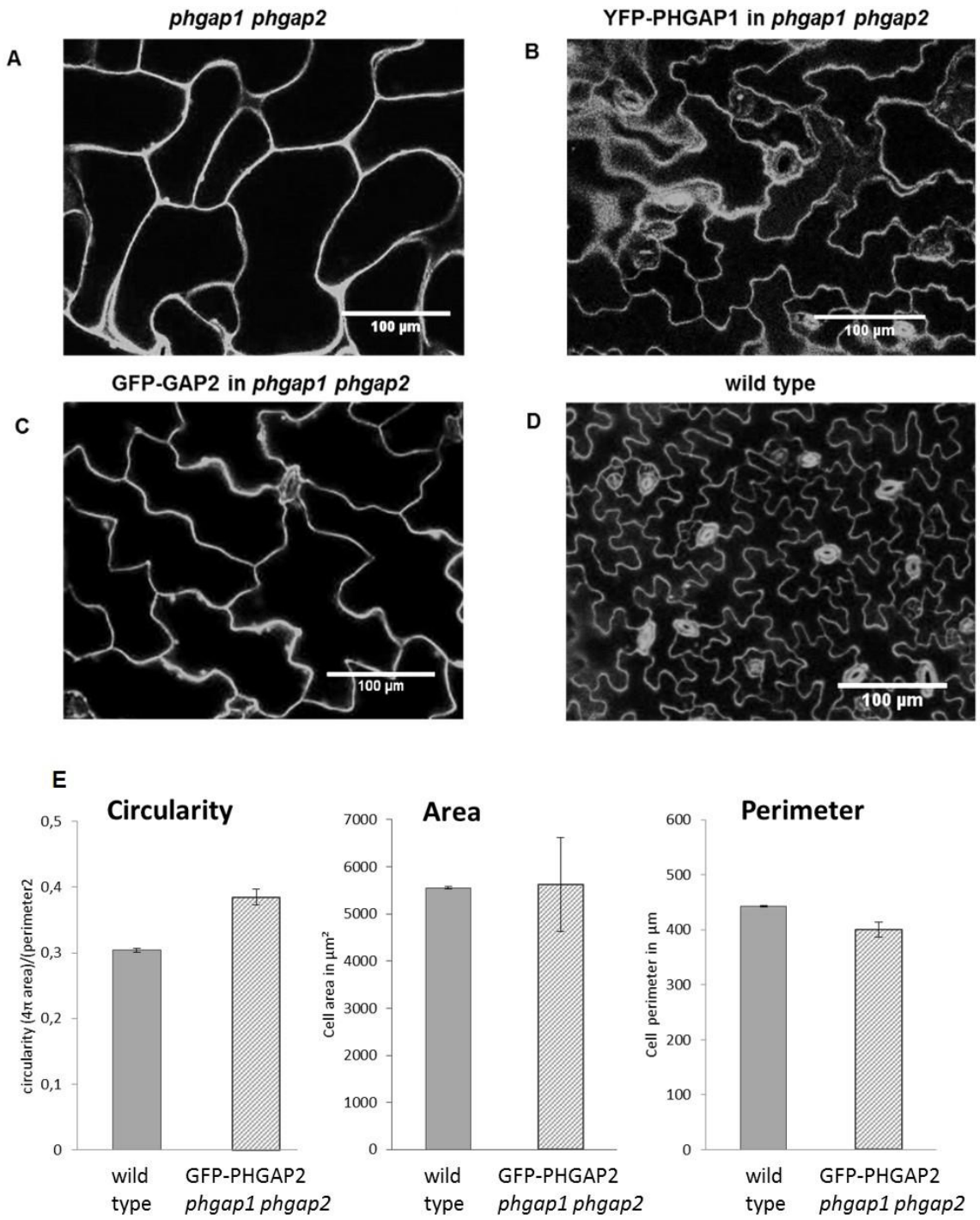

Figure 23: Analysis of the rescue ability of pavement cell shape phenotype in ten days old seedlings **(A)** *phgap1 phgap2* double mutant. **(B, C)** cDNA of *PHGAP1* and *PHGAP2* was stably trans-formed into *phgap1 phgap2* double mutant. **(D)** Wild type image for comparison. Images are maximum z-projections of confocal images. Cell walls are stained with propidium iodide. **(E)** Quantification of the pavement cell defects parameter circularity, area and perimeter were performed just as the quantification used for the *phgap1 phgap2* double mutant. Imaging was performed with Leica SP2, image processing accomplished by Photoshop CS6 extended version and statistics were done by Excel n ≥ 250 cells

5.6.10 PHGAPs are functional GTPase activating proteins

REN1 contains a conserved arginine in the GAP domain that is required for GAP activity (Hwang et al., 2008). Replacement of the arginin by a leucine resulted in loss of GAP function and the inability to rescue the *ren1* mutant phenotype (Hwang et al., 2008). To test whether PHGAPs also acted as GAPs, the distinct arginine in *pUBN*:GFP-cPHGAP1 (R203L) as well as *pUBN*:GFP-cPHGAP2 (R198L) was exchanged with leucine (Figure 24 A) and the constructs transformed into the *phgap1 phgap2* mutants. These mutations in the PHGAP proteins resulted in loss of function for both PHGAP1 and PHGAP2. No complementation of the pavement cell defects could be obtained in a population were the transgene was segregating (Figure 24 B to E)

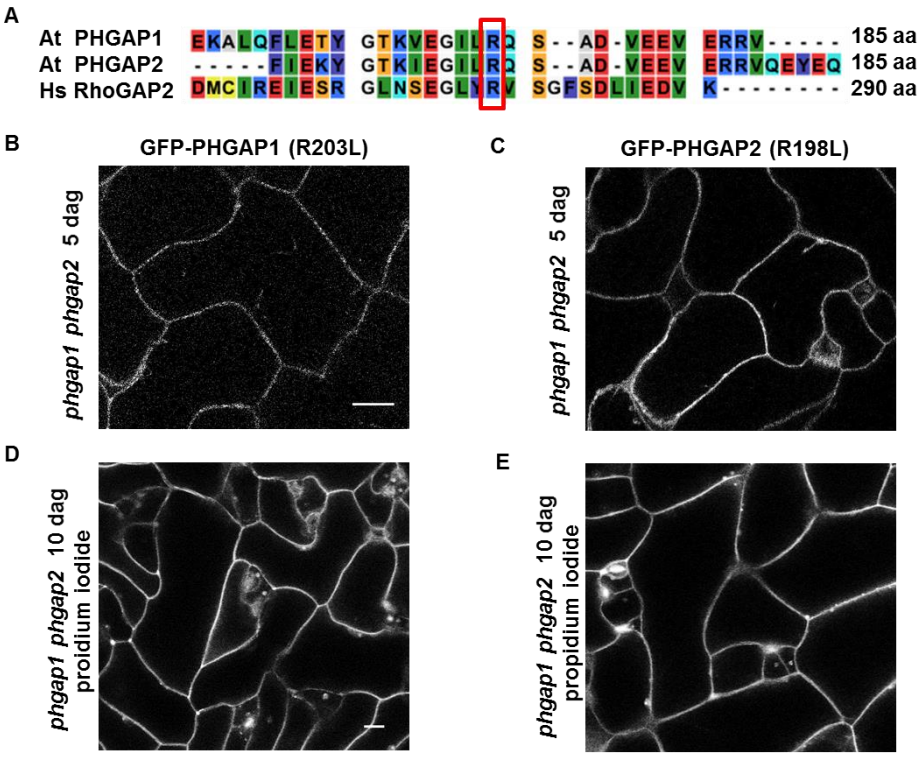

Figure 24: PHGAP1 and PHGAP2 functionality is mediated by a conserved arginin in the GAP domain. **(A)** Alignment of a subset of amino acid sequences contained in the GAP domain of the putative At ROPGAPs and Hs RhoGAP2. Mutation of the conserved arginin is indicated by the red box. **(B and C)** *pUBN*:GFP-PHGAP1-R203L and *pUBN*:GFP-PHGAP2-R198L protein expression in *phgap1 phgap2* mutants five days after germination (dag) in expanding pavement cells. **(D and E)** Observation of *pUBN*:GFP-PHGAP1-R203L and *pUBN*:GFP-PHGAP2-R198L protein expression in *phgap1 phgap2* mutants ten days after germination in fully expanded pavement cells. Cell walls are visualized by propidium iodide. Images were taken in cotyledons at confocal microscope. Bar 20 µm

5.6.11 Loss of function of the GAP domain does not influence the localization of PHGAP1 and PHGAP2 at the cortical division site

For determination, if the particular localization of PHGAP1 and PHGAP2 at the cortical division site is affected by the loss of GAP function, localization of GFP-PHGAP1-R203L and GFP-PHGAP2-R198L mutants was examined in in wild type plants. Both, GFP-PHGAP1-R203L and GFP-PHGAP2-R198L, were observed in a ring shaped manner in subset of epidermal root cells aside from the cytoplasmic localization in all cells of the root meristem (Figure 25 A and B). Thus, cortical division site localization does not depend on GAP activity, but most likely depends on interaction with POK1.

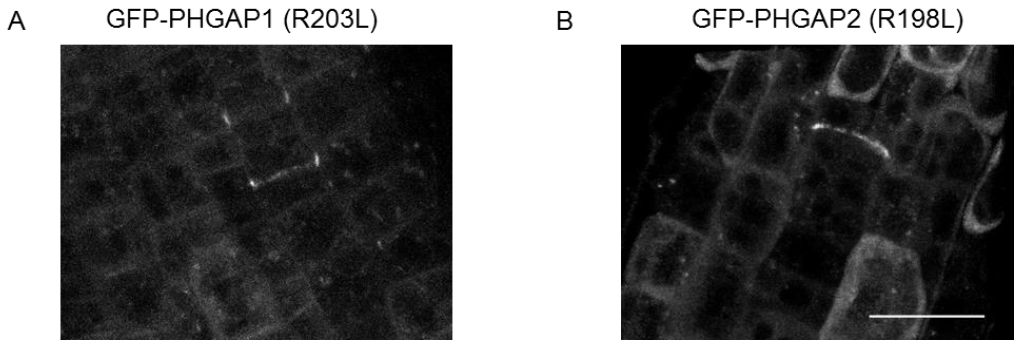

Figure 25: Localization pattern of *pUBN:*GFP-PHGAP1-R203L and *pUBN:*GFP-PHGAP2-R198L in root epidermal cells in the wild type background. Images are maximum projections of Z-stacks and were taken at the confocal microscope. Bar = 20 µm

5.7 PHGAP interaction studies

5.7.1 PHGAP2 interacts with several ROPs

For *in vivo* interaction studies between PHGAP2 and putative interacting ROPs, the ratiometric 2in1 BiFC system was used. The interactions were investigated in *A. thaliana* root protoplasts. As a control the confirmed and published interaction of REN1 and ROP1 was used and for ensuring that the interactions are not false positive TAN which is expressed in the cytoplasm as well as PHGAP2 were used as a negative control (Figure 26 E and F). Another approach for an adequate negative control, was the use of DNROP6 in combination with PHGAP2.

It could be shown that PHGAP2 can interact with ROP1, CA-ROP2, CA-ROP4, and CA-ROP6. Furthermore, the DN-ROP6 is still able to interact with PHGAP2, which was an unexpected result, since PHGAP should only interact with active ROPs. The interaction strength of PHGAP2 and DN-ROP6 was actually similar to the constitutive active form CA-ROP6 (Figure 26 A-D). Thus, it seems that PHGAPs may interact with several ROPs. This raises the question how specific PHGAP-ROP interactions might be achieved in the cell? The rBiFC system might not be the appropriate experimental setup to answer this question.

From previous studies it was known that POK1 can interact with PHGAP1 in Y2H, but this low abundant protein interaction could not replicated in the rBiFC studies, neither with POK1 nor with various putative ROP interactors. The protein expression of the potential interactors was extremely low so that measurement of these interactions was almost impossible. Nevertheless, the pavement cell phenotype only appears when both proteins, PHGAP1 and PHGAP2, were knocked down, suggesting that also PHGAP1 must regulate ROP activity.

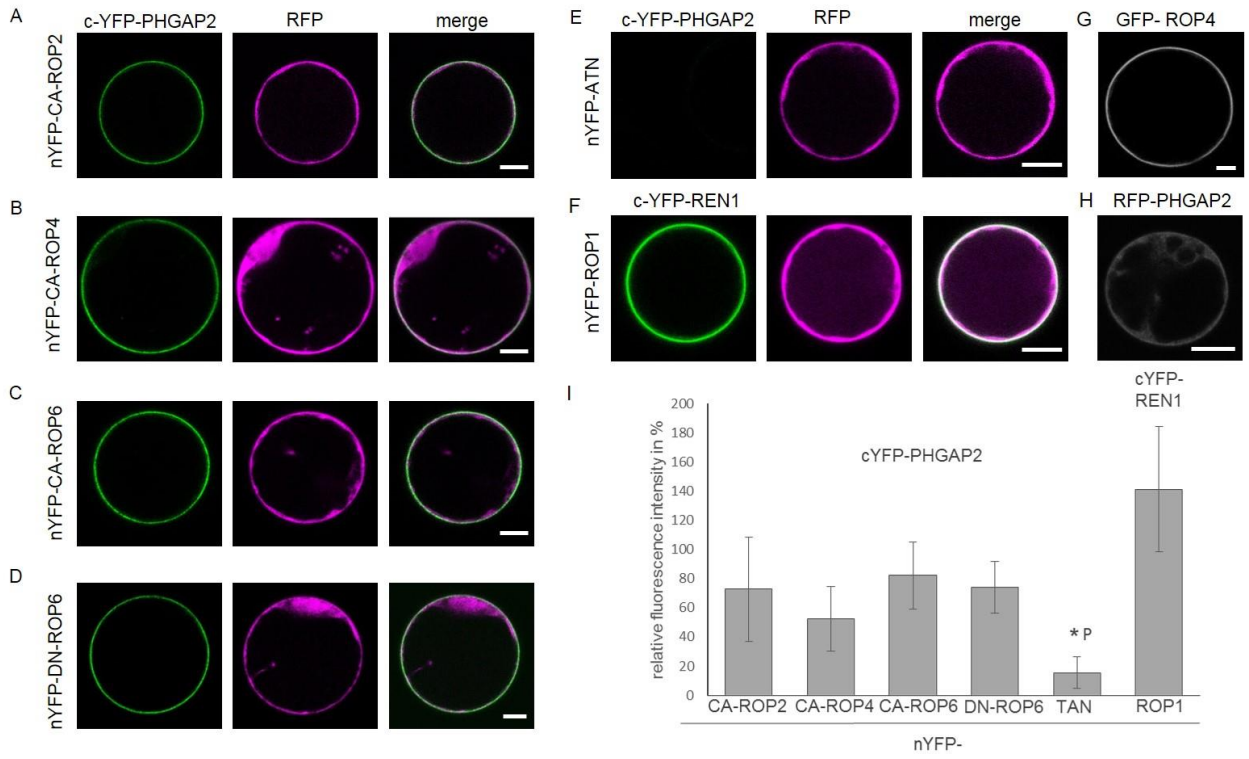

Figure 26: rBiFC interaction assay of PHGAP2 with potential interactors - ROP2, ROP4 and ROP6 expressed under the control of 35S promoter. Constitutive active forms of the eligible ROPs were used for interaction with PHGAP2. Confocal images of an *A. thaliana* protoplasts co-expressing (A) nYFP-carop2 and cYFP-PHGAP2, (B) nYFP-carop4 and cYFP-PHGAP2, (C) nYFP-carop6 and cYFP-PHGAP2, (D) nYFP-*dnrop6* and cYFP-PHGAP2, (E) nYFP-ROP1 and cYFP-REN1 as positive control or (F) non-interacting nYFP TAN and cYFP-PHGAP2 control. RFP, expressed from the same plasmid, was used as an internal control. **(G and H)** Expression of *Pro35S:*GFP-ROP4 representative localization pattern for all tested ROPs and *pro35S:*RFP-PHGAP2*.* Images are Z-projections of images stacks with z-intervals of 1 µm. Bar = 10 µm. **(I)** Quantification of the relative fluorescence intensity of the interaction partners and the control by using the YFP/RFP ratio. Data are means of n $\geq$ 34 protoplasts for each construct. Each protoplast represents an independent transformation event. The YFP/RFP ratio of the interacting partners differs significantly ($p < 0.0001$) from the non-interacting control TAN and PHGAP2.

5.8 Water homeostasis and water transport

5.8.1 Water homeostasis is altered in *phgap1 phgap2* mutants

In accordance to GTPase activity of ROP2 in pavement cell establishment, ROP2 plays a role in ABA- and CO_2-induced stomatal closure as described in Hwang et al, 2011. If the hypothesis is true that ROP2 was regulated by PHGAP1 and PHGAP2, an effect in water homeostasis in leaves should be observed. The first measurements of the fresh weight of the leaves, taken for the experiment did not show any differences. However, at the times T=2 h up to T=8 significant differences in weight between the wild type and the *phgap1 phgap2* mutant were noticed, which indicated that the double mutant lost more water in the same time period than the wild type control (Figure 27).

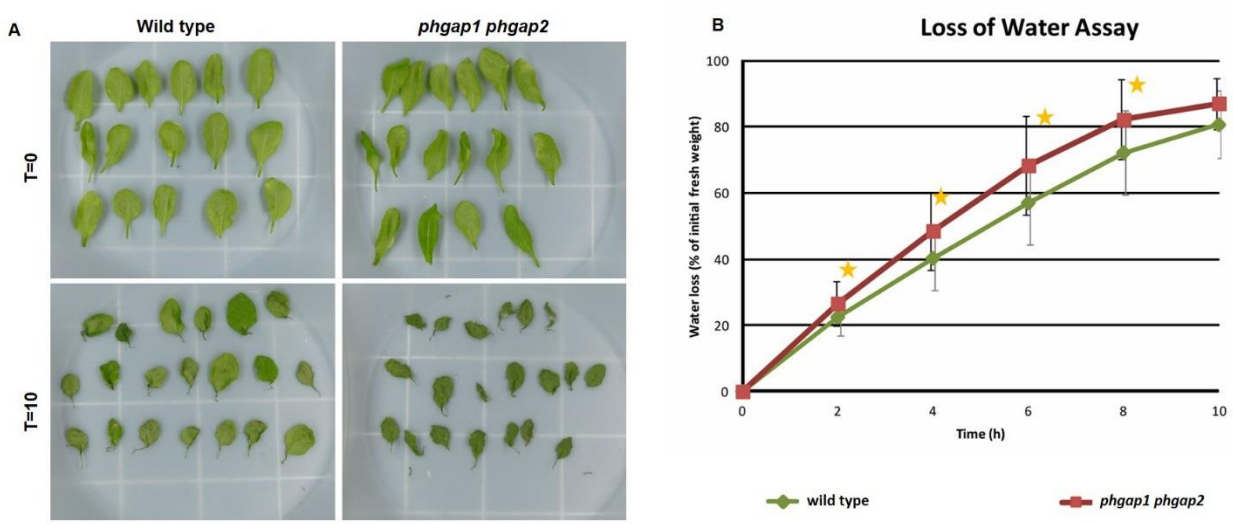

Figure 27: Comparison of water loss behavior between wild type and the *phgap1 phgap2* double mutant. **(A)** Four weeks old rosette leaves were dried at room temperature. At different time points 0, 2, 4, 6, 8, and ten hours the weight was determined. The relative water loss was blotted over time. **(B)** Graph shows relative water loss at displayed time points. Asterisks indicate significant differences.

5.8.2 Water transport is not influenced *phgap1 phgap2* mutants

Adult *phgap1 phgpap2* plants displayed a slight drought phenotype in comparison to the wild type which could be associated with the water loss indicated by the results of the previous water homeostasis experiments. Alternatively the *phgap1 phgpap2* mutants might have a defect in water uptake. That led to the investigation of the water uptake. Inflorescences from wild type and *phgap1 phgap2* mutants were placed into blue ink. After ~1 hour the ink reached the petals of the inflorescences of the wild type and the *phgap1 phgap2* mutants simultaneously, which reveals no defects in water uptake (Figure 28).

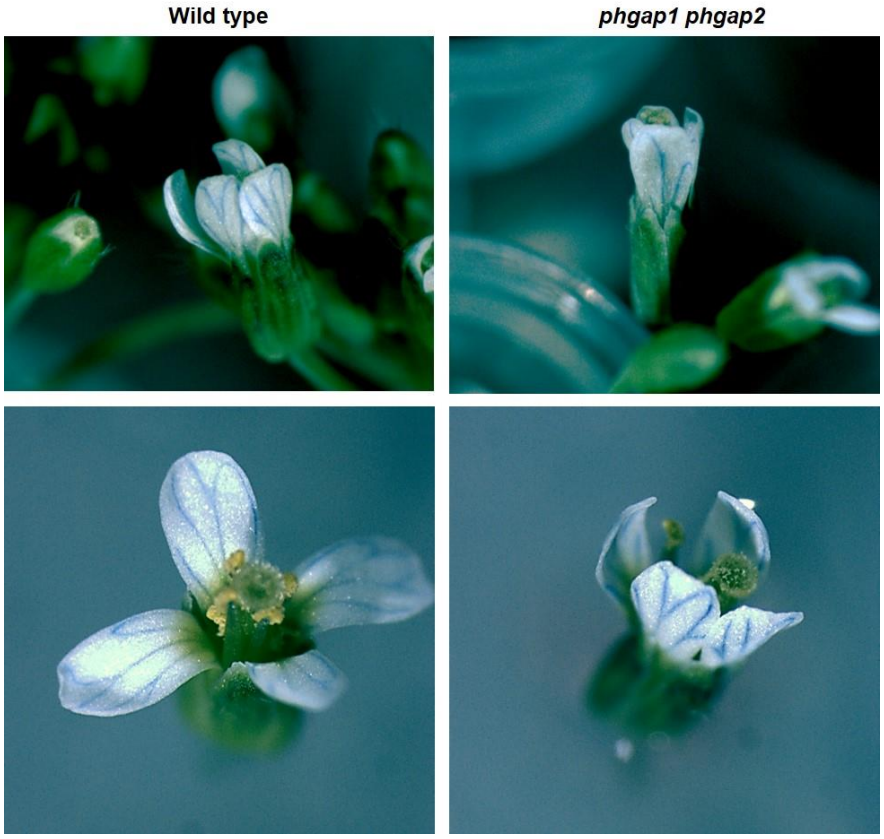

Figure 28: Comparison between wild type and *phgap1 phgap2* water conductance. The figure depicts blue ink uptake from 2 cm beneath cut inflorescences. The ink was soaked up for one hour. Images were taken at the binocula

6 Discussion

POK1 and POK2 are crucial for the maintenance of the cell division plane and the correct placement of the cell plate (Lipka et al., 2014). The interaction partners of POK1, PHGAP1 and PHGAP2, also seem to play a role in cytokinesis, but additionally they perform important functions in polar cell expansion as well. Co-expression of YFP-POK1 and RFP-PHGAP1 showed ring-shaped co-localization in cytokinetic root cells indicating their involvement in cell division. But how these PHGAP proteins are involved in this process and what is their importance is not well understood.

6.1 Contribution of PHGAPs to the cell division

While *pok1 pok2* double mutant phenotypes were mainly characterized in the root meristem of *A. thaliana*, investigation of *phgap1 phgap2* cytokinesis defects was not straight forward in roots. Root development was unaffected in *phgap1 phgap2* double mutants and neither cell division nor cell expansion defects have been observed in roots. This result is puzzling, given the interaction of POKs and PHGAPs in yeast two hybrid and BiFC experiments. However, gene expression patterns of *PHGAP1 and PHGAP2* in roots are complementary (Figure 9) and thereby double mutants do not show different phenotypes from *phgap* single mutants. Thus, other proteins must act redundantly with PHGAPs in the root. Indeed, members of the group of CRIB domain containing ROPGAPs are also expressed in the root, probably sharing redundant functions with PHGAPs (Figure 15). For tobacco it was proposed that transiently expressed tobacco RhoGAP1 is located in the pollen tube tip and acts as a lateral inhibitor to limit ROP GTPase activation (Klahre and Kost, 2006). Further investigations have shown that RhoGAP1 and REN1 act together in the polar pollen tube growth in *A. thaliana* (Hwang et al., 2010). Thus, generation of *phgap ropgap* mutants might reveal functional redundancy in cell division in the root meristem. In order to evade this issue of opposing

gene expression patterns and redundancy, embryo development was investigated to determine PHGAP function in cell division.

The importance of PHGAP1 and PHGAP2 function in cell division was confirmed during embryogenesis. In comparison to *pok1 pok2* double mutants (Muller et al., 2006), *phgap1 phgap2* mutants display mild cell division defects at low frequency in early embryo development. This could be due to the fact that *phgap1 phgap2* mutants are knock down mutants and residual PHGAP proteins might be present. However, recently a very similar embryo phenotype was observed in *rop3* knock out and dominant negative *DNrop3* mutants at low frequencies in *A. thaliana* (Huang et al., 2014). The authors suggested that ROP3 seems to play a role primarily during early embryo development while other ROPs might act later in embryo development. These findings also imply that ROP signaling pathways contribute to cell division in *A. thaliana* and are consistent with our findings on PHGAP function. In case of PHGAP1 and PHGAP2 it was proposed that the absence of these proteins mimic a constitutive active form of ROPs, leading to the conclusion that PHGAP1 and PHGAP2 most likely do not regulate ROP3. However, the *phgap1 phgap2* mutants seem to distort the balance of the ROP activity during early embryo development.

Rho GTPase function in cell division is well described in mammals. Twenty Rho GTPases are known and a large number of them is characterized (reviewed in(Heasman and Ridley, 2008). Rho GTPases play critical roles in the regulation of actin nucleation and organization in interphase and cell division. The RhoA GTPase and Cdc42 GTPase organize the assembly of the acto-myosin contractile ring and induce the acto-myosin-driven constriction of the cleavage furrow which separates the daughter cells (reviewed in(Etienne-Manneville and Hall, 2002; Barr and Gruneberg, 2007; Heng and Koh, 2010) .

Rho1 is localized in budding yeast and activated at the division area (Tolliday et al., 2002) and is necessary for secondary septum formation in late cytokinesis (Yoshida et al., 2009). However, in fission yeast it is not really known if Rho1 contributes to cytokinesis, but another member of the Rho GTPase family, the Rho4, was found localizing to the septum and seems to play a role in cytokinesis (Santos et al., 2003).

The first identified ROP-GTPase from *Pisum sativum*, named Rop1Ps, was located at the pollen tube tip which suggested involvement in cell expansion of the pollen tube. Overexpression of Rop1Ps and its *A. thaliana* orthologue Rop1At in fission yeast lead to isotropic growth. The GFP-Rop1At fusion protein localizes unpolar, bipolar and unipolar (Li et al., 1998) in yeast. In addition, Rop1Ps is localized at the septum suggesting that it might serve a conserved role in cytokinesis.

Since plants have no acto-myosin contractile ring owing to an alternative division mechanism, the question arises which function ROP GTPases fulfill in plant cell division. One example of ROP activity in asymmetric cell division is the polarization of subsidiary mother cells during stomata development in maize. In maize leaf epidermal cells of the stomata lineage, ROP2 and ROP9 activity is triggered by a leucine rich repeat receptors like kinase PANGLOSS (PAN) and participate in the reorganization of the cytoskeleton (Cartwright et al., 2009; Humphries et al., 2011). Stomata development is driven by asymmetrical cell divisions, which requires prior polarization of the cell. Subsidiary mother cells flank the guard mother cell. Subsequent formation of an actin patch at the contact site between subsidiary and guard mother cell directs nuclear migration. In *rop2/-pan/-rop9/*+ mutants, a high amount of subsidiary mother cells showed no or mis-located actin patches causing deformation of the subsidiary cells. This observation suggested that ROP GTPases actively participate in the regulation of actin organization in plant cell division (Humphries et al., 2011).

The role of actin in plant cell division is not essential. Mutations of actin genes or drug-induced depolymerization of actin leads to cell wall positioning defects but does not inhibit mitotic progression (Kojo et al., 2013). Similarly, mildly mis-oriented cell walls occur in *phgap1 phgap2* mutant embryos. Therefore, PHGAP1 and PHGAP2 might regulate ROP GTPases which in turn regulate actin organization in embryo development. Recently it was hypothesized, that F-actin might interact with microtubules via myosin VIII bridging the cell cortex and the phragmoplast in moss (Wu and Bezanilla, 2014). PHGAPs could be related to ROP regulation in this putative process. The appearance of fluorescent PHGAP fusion proteins at the CDS in dividing *A. thaliana* root cells supports the

hypothesis that PHGAPs are directly or indirectly involved in the regulation of actin organization by regulating ROP activity. Visualization of PHGAP1 and PHGAP2 during cell division using the advantages of *Tobacco* BY2 (Geelen and Inze, 2001) cells by co-expressing fluorescent fusion of an actin binding protein and interacting ROPs could be informative with respect to their regulating function. Alternatively, PHGAPs might down regulate the ROP activity in order to prevent microtubule bundling at the CDS, similar to the ROP-regulated mechanism of pavement cell shape establishment. Antagonistic ROP activities regulate actin nucleation and lobe formation, adjacent to the regions of microtubule bundling and neck formation (Fu et al., 2002; Fu et al., 2005; Fu et al., 2009; Lin et al., 2013) REF. Moreover, PHGAPs heavily decorate the cell plate after fusion with the parental cell wall (Figure 12 C). Notably, ROP4 involved in lobe formation of pavement cells was also found at the cell plate in tobacco BY-2 cells (Molendijk et al., 2001) although the relevance of this localization pattern is not clear. Taken together, these observations suggest that PHGAPs regulate ROP to limit F-actin filament network initiation.

6.2 Participation of PHGAPs in reproduction

Observations of *phgap1 phgap2* mutant siliques showed significant reduction of the number of fertilized ovules, which implies that loss of PHGAP1 and PHGAP2 might cause meiotic defects. Analysis of *phgap1 phgap2* mutants showed severely reduced transmission through the male gametophyte suggesting defects in male gametophyte development (Table 2). However, *phgap1 phgap2* mutant pollen displayed normal pollen tube growth *in vitro*.

Gene expression analysis revealed that both, *PHGAP1* and *PHGAP2*, are expressed in the female gametophyte (Figure 9). A recent publication showed that ROP signaling is

apparently involved in the actin regulation in the female gametophyte. The authors suggested that dominant negative ROP8 causes extremely reduced F-actin movement similar to a specific mutation in ACTIN (ACT8), which disrupt the F-actin in the female gametophyte preventing fusion of the sperm cell with the egg cell (Kawashima et al., 2014). The assumption that the absence of PHGAP1 and PHGAP2 mimics constitutive active ROPs implies that they might regulate not yet identified ROPs in this process, although related phenotype was observed in *phgap1 phgap2* mutants. Additional investigations are necessary regarding PHGAP activity in the reproduction process, in particularly functional redundancies need to be resolved.

6.3 The role of PHGAPs in cell expansion and shape formation

PHGAP gene expression analysis indicated that PHGAP1 and PHGAP2 might play a role in the development of young leaves (Figure 9). *phgap1 phgap2* double mutants displayed mild macroscopic defects in the first leaves and later in the rosette stage (Figure 21 A and B) which might indicate defects on the cellular level. Pavement cell shape defects in *phgap1 phgap2* mutants (Figure 21 D) showed clearly that PHGAP1 and PHGAP2 act together in pavement cell shape establishment since *phgap* single mutants did not display pavement cell defects. Furthermore, the cellular pavement cell expansion defects in *phgap1 phgap2* mutants were reminiscent of constitutively active ROP mutants (Fu et al., 2002; Fu et al., 2005; Sorek et al., 2010; Poraty-Gavra et al., 2013; Wu et al., 2013). ROP-GTPase signaling, a well characterized molecular pathway, is required for normal pavement cell shape establishment. Early findings reported that ROP2 signaling controls F-actin network organization in pavement cells (Fu et al., 2002) suggesting a functional conservation of this specific signaling pathway. In mammals, Rho/RAC GTPase signaling is also required for cell polarity establishment and actin network organization in lammelipodia and filopodia (reviewed in(Heasman and Ridley, 2008).

Further, studies showed that ROP6 was also involved in polarity establishment in pavement cells. ROP6 was found as an antagonist of ROP2 and induces microtubule

bundling. Both, ROP2 and ROP6, are necessary for normal pavement cells development (Fu et al., 2005). Dominant negative (GDP-locked) as well as constitutively active (GTP-locked) ROP2 or ROP6 mutants lead to pavement cell shape alterations. Dominant negative ROP2 and dominant negative ROP6 still display pavement cells with mild lobes while constitutive active ROP2 and constitutive active ROP6 exhibit more rectangular shapes (Fu et al., 2002; Poraty-Gavra et al., 2013). To our knowledge, nothing is known about negative a regulation of ROPs in pavement cell shape establishment. However, *phgap1 phgap2* mutants are reminiscent of the constitutively active form of ROP2 and also the constitutive active form of ROP6, further supporting the notion that PHGAPs are necessary to balance ROP activity. In support of this idea, mutations of the conserved arginine within the GAP domain of PHGAP1 (R198L) and PHGAP2 (R203L) (Hwang et al., 2008) did not rescue the *phgap1 phgap2* mutant phenotype (Figure 24). Furthermore, the localization of *pUBN*:GFP-cPHGAP1 (R198L) and *pUBN*:GFP-cPHGAP2 (R203L) is not altered compared to non-mutated fluorescent protein fusions suggesting that the activity of the GAP domain is not necessary for the localization neither in developing pavement cells nor at the cortical division site in dividing cells (Figure 26).

One important question concerning PHGAP protein function in pavement cell shape establishment is, which ROPs are regulated by the PHGAP proteins. Obvious candidates were ROP2, ROP4 and ROP6. By using ratiometric bimolecular fluorescence complementation (rBIFC) the interaction between PHGAP2 and CA-ROP2, CA-ROP4 and CA-ROP6 could be shown (Figure 27). However, it is unlikely that ROP2, ROP4 and ROP6 are regulated by the same PHGAP proteins in the same cell at the same time. Thus, it seems that PHGAP2 is able to bind ROPs non-specifically and specific interactions are achieved by spatio-temporal regulation. This is also supported by the comparatively high relative interaction ration between PHGAP2 and pollen-specific ROP1 in rBiFC experiments (Figure 26). This result is somewhat surprising since the expression of PHGAP2 in pollen tubes, did not complement the *ren1-4* pollen tube growth defect. Thus, the experiment might be repeated with the pollen-specific *pLAT52* promoter or the *REN1* promoter.

Unexpectedly, interaction was not detectable between PHGAP1 and the candidate ROPs using rBiFC experiments. This is surprising, because PHGAP1 was predicted to interact with one of the ROPs involved in pavement cell shape establishment with respect to the *phgap1 phgap2* mutant pavements cells phenotypes. A possible explanation for this negative results, would be a weak interaction which cannot be sufficiently be detected/stabilized in the rBiFC experiments. Thus, a strategy to enrich the binding partners might be required before future experimentation. In general Co-Immunoprecipitation would be a useful tool, if the protein detection can optimized for the low abundant proteins PHGAP1 and PHGAP2. Furthermore, genetic studies might be useful in support of interaction studies. The generation of *phgap1 phgap2 rop* triple mutants might be insightful about possible interactions. Investigations of *phgap1 phgap2* mutants expressing GFP-ROP6 should be informative regarding alterations in GFP-ROP6 localization and may provide a further evidence for PHGAP ROP6 interaction. Preliminary but yet unconfirmed data of membrane fractionation of 6 days old seedlings suggest, that in phgap1 phgap2 mutants, GFP-ROP6 remains bound to the plasma membrane in its active state, suggesting that PHGAPs indeed regulate ROP6. However, this finding has to be further examined.

6.4 PHGAPs role in the water homeostasis

Observations that *phgap1 phgap2* double mutants show a higher water loss than wild type indicate that PHGAP1 and PHGAP2 might be involved in stomata closure by regulating ROP activity (Figure 28). Indeed, besides its role in actin network organization during pavement cell development, ROP2 has a supportive function in stomata opening and closure. It is suggested that stomata opening and closure is driven by different physiological stimuli (Jeon et al., 2008; Hwang et al., 2011). ROP2 activation in guard cells is light induced. Hence, ROP2 negatively regulates light induced stomata opening (Jeon et al., 2008). Furthermore, ROP2 activity is involved in stomata closure in response to abscisic acid (ABA) signaling and CO_2. ABA-treated guard cells of *V. faba* showed a translocation of a GFP-ROP2 from the plasma membrane to the cytoplasm suggesting

that ABA-treatment influences ROP2 activity. Expression of constitutive active ROP2 in *A. thaliana,* as well as in *Vicia faba*, result in reduced stomata closing whereas dominant negative ROP2 and ROP2 knockout mutants promote the closure of the stomata (Hwang et al., 2011).

If PHGAP1 and PHGAP2 are indeed involved in ROP2 regulation; ROP2 would be constitutively active in *phpgap1 phgap2* mutants preventing efficient stomata closing (Hwang et al., 2011). Alternatively, it is also possible that due to the loss of pavement cell shape complexity, accompanied with less ordered microtubules in the *phgap1 phgap2* double mutants (Figure 22), the mechanical stress pattern is altered in the epidermal tissue (Sampathkumar et al., 2014) causing dysregulation of the turgor in stomata which could result in longer opening. At the moment these two possibilities for increased water loss in *phgap1 phgap2* mutants, either constitutive activation of ROP2 or altered mechanical stress, cannot be distinguished.

PHGAP2 is specifically expressed in the root vasculature of seedlings but does not seem to regulate ROP activity there; alternatively redundancy is masking PHGAP2 function in this tissue. One of the ROPs, *ROP7*, is specifically expressed during late xylem differentiation but both, *rop7* knock out and constitutive active *rop*7 mutants, did not display a phenotype in the xylem (Brembu et al., 2005). The authors suggested functional redundancy in xylem. Interestingly they observed alteration of pavement cells in constitutive active *rop7* mutants, indicating that ROP7 is also involved in cell polarity establishment of pavement cells. However, our results on the water transport using a simple water uptake experiment indicated that water transport is not influenced by PHGAPs (Figure 29), but it would be interesting to test if ROP7 is regulated by PHGAP1 and PHGAP2 during pavement cell establishment.

6.5 Filling the (PH) GAPs - Future studies and theoretical model

The mechanism of PHGAP association with the plasma membrane is unknown. During cell division it is likely that POK1 recruits PHGAP1 and PHGAP2 to the cortical division site since POK1 is already present before PHGAPs. Thus the interaction with specific domains of POK1 might be responsible for PHGAP localization at the cortical division site.

The combination of all findings and putative possibilities leads to a theoretical model. The functions of PHGAP1 and PHGAP2 in regulating ROP activity are spatio-temporally controlled. PHGAP1 and PHGAP2 have a supportive, non-essential function in cell division. One mode of action could contribute to the fine tuning of late cytokinetic events at the cortical division site, most likely affecting the F-actin organization via regulation of ROP activity. PHGAP1 and PHGAP2 localize to the cortical division site and localize to the cell plate after cell plate fusion with the parental plasma membrane. There, prevention of the induction of F-actin network would be likely and could regulate ROP4 that was observed at the cell plate (Figure 30).

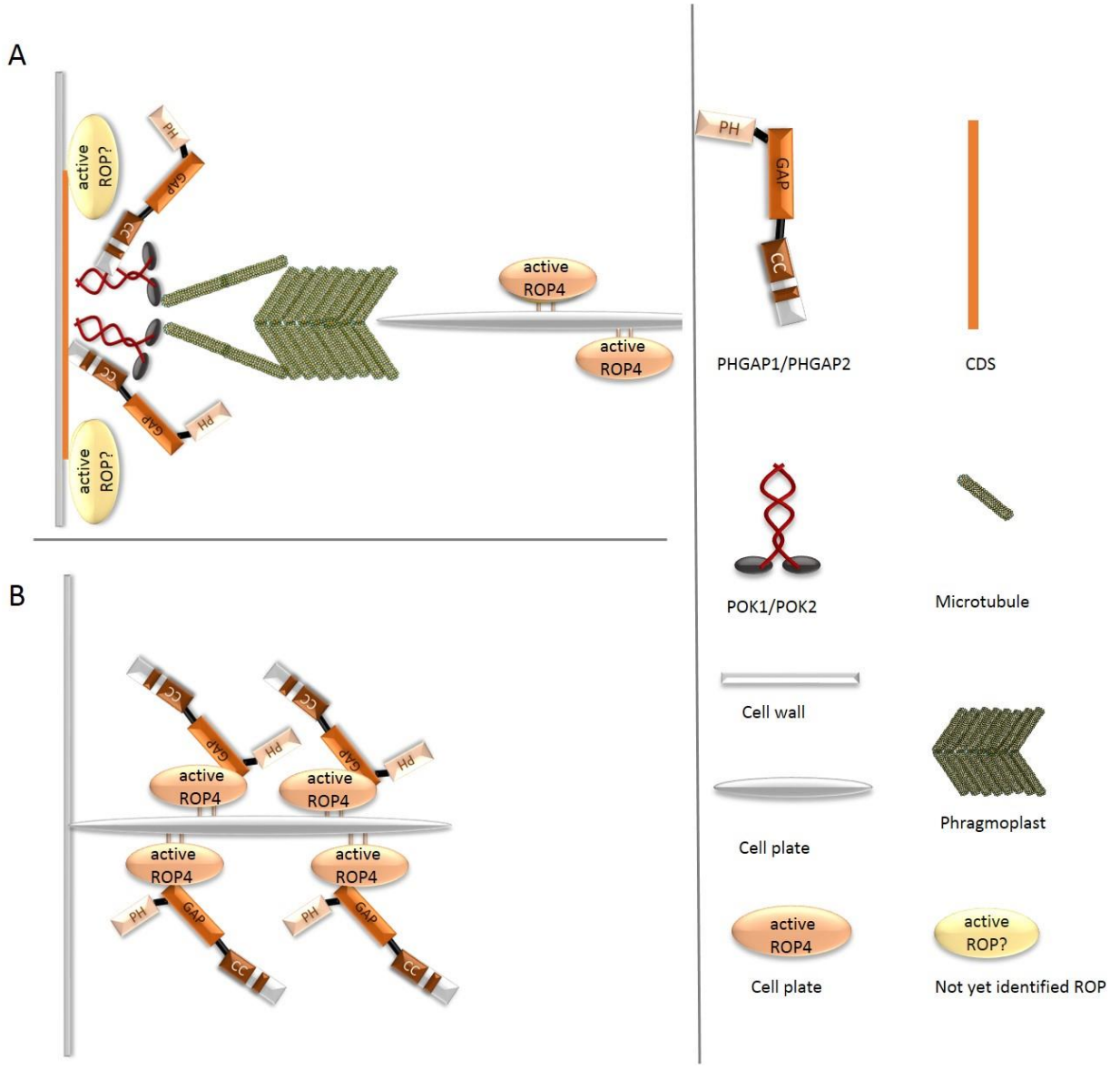

Figure 29: Hypothetical model of PHGAP function in cell division. **(A)** POK recruits cytoplasmic PHGAP via C-terminal interaction to the cortical division site. At this position PHGAPs inactivate a ROP via stimulating its intrinsic GTPase activity, preventing new actin filament network to induction facilitate preparation for the future cell plate fusion with the parental cell wall. At the same time POK1 gets immobilized at the cortical division zone and pulls arriving phragmoplast microtubules to induce fusion with the cell plate. **(B)** If the cell plate is finally attached to the parental cell wall, PHGAPs will localize to the cell plate to inactivate ROP4, which is proposed to regulate actin filament network at the cell plate. Then the PHGAPs dissociate back to cytosol.

During interphase, PHGAPs must be recruited to the sites of ROP activity. One option for plasma membrane association would be via the PH domains and their likely ability to bind to phospholipids (reviewed in(van Leeuwen et al., 2004). Furthermore, it would be possible that PHGAP1 and PHGAP2 migrate to the site of action via vesicle transport as shown for REN1. REN1 interacts with vesicles relying on the C-terminal coiled coil domain (Hwang et al., 2008). In order to investigate the contribution of protein domains to the localization and function of PHGAPs, deletion constructs of the PH domain as well as the coiled coil domain of PHGAP1 and PHGAP2 were created and transformed in *phgap1*/+ *phgap2*/+, but it still needs time to identify plants with homozygous transgenes in the different genetic backgrounds.

A third, so far utterly unexplored possibility regarding the plasma membrane recruitment of PHGAPs would involve 14-3-3 proteins. Plant 14-3-3 proteins are phosphoserine-binding proteins (Yaffe and Elia, 2001; Denison et al., 2011). It is suggested from the plant and the animal field that they can act as a shuttle (Benzing et al., 2000; Klahre and Kost, 2006; Mucha et al., 2011). Recently identified 14-3-3 binding motives for both PHGAP1 and PHGAP2 could be another possibility for PHGAP recruitment. Therefore, interaction studies would be necessary.

Furthermore, PHGAP function in pavement cells is well supported, but the underlying mechanism as well as their putative ROP interaction partners are not identified unequivocally. I propose that ROP2/4 and ROP6 are regulated by both, PHGAP1 and PHGAP2, and the recruiting mechanism of PHGAP1 and PHGAP2 to the plasma membrane could be a combination of PH-domain mediated binding to phosphoinositides and 14-3-3 protein supported shuttling to the plasma membrane (Figure 31).

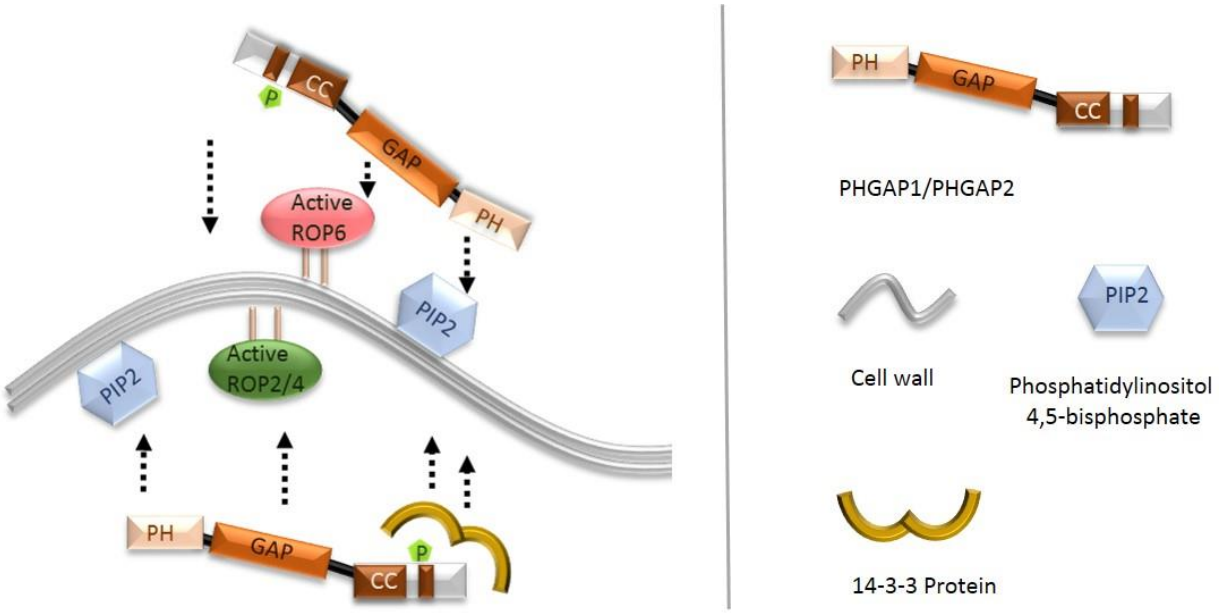

Figure 30: Putative recruitment mechanisms of PHGPAPs to ROPs in pavement cell establishment. Due to PHGPAPs domain structure different recruitment strategies are possible. The Pleckstrin Homology (PH) domain is known for its ability to interact with phosphoinositides. This could be responsible for membrane association and physical interaction with active (GTP-bound) ROPs. A further possibility is that PHGPAPs are recruited via14-3-3 protein shuttling, since PHGPs have a recognition motive for 14-3-3 binding. Of course, both mechanisms could act together as a kind of two component system.

7 Appendices

7.1 Oligonucleotides and primers used for cloning

PH-GAP1 ATG_F	GGTACCATGGAGGCTTCTCTAGCTGTTA
PH-GAP1 Stop_R	GCGGCCGCCTAATTCCATGGTGGAGAAGA
PH-GAP2-ATG_F	GGATCCATGGAGGCTTCTTTAGCGGCTTT
PH-GAP2 Stop_R	GCGGCCGCTTAGTTCCAAGGTGGAGATGAT
PH-GAP1 1.5 kb pro_F	CTGCAGAGAGACGGAAGTGAGTTGCTGACTT
PH-GAP1 1.5 kb pro_R	CTGCAGTGCAGAAGTACACACTTAATC
proPHGAP2_Not_R	GCGGCCGCTGCCTCAACAGCATAATCTCCAGAT
proPHGAP2-2R	CTGCAGAAAGAAGCCTCCATTGCCTCAACA
PHGAP1 R203L_F	AGGGATATTACTGCAGTCTGCTGAT
PHGAP1 R203L_R	ATCAGCAGACTGCAGTAATATCCCT
PHGAP2 R198L_F	AGGAATTTTACTGCAGTCTGCAGATGT
PHGAP2 R198L_R	ACATCTGCAGACTGCAGTAAAATTCCT
ROP2/ROP4 G15V_F	TCGGAGATGTTGCCGTCGGAAA
ROP2/ROP4 G15V_R	TTTCCGACGGCAACATCTCCGA
attB3 POK1C-short _F	GGGGACAACTTTGTATAATAAAGTTGTAATGGATGAAGAAGT AAAAAGGCATCGT
attB2 POK1C-short_R	GGGGACCACTTTGTACAAGAAAGCTGGGTTTTACCGATATCT TGTACCAGAGCT
attB3 TAN1_F	GGGGACAACTTTGTATAATAAAGTTGTAATGGTTGCAAGAAC CCCACAGAAGCA
attB2 TAN1_R	GGGGACCACTTTGTACAAGAAAGCTGGGTTCTACACTTTCCT GCTCTTCATTGGA
attB1 TAN1_F	GGGGACAAGTTTGTACAAAAAAGCAGGCTTAATGGTTGCAAG AACCCCACAGAAGCA
attB4 TAN1_R	GGGGACAACTTTGTATAGAAAAGTTGGGTGCTACACTTTCCT GCTCTTCATTGGA
attB3 ROP1 _F	GGGGACCACTTTGTACAAGAAAGCTGGGTTTCATAGAATGGA GCATGCCTTCT
attB2 ROP1_R	GGGGACAACTTTGTATAATAAAGTTGTAATGAGCGCTTCGAG GTTCGTAA
attB3 ROP4_F	GGGGACAACTTTGTATAATAAAGTTGTAATGAGTGCTTCGAG GTTTATAAAGTGT
attB2 ROP4_R	GGGGACCACTTTGTACAAGAAAGCTGGGTTTCACAAGAACAC GCAGCGGTTCTT
attB3 ROP2_F	GGGGACAACTTTGTATAATAAAGTTGTAATGGCGTCAAGGTT TATAAAGTGT
attB2 ROP2_R	GGGGACCACTTTGTACAAGAAAGCTGGGTTTCACAAGAACGC GCAACGGTTCTT
attB3 ROP6_F	GGGGACAACTTTGTATAATAAAGTTGTAATGAGTGCTTCAAG GTTTATCAAGT
attB2 ROP6_R	GGGGACCACTTTGTACAAGAAAGCTGGGTTTCAGAGTATAGA ACAACCTTTCTG
attB1 PHGAP1_F	GGGGACAAGTTTGTACAAAAAAGCAGGCTTAATGGAGGCTTC TCTAGCTGTTATA

attB4 PHGAP1_R	GGGGACAACTTTGTATAGAAAAGTTGGGTGCTAATTCCATGG TGGAGAAGAGGAT
attB1 PHGAP2_F	GGGGACAAGTTTGTACAAAAAAGCAGGCTTAATGGAGGCTTC TTTAGCGGCTTT
attB4 PHGAP2_R	GGGGACAACTTTGTATAGAAAAGTTGGGTGTTAGTTCCAAGG TGGAGATGATG
attB1 REN1_F	GGGGACAAGTTTGTACAAAAAAGCAGGCTTAATGGCTAACAA AAACGCAGAATCA
attB4 REN1_R	GGGGCACTTTGTATAGAAAAGTTGGGTGTCATCTGGAGAAGG TCCTTGGTG

7.2 Oligonucleotides and primers used for genotyping

PHGAP1_ATG_F	GGTACCATGGAGGCTTCTCTAGCTGTTA
PHGAP1_EcoRI-R	TCTTCAGGACTGAATTCTGTCTT
L4	TGATCCATGTAGATTTCCCGGACATGAAG
PHGAP2_01F	TCCGGAACCTAATAGACGTCTAC
PHGAP2_ATG_F	GGATCCATGGAGGCTTCTTTAGCGGCTTT
PHGAP2_03R,	GGATCCATGGAGGCTTCTTTAGCGGCTTT
LBa1	TGGTTCACGTAGTGGGCCATCG
PH-GAP1_EcoR1-F	AGGCAAGACAGAATTCAGTCCTGAA
PH-GAP1 1506_R	TACTGGGAGTAACTGAGGGTATA
LBDs-Lox	AACGTCCGCAATGTGTTATTAAGTTGTC
PHGAP2 02_R	ATCTGCTCTCCAGCTTGTTGAT
PHGAP-g4913_F	TGCTGAAGCTGATGTCGCAAGGT
PHGAP1-01_R	ATACAGAGGCTCGAGCACATG
PHGPAP1-p954_F	ACTCTTATGTACACTACATCTA
REN1-02_F	TTGTAGAGGTCTCGACAAGTGA
REN1-03-R	AGCTACCTCTTGCAGATCTT

7.3 Publication

Title: The phragmoplast-orienting kinesin-12 class proteins translate the positional information of the preprophase band to establish the cortical division zone in Arabidopsis

Elisabeth Lipka[1], Astrid Gadeyne[2,3], Dorothee Stöckle[1], Steffi Zimmermann[1], Geert De Jaeger[2,3], David W. Ehrhardt[4], Viktor Kirik[5], Daniel Van Damme[2,3], Sabine Müller[1]*

[1] Center for Plant Molecular Biology, ZMBP, Developmental Genetics, University of Tübingen, 72076 Tübingen, Germany
[2] Department of Plant Systems Biology, VIB, Technologiepark 927, B-9052 Gent, Belgium
[3] Department of Plant Biotechnology and Bioinformatics, Ghent University, B-9052 Gent, Belgium
[4] Department of Plant Biology, Carnegie Institution for Science, Stanford, California 94305, USA
[5] School of Biological Sciences, Illinois State University, Normal, Illinois 61790, USA

Running title: Kinesin dependent phragmoplast guidance

* Corresponding author: Sabine Müller
Center for Plant Molecular Biology, ZMBP
Developmental Genetics
University of Tübingen
Auf der Morgenstelle 32
72076 Tübingen, Germany

13 pages

The author responsible for distribution of materials integral to the findings presented in this article in accordance with the policy described in the Instructions for Authors (www.plantcell.org) is: Sabine Müller (sabine.mueller@zmbp.uni-tuebingen.de)

Synopsis: Kinesin-12 class motor proteins at the cortical division site maintain cortical division site identity proteins for efficient guidance of the phragmoplast in late cytokinesis.

Abstract

The preprophase band (PPB) is a faithful but transient predictor of the division plane in somatic cell divisions. Throughout mitosis the PPBs positional information is preserved by factors that continuously mark the division plane at the cell cortex, the cortical division zone (CDZ), by their distinct spatio-temporal localization patterns. However, the mechanism maintaining these identity factors at the plasma membrane after PPB disassembly remain obscure.

The pair of kinesin-12 class proteins PHRAGMOPLAST ORIENTING KINESIN (POK) 1 and POK2 are key players in division plane maintenance. Here we show that POK1 is continuously present at the cell cortex, providing a spatial reference for the site formerly occupied by the PPB. FRAP analysis combined with microtubule-destabilization revealed dynamic microtubule-dependent recruitment of POK1 to the PPB during prophase, while POK1 retention at the cortical division zone in the absence of cortical microtubules appeared static.

POK function is strictly required to maintain the division plane identity factor TANGLED (TAN) post PPB disassembly, although POK1 and TAN recruitment to the PPB occur independently during prophase. Together our data suggest that POKs represent fundamental early anchoring components of the cortical division zone, translating and preserving the positional information of the PPB by maintaining downstream identity markers.

Introduction

The plant microtubule (MT) cytoskeleton demonstrates remarkable plasticity in its ability to form complex arrays characteristic of distinct cell cycle phases and required for specific cellular functions. In expanding interphase cells, parallel aligned cortical MTs guide cellulose synthase complexes along transverse trajectories and permit cell expansion in a perpendicular direction (Paredez et al., 2006). Furthermore, vascular plants developed a specialized cytoskeletal array aiding the correct positional execution of cytokinesis. Entry into mitosis is characterized by the preprophase band (PPB) (Pickett-Heaps and Northcote, 1966), an equatorial assembly of actin filaments and cortical MTs shaped by differential modulation of MT dynamic instability and selective MT stabilization in distinct regions of the cell cortex (Dhonukshe and Gadella, 2003; Vos et al., 2004). PPB formation requires the enzymatic action of a PP2A phosphatase holo-enzyme complex containing FASS as a regulatory B subunit, complexed with the helper/assembly proteins TON1a and b, which is targeted to the MTs via the Tonneau Recruitment Motif (TRM) proteins (Spinner & Gadyne et al., 2013). However, the PPB persists only transiently until pro-metaphase when its disassembly fuels the polymerization of spindle MT. After chromosome segregation and the subsequent condensation of daughter nuclei, the cytokinetic phragmoplast, a dual array of parallel-oriented MTs connecting at the cell division plane, evolves from the anaphase spindle remnants and assists in the synthesis of the cell plate, a *de novo* established membrane compartment generated by transport and fusion of endomembrane derived vesicles to the division plane, to bisect the daughter cells. The cell plate grows centrifugally and physically separates the daughter nuclei upon fusion with the plasma membrane at the end of plant cytokinesis. Intriguingly, the PPB anticipates the site of fusion between the cell plate and the parental cell wall despite the considerable time lag between the PPB's disassembly at pro-metaphase and the end of cytokinesis when the position of the PPB is converted into the actual cell plate position (Gunning and Wick, 1985).

The correlation between PPB position and the site of cell plate fusion led to the hypothesis that the PPB determines the plane of cell division and recruits molecules that serve as positional information to establish and maintain the cortical division zone (CDZ) identity

throughout mitosis (reviewed in Rasmussen et al., 2013). However, the first proteins described to serve as a reference beyond PPB disassembly were negative markers such as F-actin (Mineyuki and Palevitz, 1990; Cleary et al., 1992) and later the *Arabidopsis* kinesin-14 KCA1, both characterized by their low protein abundance or deficiency at the CDZ (Sano et al., 2005, Vanstraelen et al., 2006). In *Arabidopsis* the microtubule binding protein TANGLED (TAN) and the Ran GTPase regulatory protein RanGAP1 both co-localized with the PPB and remained at the CDZ throughout mitosis (Walker et al., 2007; Xu et al., 2008). During the course of mitosis the CDZ seems to alter from an initially wide zone (the cortical division zone, CDZ) to a narrow site (cortical division site, CDS) at the end of cytokinesis (Van Damme, 2009). The initial recruitment of both TAN and RanGAP1 to the cell cortex requires PPB formation (Walker et al., 2007; Xu et al., 2008), whereas TAN residency at the CDZ/CDS post PPB disassembly does not require MTs (Walker et al., 2007). In *Arabidopsis*, both TAN and RanGAP1 maintenance at the CDZ is abolished in a mutant background lacking a pair of kinesin-12 proteins, PHRAGMOPLAST ORIENTING KINESIN (POK) 1 and 2 (Walker et al., 2007; Xu et al., 2008). *Arabidopsis pok1 pok2* double mutants display severe cell wall positioning defects, reminiscent of the *Zea mays* (maize) *tan1* phenotype (Smith et al., 1996). The majority of phragmoplasts in the *pok1 pok2* double mutant do not correspond to a transverse orientation relative to the cell longitudinal axis, while PPBs were predominantly transverse with respect to the long axis of the cell supporting a role of POKs in the spatial control of cytokinesis (Muller et al., 2006). TAN and RanGAP1 have been shown to interact with the C-terminal domain of POK1 (Muller et al., 2006, Xu et al., 2008), suggesting that POK1, TAN and RanGAP1 are part of a functional module required for CDZ identity maintenance. The exact nature of this module remains however unclear due to the lack of positional information on the POK kinesins.

Here we provide novel insight into POK function by characterizing a novel *pok2* allele from a mutant screen for *pok1-1* enhancers. *In vivo* observations of the novel allele combination *pok1-1 pok2-3* revealed lengthy cytokinesis due to a reduced rate of phragmoplast expansion and frequent tilting of late phragmoplasts from their initial orientation. Nevertheless, fusion of the cell plate with the parental wall occurred at seemingly indiscriminate sites resulting in a highly dis-organized framework of cell walls,

underpinning POKs role in an efficient phragmoplast guidance mechanism and the timely progression through cytokinesis.

Localization studies using a functional YFP-POK1 fusion protein showed that POK1 is recruited to the PPB and remains at the cortex throughout mitosis. Similar to TAN, POK1 initially marks the CDZ and its localization domain narrows down to the CDS prior to cell plate fusion with the parental plasma membrane. POK1 is progressively and dynamically loaded onto the PPB from the cytosol in prophase while its association with the plasma membrane at the CDZ following PPB degradation appears static. Throughout telophase, the ring-shaped localization narrows from an initial broad band to a sharp string like pattern that disappears shortly after cell plate fusion. In *pok1 pok2* mutants, the cortical division zone marker TAN disappeared from the CDZ upon entry into metaphase, emphasizing that the POK kinesins function as molecular anchors for other CDZ/CDS identity markers.

Results

POK1 and POK2 are required for guidance of the phragmoplast toward the cortical division site

Previously, we described two independent *pok1 pok2* double mutant allele combinations, with similar phenotypic defects differing predominantly in their growth rate (Müller et al., 2006). In a sensitized EMS-induced mutant screen to identify second site mutations in phenotypically wild-type looking *pok1-1* single mutants, we discovered a severe mutant reminiscent of previously characterized *pok1 pok2* double mutants. The novel mutant co-segregated with the *pok1-1* genotype (Supplemental Figure 1A, B online) and did not complement the *pok1 pok2* double mutant phenotype in test-crosses, suggesting that the mutation was located in *POK2*. Sequencing of *POK2* revealed a C to T substitution in exon 16, 2197 bp of the coding sequence downstream of the ATG (Figure 1A). The mutation resulted in a premature STOP codon predicted to obliterate about three quarters of the POK2 protein. The allele was designated *pok2-3*. Due to the close linkage of *POK1* and *POK2* on chromosome III, *pok2-3* single mutants were not accessible for analysis.

Overall, the *pok1-1 pok2-3* double mutant displayed an aggravated phenotype compared to the previously described allele combinations *pok1-1 pok2-1* and *pok1-2 pok2-2* (Supplemental Figure 1 A online, Müller et al., 2006). We reasoned that POK activity was further diminished in these plants and thus the novel mutant was used to expand on the *in vivo* characterization of POK function. The *pok1-1 pok2-3* seedlings displayed shorter and wider roots and hypocotyls and succulent leaves (Figure 1B and D). Mature plants were dwarfed similar to weak *ton2* alleles (Kirik et al., 2012; Spinner & Gadeyne et al., 2013), but in contrast to *ton2*, *pok1-1 pok2-3* mutants were fertile (Supplemental Figure 1A online). Double *pok1-1 pok2-3* mutants grew significantly shorter roots (Figure 1C) and displayed smaller leaves than *pok1-1 pok2-1* or *pok1-1* (Figure 1D). Although organ formation apparently was not affected, at the cellular level, cell division patterns were dramatically disturbed in *pok1-1 pok2-3* double mutants (Figure 1E right panel), compared to wild type and single mutant *pok1-1* root meristems (Figure 1E, left panel).
Previously, immuno-localization of tubulin in root squashes established that phragmoplasts in *pok1 pok2* did not expand in the direction of the former PPB (Muller et al., 2006). To investigate phragmoplast guidance *in vivo*, the MT reporter line GFP-MBD was introgressed into the *pok1-1 pok2-3* double mutants. As in *pok1-1 pok2-1* and *pok1-2 pok2-2* (Muller et al., 2006), PPB, spindles and phragmoplasts formed normally in the *pok1-1 pok2-3* double mutant root meristem cells (Supplemental Fig. 2 online). Time lapse recordings of phragmoplast expansion, encompassing the stage of spindle-to-phragmoplast transition until completion of phragmoplast disassembly, revealed that phragmoplasts frequently tilted (Figure 2A, 2B, 2D, Supplementary movies 1 and 2, Sup. Fig. 3A, B), and that the duration of cytokinesis was prolonged in *pok1-1 pok2-3* double mutants (Figure 2C). While in the wild type cytokinesis lasted 37 min ± 11 min (n= 24) on average, in the double mutant cytokinesis lasted on average 57 min ± 24 min (n = 17, *$P<0.05$) (Figure 2C). In wild type meristems, optical sections through phragmoplasts typically display the transverse double layer of anti-parallel MTs connecting in the midzone (Figure 2A), which expands laterally throughout cytokinesis. In the wild type, periclinal root divisions, allowing a view of the phragmoplast torus/ring while it expands, occur with a very low frequency close to the root apical meristem as the *Arabidopsis* root contains a single layer of epidermal, cortical and endodermal tissue. Remarkably, 23% of

cytokinetic cells in *pok1-1 pok2-3* double mutants displayed the phragmoplast ring-view (Figure 2D), while only 2.4% of cytokinetic cells in the wild type exhibited the phragmoplast ring, in agreement with altered division plane orientations in *pok1-1 pok2-3*.

To determine whether the rate of phragmoplast expansion contributed to the prolonged cytokinesis in the *pok1-1 pok2-3* double mutant, we compared the rate of phragmoplast expansion using kymograph analysis (Figure 2E and 2F). Regardless of the genotype, most phragmoplasts displayed an expansion asymmetry as reflected by varying inclines of the kymograph (Figure 2F, left panel). This demonstrated that lateral expansion of the phragmoplast did not occur at a steady velocity, also indicated by the high standard deviation (Figure 2G). Nevertheless, in *pok1-1 pok2-3* double mutants, the average expansion rate was moderately, but significantly reduced (0.18 ± 0.09 µm/min; **P<0.02,* n = 22) compared to the wild type (0.21 ± 0.09 µm/min; n = 43) (Figure 2G), suggesting that slowing of the expansion rate in the double mutant contributes to the observed prolonged cytokinesis together with the frequent tilting of the phragmoplast.

POK1 interacts with TAN through its C-terminal domain and is required for TAN maintenance at the CDZ, but not for its recruitment

As previously reported, TAN maintenance at the CDZ requires POK function, while recruitment to the PPB occurred, although inefficient, in *pok1 pok2* mutants (Walker et al., 2007), in agreement with two distinct TAN protein domains mediating TAN recruitment to the CDZ before and after PPB disassembly (Rasmussen et al., 2011). To clarify the role of POKs in TAN recruitment, we analyzed TAN localization in the severe po*k1-1 pok2-3* allele combination (Figure 3). In the wild type, the majority of cells displaying either the PPB (95%, n = 19 cells), pro-spindle (100%, n = 6 cells), spindle (92%, n = 12 cells) or phragmoplast (98%, n = 43 cells) also contained associated cortical TAN-rings (Figure 3A to 3D). In contrast, the TAN recruitment in cells with PPBs (55%, n = 11 cells seemed less efficient or delayed, but not abolished in *pok1-1 pok2-3* double mutants, consistent with results from previous studies. Interestingly, the cortical association of TAN in cells containing pro-spindles was high (89%, n = 9 cells, Figure 3E), suggesting that POK function was not critically required for TAN localization at prophase. However, the

percentage of TAN rings in cells displaying spindles in metaphase dropped to 19% (n = 16 cells, Figure 3F, G and I), indicating that binding of POK1 and TAN becomes essential during this cell cycle stage. Moreover, TAN rings were entirely absent from cells with phragmoplasts (0%, n =18 cells, Figure 3H) in *pok1 pok2* double mutants. This result further supports the partial POK-dependence of TAN at the PPB and the essential POK1-dependent maintenance of TAN following prophase. In addition, we showed *in planta* interaction of nYFP-POK1$_{1683-2066}$ and cYFP-TAN in *Arabidopsis* protoplasts using BiFC (Figure 3J and K), supporting that interaction between TAN and POK1 mediates TAN maintenance at the CDZ. In contrast to control experiments (Figure 3L to 3N), strong expressing protoplasts displayed a filamentous YFP pattern reminiscent of cortical MTs (Figure 3O), suggesting that stabilization of POK1 and TAN interaction increases their capacity for MT binding

POK1 localizes to the cortical division zone

We analyzed the localization pattern of a functional YFP-POK1 fusion (Supplemental Figure 1C, and D) in four- to six-day-old wild type seedlings (Figure 4, Sup. Fig. 3). Only a subset of meristematic cells displayed a fluorescent YFP-POK1 signal, suggesting cell cycle-controlled expression or degradation of POK1. POK1-expressing cells displayed distinct fluorescent patterns of broad bands, sharp bands or pairs of focused spots (Figure 4A) in single optical sections. Three-D reconstruction of confocal image stacks revealed that YFP-POK1 formed continuous rings at the cell cortex.

To correlate the distinct YFP-POK1 rings with the corresponding cell cycle stages, we co-expressed YFP-POK1 and the MT reporter RFP-MBD. In root and leaf meristems, YFP-POK1 rings were associated with mitotic cells exhibiting PPBs, spindles and phragmoplasts (Figure 4B, Supplemental Figure 4A and B online). The observed YFP-POK1 patterns were reminiscent of the ring-shaped localization observed for the two POK1 inter-actors TAN and RanGAP1, which both co-localize with the PPB and continuously mark the CDZ throughout mitosis (Walker et al., 2007; Xu et al., 2008).

The short C-terminal fragment POK1$_{1683-2066}$ shown to be sufficient to bind TAN (Müller et al., 2006 and this study) and RanGAP1 (Xu et al., 2008) fused to YFP (*Pro35S*:YFP-POK1$_{1683-2066}$, Figure 4C) accumulated mainly in aggregates in *Arabidopsis* root meristem

cells (Supplemental Figure 4C online), constraining detection of a potential cortex localization.

Since POK1$_{1683-2066}$ showed substantial aggregation, we tested whether aggregation could be prevented by expressing longer fluorophore-tagged constructs of the POK1 C-term (*Pro35S:GFP-POK1$_{1213-2066}$*) and (*ProTP1:dTom-POK1$_{1265-2066,}$* Supplemental Figure 4D online). Both fusion proteins displayed a cell cycle-dependent subcellular localization pattern similar to the full-length YFP-POK1 and vastly diminished aggregation (Supplemental Figure 4E and 4F).

POK1 cortical recruitment shows cell phase-dependent dynamicity

To further characterize POK1 cortical recruitment, FRAP analysis was performed (Figures 5 and 6). In the *Arabidopsis* root meristem, epidermis cells in pro- and metaphase were selected based on the presence or absence of condensed nuclei in bright field. In transverse sections, YFP-POK1 localized to both lateral cell sides (Figure 5A to D). YFP-POK1 was specifically bleached at one side of the confocal section and migration of fluorescent signal into the bleached region was subsequently monitored. In prophase cells, fluorescence clearly recovered during the observation period (Figure 5A, 5C, 5E,). By contrast, metaphase YFP-POK1 fluorescence hardly recovered (Figure 5B, 5D, 5E), indicating a more dynamic YFP-POK1 recruitment or dispersal mechanism during prophase and a fairly static maintenance mechanism during subsequent cell cycle phases. The POK1 C-terminal fragment GFP-POK1$_{1213-2066}$ in BY-2 cells displayed differential dynamicity in FRAP experiments similar to YFP-POK1 in *Arabidopsis* (Figure. 6A to D). Also in prophase BY-2 cells, fluorescent signal recovered, although at a longer half time (Figure 6D) than YFP-POK1 (Figure 5E), while BY-2 metaphase cells displayed sluggish GFP-POK1$_{1213-2066}$ signal recovery similar to YFP-POK1. Due to the superior imaging accessibility, we clarified whether the initial recruitment of POK1 to the CDZ requires MTs, using BY-2 cells. Prophase cells expressing *ProS35:POK1$_{1213-2066}$-GFP* were treated with oryzalin and subjected to FRAP analysis. The oryzalin treatment completely abolished fluorescence recovery to the CDZ at prophase following photobleaching (n=6) (Figure 6E to L), suggesting the MT-dependent recruitment of POK1$_{1213-2066}$-GFP.

In *Arabidopsis*, a proportion of mitotic cells accumulated full-length YFP-POK1 signal in the cytoplasm, both in the absence and presence of YFP-POK1 cortical rings (Figure 4A, asterisk). We determined the proportion of cells containing cytoplasmic YFP-POK1 and/or YFP-POK1 at the CDZ for each cell cycle stage (Sup. Figure 4A). In the presence of PPBs, YFP-POK1 accumulates in the cytoplasm and progressively associates with the PPB and the CDZ in pro-metaphase, suggesting that YFP-POK1 is dynamically recruited to the CDZ. From metaphase until the termination of cytokinesis, the majority of YFP-POK1 was found to be associated with the CDZ. Taken together, our data suggest a cell cycle-dependent re-localization from cytoplasmic to cortical, CDZ/CDS resident YFP-POK1.

Similar to TAN (Walker et al., 2007, Rasmussen et al., 2011 and Sup. Fig. 4B, C) and RanGAP1 (Xu et al., 2008), the ring-shaped localization of POK1 narrowed during cytokinesis in BY-2 cells (Figure 6B, C, Supplemental Figure 5D, E) and *Arabidopsis* (Figure 5A and B) in a cell cycle progression-dependent manner. While the sharp punctate signal corresponds to the site of cell plate fusion, the CDS, the broad POK1 signal corresponded to the wider CDZ.

YFP-POK1 CDZ/CDS localization is independent of microtubules

To analyze the microtubule dependency of the subcellular YFP-POK1 localization, seedlings co-expressing YFP-POK1 and RFP-MBD were treated with the MT polymerization inhibitor oryzalin. The effect of oryzalin was visualized by the depolymerization of RFP-MBD-labeled MTs. While mitotic MT arrays disappeared upon oryzalin treatment (Figure 5F and 5H), YFP rings associated with cells containing PPBs (Figure 5G), spindles or phragmoplasts prior to oryzalin treatment were still present after MT de-polymerization (Figure 5G and 5I and Table 1). In two instances, the PPB was not associated with a YFP-POK1 ring (Table 1, n = 10 PPBs), which is consistent with the progressive recruitment of POK1 to the CDZ during prophase. In addition to the YFP-POK1 rings present in cells with phragmoplasts (n=15), five more (sharp) YFP-POK1 rings associated with recently synthesized cell walls (Table 1), which we also frequently observed in untreated cells. Maintenance of cortical POK1 upon oryzalin treatment demonstrates the MT-independent maintenance of CDZ-resident YFP-POK1.

Taken together, these results suggest that dynamic POK1 is continuously recruited to the CDZ in a microtubule-dependent manner during prophase, most likely from a cytoplasmic pool that is depleted prior to metaphase. Upon PPB disassembly, POK1 becomes immobilized and its localization subsequently narrows as mitosis progresses likely involving a self-associating mechanism. Independently of POK function, TAN and RanGAP1 arrive at the PPB where they become tethered by a POK-dependent mechanism. Together these proteins constitute a modular hub to maintain the positional information of the division plane and to guide the phragmoplast during cytokinesis.

Discussion

The correlation between the orientation of the PPB and the direction of phragmoplast expansion is a long-standing dogma in plant cell biology (Gunning and Wick, 1985). Cell biological studies on cell cultures and the use of a variety of chemicals interfering with cytoskeletal organization/dynamics as well as mutant analysis demonstrated the causal relation of PPB position and guidance of the phragmoplast towards the site specified by the PPB (Torres-Ruiz and Jurgens, 1994; Traas et al., 1995; Smith et al., 1996; Camilleri et al., 2002; Sano et al., 2005). Yet the molecular mechanisms involved remain poorly characterized. In contrast, upstream processes such as auxin-dependent transcriptional control of local cell divisions, essential for embryonic patterning, are intensively studied (reviewed in Lau et al., 2012). For instance, the ectopic expression of the bHLH transcription factor TMO5 is sufficient to induce periclinal divisions (De Rybel et al., 2013). The proteins TAN and the POK kinesin-12 proteins were implicated in phragmoplast guidance due to the mis-positioning of cell walls in the corresponding mutants with respect to the former PPB position (Smith et al., 1996; Muller et al., 2006), but how these proteins functionally interacted was unclear due to the lack of subcellular data regarding the POK kinesins. Our *in vivo* analysis confirmed the frequent mis-match of PPB and phragmoplast orientation in dividing *pok1 pok2* cells, showing that the POK kinesins function downstream of PPB formation and division plane determination. In contrast, in

mutant alleles of microtubule associated proteins such as CLASP (Ambrose et al., 2007; Kirik et al., 2007), PP2A subunit mutants (Spinner & Gadeyne et al., 2013) and the putative membrane protein SABRE (Pietra et al., 2013), oblique cell walls and mis-guidance of the phragmoplast are a consequence of mis-positioning of the PPB or lack thereof and thus these proteins act upstream of the POKs.

Consistent with phragmoplast expansion in BY-2 cells (Buschmann et al., 2010), we determined distinct expansion velocities for the left and right edge of wild type and *pok1-1 pok2-3* phragmoplasts. The rate of phragmoplast expansion was diminished in *pok1-1 pok2-3* cytokinesis, but could not solely account for the difference with respect to wild type cytokinesis duration. Tilting of the *pok1-1 pok2-3* phragmoplast contributes to the extended duration of *pok1-1 pok2-3* cytokinesis as well, since the tilted cell plate apparently does not follow the shortest distance rule (Rasmussen et al., 2013) in the absence of POK-dependent phragmoplast guidance. The postulated direct correlation of cytokinesis duration and cell size (Gorst et al., 1986) is consistent with this assumption.

The cell cycle-dependent association of POK1 with the CDZ/CDS closely resembles the localization of CDZ/CDS identity markers TAN and RanGAP1 (Walker et al., 2007; Xu et al., 2008). Interaction of POK1-Cterm with TAN as determined by BiFC (Figure 3) and the phenotype similarity of the maize mutant *tan* (Smith et al., 1996; Cleary and Smith, 1998) and the *pok1 pok2* double mutant in *Arabidopsis* further support a joint function of POK1 and TAN in the phragmoplast guidance mechanism.

POK1, TAN (Walker et al., 2007) and RanGAP1 (Xu et al., 2008) share the feature of narrowing from a broad towards a sharp ring during cytokinesis, suggesting that the proteins are co-regulated and/or act in a complex. POK1 seems to be particularly important for CDZ identity maintenance throughout mitosis, since both TAN (this study and Walker et al., 2007) as well as RanGAP1 (Xu et al., 2008) fail to remain present in *pok1 pok2* double mutants upon the metaphase/anaphase transition. Thus, the narrowing of TAN (Walker et al., 2007) and RanGAP1 (Xu et al., 2008) might reflect the narrowing of POK1 at the CDZ. With respect to TAN and RanGAP1 maintenance, POK1 provides a scaffolding function to retain CDZ resident proteins, thereby sustaining CDZ identity. Although the C-terminal POK1$_{1683\text{-}2066}$ is sufficient for TAN interaction, GFP-POK1$_{1683\text{-}2066}$

localization at the CDZ could not be unambiguously confirmed, in contrast to GFP-POK1$_{1213-2066}$, indicating that the necessary additional domain for efficient POK1 targeting to the PPB and CDZ lies directly upstream of POK1$_{1683-2066}$. With few exceptions, most kinesin class proteins act as homo- or heterodimers (Endow et al., 2010), mediated by multiple coiled coil domains, which are also predicted for POK1 and POK2 C-termini (Figure. 4C). Thus, the POK1C-terminal fusion proteins might associate with the PPB/CDZ through self-dimerization or with endogenous full-length POKs. Alternatively, the POK1C-terminal might be necessary and sufficient to recruit POK1 to the PPB and CDZ via interactions with yet unknown membrane-anchored binding partners.
Although the localization of POK2 was not directly investigated here, the rescue ability of the full-length YFP-POK1 fusion protein and the absence of aberrant single mutant phenotypes indicate functional redundancy of POK1 and POK2 and therefore also similarity in localization. In light of functional redundancy of POK1 and POK2, the aggravated phenotype of the novel *pok1-1 pok2-3* allele combination can be explained by the fact that some POK2 activity might still be present in previously described double mutants.

Genetic evidence suggests that TAN arrives at the PPB independently of POK1, and yet, both POK1 and TAN1 (Walker et al., 2007) recruitment to the PPB require an intact microtubule cytoskeleton. To clarify the sequence of independent recruitment events at the PPB, time-resolved *in vivo* co-localization studies of POK1, TAN and RanGAP1 proteins would proove useful, since genetic analysis in *Arabidopsis* is hampered by the lack of clear *tan* loss of function alleles as well as the pleiotropic phenotypes of *ran gap* double knock down mutants (Xu et al., 2008) and gametophytic lethality of *ran gap* double knock out mutants (Rodrigo-Peiris et al., 2011), respectively.

Based on homology of the motor domains, POK1 clusters with kinesin-12 class proteins, predicted to display MT plus end directed motility (Lee and Liu, 2004; Muller et al., 2006; Lipka and Muller, 2012). Although POK1 motor activity has not been investigated, given its localization at the plasma membrane, it potentially contributes to the phragmoplast guidance mechanism by directly binding to peripheral phragmoplast MTs and exerting a

motor-activity-related force. Alternatively, POK, together with TAN might simply function to stabilize outreaching MTs. Indeed, TAN is a highly basic protein that co-sedimented with MTs *in vitro* (Smith et al., 2001), showing that it has MT-binding capacities. In this hypothesis, the motor-activity required for orienting the phragmoplast might be delivered by phragmoplast-associated kinesins. Stabilization of the POK1$_{1683-2066}$ and TAN protein complex by reconstitution of YFP in the BiFC experiment drew the complex to filamentous cellular structures, closely resembling MTs, thus likely unmasking a normally transient interaction of the POK1-TAN protein complex with MTs (Figure 3). This observation raises the exciting possibility that the CDZ resident POK1-TAN complex might indeed stabilize transient interactions with phragmoplast emanating MTs that approach the CDS, to direct the phragmoplast/cell plate to its final destination.

Intriguingly, the localization pattern of POK1 is complementary to that of the cell cycle-regulated kinesin-14, KCA1 (Vanstraelen et al., 2006). KCA1 interacts with PPB-localized CDKA;1 (Vanstraelen et al., 2006), the MT severing protein katanin (Boutte et al., 2010) and the actin cytoskeleton (Suetsugu et al., 2010). *kca1 kca2* double mutants are primarily affected in chloroplast movement (Suetsugu et al., 2010). The predicted MT minus end directed motor activity of KCA1 seems well suited to accomplish a cortical pulling force to orient a mitotic MT array, similar to dynein, which is required for spindle/division plane orientation in animals (Kiyomitsu and Cheeseman, 2013). The complementary localization at the plasma membrane of two sets of kinesins leads to the intriguing hypothesis that the KCA and POK kinesin proteins might act antagonistically to position/guide mitotic MT arrays. However, the role of KCA1 in division plane orientation awaits further scrutiny.

The overall phenotype of *pok1-1 pok2-3* seedlings is strikingly similar to weak alleles of *ton2* (Kirik et al., 2012; Spinner & Gadeyne et al., 2013). Intriguingly, the POK-independent TAN and RanGAP1 recruitment to the CDZ correlates with the presence of TON2 at the CDZ, which disappears from the CDZ upon anaphase, as was shown for the TON2 homolog DCD1 in maize (Wright et al., 2009) and for *A. thaliana* TON1 and FASS (Spinner & Gadeyne et al., 2013). Interestingly, the MAPK cascade controlling MT turnover in the expanding phragmoplast is initiated by interaction of the HINKEL/At-

NACK1 kinesin with the respective MAPKKK NPK1. Phosphorylation of both proteins by CDKs prevents their binding, while their dephosphorylation at the metaphase/anaphase transition is critically required for successful cytokinesis (Sasabe et al., 2011). Similarly, phospho-regulation might direct the anchoring of POK1 at the cell cortex upon PPB disassembly and/or control the binding of TAN and POK1 involving TON2-dependent dephosphorylation. Indeed, TAN is a potential target of phospho-regulation, as pharmacological inhibition of phosphatases as well as genetic interference with TON2 function prevented its cortical localization (Rasmussen et al., 2011, Walker et al., 2007).
In summary, we provide evidence for POK's critical function for the maintenance of CDZ/CDS identity. In a MT-dependent manner, dynamic POK1 is continuously recruited to the CDZ during prophase, most likely from a cytoplasmic pool that is depleted prior to metaphase. Upon its arrival at the CDZ, POK1 becomes immobilized and subsequently its localization narrows by a yet unknown mechanism as mitosis progresses (Figure 7). Independent from POK function, TAN and RanGAP1 arrive at the CDZ, where they become tethered by a POK-dependent mechanism possibly involving TON2-mediated dephosphorylation of TAN (Figure 7).
Together these proteins provide positional information of the division plane and might even actively participate in the phragmoplast guidance mechanism. However, at this point it still remains to be elucidated whether POKs are actively engaged in the phragmoplast guidance mechanism or whether their function is primarily a scaffolding activity to provide a spatial reference for CDZ components following PPB disassembly. Future studies are geared towards resolving these open questions.

Plant Material

Arabidopsis thaliana plants, accession Columbia, were used throughout the study unless otherwise indicated. SALK T-DNA insertion lines for *pok1-1, pok1-2, pok2-1* and *pok2-2*, as well as the double mutants *pok1-1pok2-1* and *pok1-2pok2-2* have been described previously (Muller et al., 2006). *Agrobacterium*-mediated transformation to create diverse transgene lines was performed according to (Clough and Bent, 1998).

Growth Conditions

For examination of mutant phenotypes and localization studies at the seedling stage, seedlings were grown on plates containing Murashige and Skoog basal medium (Sigma-Aldrich) and 1% agarose or agar. For reproduction and crossing, plants were grown in soil. Plates and pots were incubated at 20ºC–22ºC on a 16-h-light/8-h-dark cycle.

EMS mutagenesis and identification of *pok2-3*

Plants homozygous for the *pok1-1* mutation where imbibed in dH_2O, mutagenized with 0.3% ethylmethansulfonate overnight and thoroughly washed subsequently. Five-hundred M1 progeny were scored for short roots on standard MS medium plates and seeds were collected individually for each M1 plant. Among eight preselected M2 families, one segregated the *pok1-1 pok2-3* phenotype. We performed test crosses with *pok1-1 pok2-1* and since the progeny (n = 120) showed the *pok1 pok2* phenotype we concluded that *POK2* was mutated. Sequencing of the *POK2* locus identified a C to T substitution in exon 16 leading to a premature stop codon.

Microtubule marker line

The MT binding domain MBD contained in a Gateway® (Invitrogen) compatible destination vector pEG104-*Pro35S*:mCherry-MBD (Gutierrez et al., 2009) was recombined into pDONR207 (Invitrogen) by the BP clonase reaction. Subsequently, the LR reaction was performed with the destination vector *pUBN*:RFP containing the *Arabidopsis* Ubiquitin10 promoter (Grefen et al., 2010). Transgenic plant lines expressing XFP-MBD fusion protein have been used as a faithful MT marker (Marc et al., 1998; Gutierrez et al., 2009).

Generation of YFP-POK1 fusion protein

A recombineering-based approach was used to genetically insert the YFP tag at the 5’ of *POK1.* All recombineering steps were essentially performed as described in (Tursun et al., 2009). In brief, recombineering primers (Supplemental Table 1 online) encoding 50 nt of POK1 homology arms immediately upstream and downstream of the ATG and about

50 nt of a plasmid pBALU6 (Tursun et al., 2009), containing a YFP and GalK cassette, were used to amplify the fluorophore and the GalK selection marker. The binary BAC 79I20 carrying the genomic region of *POK1* was transformed into *E. coli* strain SW105, which allowed homologous recombination upon heat induction. Electro-competent SW105 containing BAC 79I20 were incubated at 42°C for 15 min to induce *λ red* recombinase and subsequently transformed with the PCR product amplified from the YFP-GalK cassette. Then cells were propagated for 3 h at 32°C and plated on galactose minimal medium. Colonies were streaked on McConkey indicator plates to screen for Galactokinase activity, which lead to changes in pH of the medium turning colonies pink. Positive clones were further analyzed by PCR for the integration of the cassette into the BAC. Selected clones were cultured in liquid medium and split after propagation. One aliquot was supplied with 1/100 volume of 10% Arabinose solution for induction of FLP recombinase to remove the GalK selection marker. Both aliquots were propagated for two additional hours before DNA was extracted. Induced and non-induced samples were analyzed by PCR with primers (Supplemental Table 1 online) flanking the recombination site. Clones where GalK was efficiently excised were sequence verified and used for transformation into Agrobacterium strain GV3101. After *Arabidopsis* transformation, five independent T1 lines were recovered on nutrient agar plates containing 0.05% phosphinotrycin, PPT) and T2 plants were inspected for YFP-POK1 localization. Two independent T2 lines showed YFP fluorescence and were selected for further analysis. Both lines rescued the *pok1 pok2* double mutant phenotype and showed an identical localization pattern of the YFP-POK1 fusion protein in Col and *pok1 pok2* rescue plants.

TAN with and without stop codon was amplified from full-length cDNA clones obtained from the RIKEN institute (pda14314) (primers are listed in Supplemental Table 2 online). Because these primers were flanked with the minimal attB sites, all PCR products were amplified with the full-length attB1F and attB2R primers (Supplemental Table 2 online) and cloned into pDONR221 via a Gateway BP reaction (Invitrogen). $POK1_{1213\text{-}2066}$ coding sequences with and without stop codon were amplified from entry clone pENTR-POK1 described in (Xu et al., 2008).

The dTom-POK1$_{1265-2066}$ fusion construct was created in the pK7m34GW vector (Karimi et al., 2007) using the dTomato coding sequence and the POK cDNA fragment corresponding to amino acids 1265-2066 (Supplemental Table 3 online) under control of the constitutive promoter from the At3g16640 gene (Berkowitz et al., 2008).

The short -terminal fragment POK1$_{1683-2066}$ was cloned into pENTR3C via EcoRI/XhoI from pAD-POK1C (Müller et al., 2006) and recombined with pEG104 (Earley et al., 2006) to create *Pro35S:YFP-POK1$_{1683-2066.}$*

Pro35S:RFP-MBD expressed in BY-2 cells was described elsewhere (Marc et al., 1998; Van Damme et al., 2004). Entry clones of POK1C$_{1213-2066}$, and TAN with stop codon (Supplemental Table 2 online were used in a single Gateway LR reaction with pK7WGF2 to generate N-terminal GFP fusion proteins. Entry clones of POK1C without stop codon were combined with pK7FWG2 to create C-terminal GFP fusion proteins.

Subcellular distribution fo YFP-POK1 signal (Supplemental Figure 5 online) was analyzed in indirect immuno-localization experiments using anti-GFP (Invitrogen) and anti-tubulin (YL1/2, Abcam) and secondary antibodies anti-rabbit-Alexa488 (Invitrogen) and anti-rat-Cy3 (Jackson Immuno Research).

Confocal imaging and image processing

Imaging was performed on a Leica SP2 equipped with a point scanner and a Leica SP8 confocal microscope equipped with a Resonant Scanner. A 63 x, N.A. = 1.20, water-immersion objective lens was used for image acquisition. YFP fluorescence was excited by the 514 nm laser line from an Argon/Krypton laser and detected with a standard PTM on the SP2 or a HyD detector on the SP8 set to a detection window between 520 nm and 550 nm. RFP was excited with a 561 nm He/Ne laser and fluorescence was detected with a standard PMT or a HyD detector set at 570 nm to 650 nm. GFP was excited with a 488 nm laser line from an Argon/Krypton laser and detected with a PMT or a HyD detector at 500 nm to 550 nm.

BY-2 cells were imaged on an Olympus FV1000 inverted confocal microscope equipped with a water-corrected 60x objective (N.A.= 1.2) using a 488 nm laser excitation and a spectral detection bandwidth of 500-530 nm for EGFP and a 559 nm laser excitation together with a spectral detection bandwidth of 570-670 nm for RFP detection and with a

Zeiss 710 inverted confocal microscope with the ZEN 2009 software package and equipped with a 63x water corrected objective (N.A. = 1.2). GFP was visualized using 488 nm laser excitation and 500-530 nm spectral detection; RFP was visualized using 458 nm laser excitation and 592-754 nm spectral detection.

Two-dimensional projections and three-dimensional reconstructions of Z stacks were generated with either ImageJ v.1.48a (http://rsb.info.nih.gov/ij/) or Leica LF Image processing. Color merges were carried out with NIH ImageJ v.1.48s or Adobe Photoshop CS5 v12.0.4 (Adobe Systems). Only linear adjustments to pixel values were applied.

To determine the duration of cytokinesis and the orientation of phragmoplasts (transverse versus torus view), a *pok1-1 pok2-3* segregating population derived from a cross with the GFP-MBD marker line described in Marc et al. (1998) was used. Time lapse imaging of cells displaying spindle stages was performed and continued throughout mitosis at 3 to 5 min intervals. Time intervals were shorter at the beginning of the time lapse to determine the transition from spindle to phragmoplast and at the end of cytokinesis, while longer interval times were chosen during phragmoplast expansion. The duration was timed from the spindle/phragmoplast transition until phragmoplast disassembly.

The rate of phragmoplast expansion was determined using kymograph analysis (Buschmann et al., 2010). We recorded time lapse images of cells displaying spindles or earlier cell cycle stages at 2.5 min intervals until the phragmoplast made contact with the cell wall. In ImageJ, the segmented line tool was used to select the distance for the measurement, spanning the diameter of the phragmoplast. To determine relative velocities and to visualize the narrowing of the POK1C or TAN localization at the CDZ, the ImageJ kymograph plugin (http://www.embl.de/eamnet/html/body_kymograph.html) was used. Based on these measurements, the velocities of phragmoplast expansion were calculating in Excel.

rBiFC

The ratiometric bimolecular fluorescence complementation Gateway compatible 2in1 System (Grefen and Blatt, 2012) was used to examine interaction between POK1$_{1683-2066}$ and TAN. ROP2 was used as a negative control since, like POK1, it localized to the plasma membrane. The potential binding partners were expressed under the control of the Pro35S promoter on the same plasmid, which also carries RFP as an internal expression control. The ratio between YFP and RFP is used to estimate interaction strength. The primers used to amplify the cDNA of binding partners are listed in Supplemental Table 2 online. Amplicons were cloned via the BP reaction into pDONR221-P1P4 or pDONr221-P2P3, respectively. The resulting entry clones were used in subsequent LR reactions with destination vector pBiFCt-2in1-NN. All steps were performed according to Grefen and Blatt, 2012. Protoplasts from *Arabidopsis thaliana* suspension culture were transformed with the pBiFCt-2in1-NN plasmids according to (Schütze et al., 2009). YFP and RFP fluorescence were excited with 514 nm and 561 nm excitation wavelength by sequential scan using the Leica TCS SP8 resonant scanner and hybrid detector HyD2 set to 518 nm to 552 nm for YFP fluorescence and PMT4 set to 645 to 731 nm for RFP fluorescence. All images were taken at identical settings. Quantification of fluorescence intensity was performed in ImageJ. The segmented line tool, set to a 7.5 pixel width, was used to trace the protoplasts and mean fluorescence intensity was measured along this line. Calculation of mean YFP/RFP ratio and the graph were performed in Excel. The mCherry-ROP2 control was generated using CreLox according to Geldner et al., via recombination of *pUNI-ROP2* with pNIGL17 (Geldner et al., 2009). As localization control for TAN, the plasmid *pEZRK:TAN-YFP* described in Walker et al., 2007, was used.

BY-2 transformation

Stable BY-2 transformation was carried out as described before (Geelen and Inzé, 2001). BY-2 cell lines expressing two fluorescent constructs were created by consecutive super-transformation of single transformed lines. Stably transformed calli were screened for fluorescence and localization patterns of tagged proteins were confirmed by analyzing several independent transformants.

FRAP analysis

FRAP experiments for the POK1 C-terminal fragment GFP-POK1$_{1213-2066}$ were conducted on an Olympus FluoView1000 inverted confocal microscope. One pre bleach images was taken. A certain region of interest (ROI) was bleached for 10 s with 100% laser power. Subsequent images were taken every 60 s. BY-2 cells were mounted in a chambered cover glass system (Lab-Tek) in 1% low melting point agarose containing BY-2 medium. The average fluorescence intensity of the bleached region (ROI1) was measured using ImageJ (I(t)). The position of ROI1 was adjusted manually during the time lapse to correct for cell drifting. The average intensity of a second ROI (ROI2) outside the cell was measured to compensate for background fluorescent signal (Ibase). Because Ibase approaches a constant value, we subtracted the average Ibase from I(t) to obtain the actual fluorescence intensity Ifrap(t) (I(t)-average(Ibase)=Ifrap(t)). To estimate the amount of photobleaching due to image acquisition, we measured the average intensity of the whole cell (ROI3). From these values we also subtracted the background signal (average Ibase). These values were set out in a scatter plot and fitted to a linear trendline, which allowed us to determine the theoretical reduction in fluorescence intensity due to image acquisition for each time point (Ibleach(t)).

To obtain a normalized value for fluorescence recovery (Inorm(t)), we first determined the ratio of fluorescence loss due to Image acquisition:

Ibleach(t=0)/Ibleach(t) (1)

Next, the remaining fluorescence intensity after photobleaching (Ifrap(post)) was set to zero and all intensity values were adjusted accordingly:

Ifrap(t)-Ifrap(post) (2)

Ifrap(t=0)-Ifrap(post) (3)

Finally, to obtain the normalized values for fluorescence recovery after photobleaching (Inorm(t)), the previous equations were combined as follows:

Inorm(t)=(1)*((2)/(3))

The average Inorm(t) (FRAP Figure 6D: prophase cells, n=4; metaphase cells, n=7; FRAP Figure 6L, n=6) was set out in a scatter plot using Sigmaplot 12. A single

exponential regression with rise to a maximum (y=a*(1-exp(-b*t))) was fitted to the data points. The half time ($t_{1/2}$) for fluorescence recovery was calculated using the above formula with the fluorescence intensity value corresponding to half of the fitted maximum recovery at the latest timepoint as y.

FRAP experiments of full-length YFP-POK1 were performed using 4- to 7-day-old seedlings expressing *ProPOK1*:YFPgPOK1 in the *pok1-1 pok2-3* background. Seedlings were mounted in water on solid half strength nutrient (0.5 x MS salt, 1.5% agar). Using the LEICa SP8, four pre-bleach images were taken, and then the selected region of interest (ROI1) was bleached with identical laser settings for each experiment. Fluorescent signal recovery was imaged at 60 s time intervals for 30 min. FRAP data analysis was performed as described for GFP-POK1C. The background was determined outside of the root (ROI2) and the average intensity of the whole cell (ROI3) was used to correct for photobleaching during image acquisition without trendline fitting.

Oryzalin treatment

Four- to five-day-old seedlings co-expressing YFP-POK1 and RFP-MBD were imaged and subsequently treated by exchanging mounting medium with 10 µM oryzalin solution. Fluorescence of cells that had PPBs, spindles or phragmoplasts and YFP-POK1 prior to oryzalin treatment were re-analyzed at 5 min intervals for 10 to 30 min. BY-2 cells were mounted in a chambered cover glass system (Lab-Tek). Cells were immobilized in a thin layer (1 mL) of BY-2 medium containing vitamins (Geelen and Inze 2001), 0.8-1% low-melting-point agarose (Invitrogen) and 10 µM oryzalin. BY-2 cells were imaged to the point where MT depolymerization was evident followed by FRAP analysis.

Accession Numbers

Sequence data from this article can be found in the Arabidopsis Genome Initiative or GenBank/EMBL databases under the following accession numbers: At3g17360, At3g19050, At3g05330.

Supplemental Data

The following materials are available in the online version of this article.

Supplemental Movie Legends.

Supplemental movie 1: Time lapse of wild type cell division at 1.5 fps. Yellow arrowheads indicate position of PPB. The insertion of the cell plate at the end of cytokinesis corresponds with the position of the PPB. This movie corresponds to Supplementary Figure **3A**. Scale bar indicates 10 µm.

Supplemental movie 2: Time lapse of *pok1-1 pok2-3* cell division at 1.5 fps. Yellow arrowheads indicate the position of the PPB. The white arrows indicate the cell plate insertion site, which deviates from the PPB position. This movie corresponds to Supplementary Figure **3B**. Scale bar indicates 10 µm.

Acknowledgements

We acknowledge the ABRC and NASC for distribution of seed used in this study. The instructive advice and provision of *E.coli* SW105 and the recombineering plasmid collection by Baris Tursun is gratefully acknowledged. We thank Dr. Christopher Grefen for advice and the rBiFC plasmids. We thank Daniela Daumüller, Phillip Reichert, Hs Lee, Richard Gavidia, Angela Kirik and Samantha Atkinson for help with data collection. We thank Katharina Brancato from the ZMBP Transformation service. We appreciate the support from the Department of Developmental Genetics lead by Prof. Gerd Jürgens. Funding for this work was provided by Deutsche Forschungsgemeinschaft grant to S.M. (DFG MU 3133/1-1) and by the National Institute of Health grant (1R15GM102839)-01A1 (VK)**.** AG was indebted to the Agency for Innovation by Science and Technology for a predoctoral fellowship.

Authors contributions: E.L, A.G., D.V.D, G.D.J, D.E., V.K. and S.M. designed the research; E.L., A.G., D.S., S.Z., D.V.D, V.K. and S.M. performed research; E.L., A.G., D.S, D.V.D, V.K. and S.M. analyzed data; D.V.D. and S.M. wrote the paper.

References

Ambrose, J.C., Shoji, T., Kotzer, A.M., Pighin, J.A., and Wasteneys, G.O. (2007). The *Arabidopsis* CLASP gene encodes a microtubule-associated protein involved in cell expansion and division. Plant Cell **19,** 2763-2775.

Berkowitz, O., Jost, R., Pollmann, S., and Masle, J. (2008). Characterization of TCTP, the Translationally Controlled Tumor Protein, from Arabidopsis thaliana. The Plant Cell Online **20,** 3430-3447.

Boutte, Y., Frescatada-Rosa, M., Men, S., Chow, C.M., Ebine, K., Gustavsson, A., Johansson, L., Ueda, T., Moore, I., Jurgens, G., and Grebe, M. (2010). Endocytosis restricts Arabidopsis KNOLLE syntaxin to the cell division plane during late cytokinesis. EMBO J **29,** 546-558.

Buschmann, H., Sambade, A., Pesquet, E., Calder, G., and Lloyd, C.W. (2010). Chapter 20 - Microtubule Dynamics in Plant Cells. In Methods in Cell Biology, C. Lynne and T. Phong, eds (Academic Press), pp. 373-400.

Camilleri, C., Azimzadeh, J., Pastuglia, M., Bellini, C., Grandjean, O., and Bouchez, D. (2002). The *Arabidopsis TONNEAU2* gene encodes a putative novel protein phosphatase 2A regulatory subunit essential for the control of the cortical cytoskeleton. Plant Cell **14,** 833-845.

Cleary, A.L., and Smith, L.G. (1998). The *Tangled1* gene is required for spatial control of cytoskeletal arrays associated with cell division during maize leaf development. Plant Cell **10,** 1875-1888.

Cleary, A.L., Gunning, B.E.S., Wasteneys, G.O., and Hepler, P.K. (1992). Microtubule and F-Actin Dynamics at the Division Site in Living Tradescantia Stamen Hair-Cells. J. Cell Sci. **103,** 977-988.

Clough, S.J., and Bent, A.F. (1998). Floral dip: a simplified method for Agrobacterium-mediated transformation of Arabidopsis thaliana. Plant J **16,** 735-743.

De Rybel, B., Möller, B., Yoshida, S., Grabowicz, I., Barbier de Reuille, P., Boeren, S., Smith, Richard S., Borst, Jan W., and Weijers, D. (2013). A bHLH Complex Controls Embryonic Vascular Tissue Establishment and Indeterminate Growth in Arabidopsis. Developmental cell **24,** 426-437.

Dhonukshe, P., and Gadella, T.W., Jr. (2003). Alteration of microtubule dynamic instability during preprophase band formation revealed by yellow fluorescent protein-CLIP170 microtubule plus-end labeling. Plant Cell **15,** 597-611.

Earley, K.W., Haag, J.R., Pontes, O., Opper, K., Juehne, T., Song, K., and Pikaard, C.S. (2006). Gateway-compatible vectors for plant functional genomics and proteomics. The Plant Journal **45,** 616-629.

Endow, S.A., Kull, F.J., and Liu, H. (2010). Kinesins at a glance. Journal of Cell Science **123,** 3420-3424.

Geelen, D.N.V., and Inzé, D.G. (2001). A Bright Future for the Bright Yellow-2 Cell Culture. Plant Physiology **127,** 1375-1379.

Gorst, J., Wernicke, W., and Gunning, B.E.S. (1986). Is the preprophase band a of microtubules a marker of organization in suspension-cultures. Protoplasma **134,** 130-140.

Grefen, C., and Blatt, M.R. (2012). A 2in1 cloning system enables ratiometric bimolecular fluorescence complementation (rBiFC). Biotechniques **53,** 311-314.

Grefen, C., Donald, N., Hashimoto, K., Kudla, J., Schumacher, K., and Blatt, M.R. (2010). A ubiquitin-10 promoter-based vector set for fluorescent protein tagging facilitates temporal stability and native protein distribution in transient and stable expression studies. Plant J **64,** 355-365.

Gunning, B.E.S., and Wick, S.M. (1985). Preprophase Bands, Phragmoplasts, and Spatial Control of Cytokinesis. J. Cell Sci.**,** 157-179.

Gutierrez, R., Lindeboom, J.J., Paredez, A.R., Emons, A.M., and Ehrhardt, D.W. (2009). Arabidopsis cortical microtubules position cellulose synthase delivery to the plasma membrane and interact with cellulose synthase trafficking compartments. Nat Cell Biol **11,** 797-806.

Karimi, M., Depicker, A., and Hilson, P. (2007). Recombinational Cloning with Plant Gateway Vectors. Plant Physiology **145**, 1144-1154.

Kirik, A., Ehrhardt, D.W., and Kirik, V. (2012). TONNEAU2/FASS Regulates the Geometry of Microtubule Nucleation and Cortical Array Organization in Interphase Arabidopsis Cells. The Plant Cell **24,** 1158-1170

Kirik, V., Herrmann, U., Parupalli, C., Sedbrook, J.C., Ehrhardt, D.W., and Hülskamp, M. (2007). CLASP localizes in two discrete patterns on cortical microtubules and is required for cell morphogenesis and cell division in Arabidopsis. Journal of Cell Science **120,** 4416-4425.

Kiyomitsu, T., and Cheeseman, Iain M. (2013). Cortical Dynein and Asymmetric Membrane Elongation Coordinately Position the Spindle in Anaphase. Cell **154,** 391-402.

Lau, S., Slane, D., Herud, O., Kong, J., and Jürgens, G. (2012). Early Embryogenesis in Flowering Plants: Setting Up the Basic Body Pattern. Annual Review of Plant Biology **63,** 483-506.

Lee, Y.R., and Liu, B. (2004). Cytoskeletal motors in Arabidopsis. Sixty-one kinesins and seventeen myosins. Plant Physiol **136,** 3877-3883.

Lipka, E., and Muller, S. (2012). Potential roles for Kinesins at the cortical division site. Front Plant Sci **3,** 158.

Marc, J., Granger, C.L., Brincat, J., Fisher, D.D., Kao, T., McCubbin, A.G., and Cyr, R.J. (1998). A GFP-MAP4 reporter gene for visualizing cortical microtubule rearrangements in living epidermal cells. Plant Cell **10,** 1927-1940.

Mineyuki, Y., and Palevitz, B.A. (1990). Relationship between Preprophase Band Organization, F-Actin and the Division Site in Allium - Fluorescence and Morphometric Studies on Cytochalasin-Treated Cells. Journal of Cell Science **97,** 283-295.

Müller, S., Han, S., and Smith, L.G. (2006). Two kinesins are involved in the spatial control of cytokinesis in Arabidopsis thaliana. Curr Biol **16,** 888-894.

Paredez, A.R., Somerville, C.R., and Ehrhardt, D.W. (2006). Visualization of cellulose synthase demonstrates functional association with microtubules. Science **312,** 1491-1495.

Pickett-Heaps, J.D., and Northcote, D.H. (1966). Organization of microtubules and endoplasmic reticulum during mitosis and cytokinesis in wheat meristems. J Cell Sci **1,** 109-120.

Pietra, S., Gustavsson, A., Kiefer, C., Kalmbach, L., Hörstedt, P., Ikeda, Y., Stepanova, A.N., Alonso, J.M., and Grebe, M. (2013). Arabidopsis SABRE and

CLASP interact to stabilize cell division plane orientation and planar polarity. Nature communications **4,** doi: 10.1038/ncomms3779

Rasmussen, C.G., Sun, B., and Smith, L.G. (2011). Tangled localization at the cortical division site of plant cells occurs by several mechanisms. J Cell Sci **124,** 270-279.

Rasmussen, C.G., Wright, A.J., and Müller, S. (2013). The role of the cytoskeleton and associated proteins in determination of the plant cell division plane. The Plant Journal **75,** 258-269.

Rodrigo-Peiris, T., Xu, X.M., Zhao, Q., Wang, H.-J., and Meier, I. (2011). RanGAP is required for post-meiotic mitosis in female gametophyte development in Arabidopsis thaliana. Journal of Experimental Botany **62,** 2705-2714.

Sano, T., Higaki, T., Oda, Y., Hayashi, T., and Hasezawa, S. (2005). Appearance of actin microfilament 'twin peaks' in mitosis and their function in cell plate formation, as visualized in tobacco BY-2 cells expressing GFP-fimbrin. Plant J **44,** 595-605.

Sasabe, M., Boudolf, V., De Veylder, L., Inzé, D., Genschik, P., and Machida, Y. (2011). Phosphorylation of a mitotic kinesin-like protein and a MAPKKK by cyclin-dependent kinases (CDKs) is involved in the transition to cytokinesis in plants. Proceedings of the National Academy of Sciences **108,** 17844-17849.

Schütze, K., Harter, K., and Chaban, C. (2009). Bimolecular Fluorescence Complementation (BiFC) to Study Protein-protein Interactions in Living Plant Cells. In Plant Signal Transduction, T. Pfannschmidt, ed (Humana Press), pp. 189-202.

Smith, L.G., Hake, S., and Sylvester, A.W. (1996). The tangled-1 mutation alters cell division orientations throughout maize leaf development without altering leaf shape. Development **122,** 481-489.

Spinner, L., Gadeyne, A., Belcram, K., Goussot, M., Moison, M., Duroc, Y., Eeckhout, D., De Winne, N., Schaefer, E., Van De Slijke, E., Persiau, G., Witters, E., Gevaert, K., De Jaeger, G., Bouchez, D., Van Damme, D., and Pastuglia, M. (2013). A protein phosphatase 2A complex spatially controls plant cell division. Nature communications **4,** 1863.

Suetsugu, N., Yamada, N., Kagawa, T., Yonekura, H., Uyeda, T.Q.P., Kadota, A., and Wada, M. (2010). Two kinesin-like proteins mediate actin-based chloroplast movement in Arabidopsis thaliana. Proceedings of the National Academy of Sciences **107,** 8860-8865.

Torres-Ruiz, R.A., and Jurgens, G. (1994). Mutations in the FASS gene uncouple pattern formation and morphogenesis in Arabidopsis development. Development **120,** 2967-2978.

Traas, J., Bellini, C., Nacry, P., Kronenberger, J., Bouchez, D., and Caboche, M. (1995). Normal differentiation patterns in plants lacking microtubular preprophase bands. Nature **375,** 676-677.

Tursun, B., Cochella, L., Carrera, I., and Hobert, O. (2009). A toolkit and robust pipeline for the generation of fosmid-based reporter genes in C. elegans. PLoS One **4,** e4625.

Van Damme, D. (2009). Division plane determination during plant somatic cytokinesis. Current Opinion in Plant Biology **12,** 745-751.

Van Damme, D., Van Poucke, K., Boutant, E., Ritzenthaler, C., Inze, D., and Geelen, D. (2004). In vivo dynamics and differential microtubule-binding activities of MAP65 proteins. Plant Physiol **136,** 3956-3967.

Vanstraelen, M., Van Damme, D., De Rycke, R., Mylle, E., Inze, D., and Geelen, D. (2006). Cell cycle-dependent targeting of a kinesin at the plasma membrane demarcates the division site in plant cells. Curr Biol **16,** 308-314.

Vos, J.W., Dogterom, M., and Emons, A.M. (2004). Microtubules become more dynamic but not shorter during preprophase band formation: a possible "search-and-capture" mechanism for microtubule translocation. Cell Motil Cytoskeleton **57,** 246-258.

Walker, K.L., Muller, S., Moss, D., Ehrhardt, D.W., and Smith, L.G. (2007). Arabidopsis TANGLED identifies the division plane throughout mitosis and cytokinesis. Curr Biol **17,** 1827-1836.

Wright, A.J., Gallagher, K., and Smith, L.G. (2009). discordia1 and alternative discordia1 function redundantly at the cortical division site to promote preprophase band formation and orient division planes in maize. Plant Cell **21,** 234-247.

Xu, X.M., Zhao, Q., Rodrigo-Peiris, T., Brkljacic, J., He, C.S., Muller, S., and Meier, I. (2008). RanGAP1 is a continuous marker of the Arabidopsis cell division plane. Proc Natl Acad Sci U S A **105,** 18637-18642.

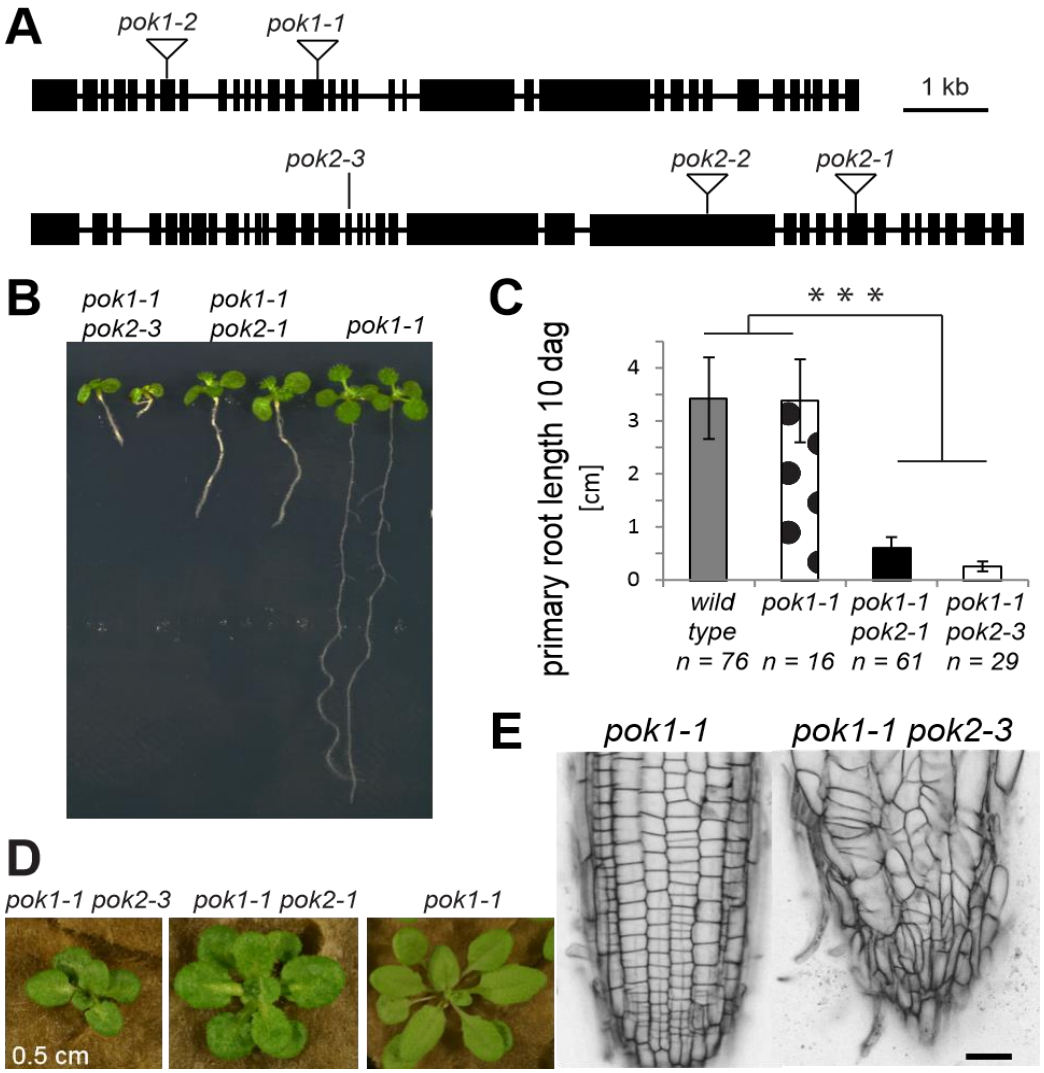

Figure 1: Mutant alleles and mutant phenotypes. (A) Schematic representation of *POK1* and *POK2* gene structure and position of mutations. SALK-TDNA insertions in alleles *pok1-1* (exon 15), *pok1*-2 (exon 7), *pok2-1* (exon 28) and *pok2-2* (exon 23) are indicated by triangles. The ethylmethansulfonate induced nonsense mutation in allele *pok2-3* is a C to T substitution (exon 16, at position 3845 bp), causing a premature Stop at amino acid 733 (Gln to *). Bars indicate exons. (B) Seedling phenotypes of (right to left) the *pok1-1* single mutant, *pok1-1 pok2-1* double mutant and *pok1-1 pok2-3* double mutant. (C) Comparison of average primary root length 10 days after germination (dag). Grey bar indicates wild type (3.4 cm ± 0.8), dotted bar indicates *pok1-1* (3.4 cm ± 0.8), black bar indicates *pok1-1pok2-1* (0.6 cm ± 0.2), grey bar indicates *pok1-1pok2-3* (0.25 cm ± 0.09). The average root length of *pok1-1 pok2-1* and *pok1-1 pok2-3* is significantly (****P<<0.005,* Student's *t*-test) shorter than in wild type and *pok1-1*. Number of samples (n) is indicated. Error bars indicate ± SD. (D) Comparison of rosettes of three-week-old *pok1-1* single mutant, *pok1-1 pok2-3* double mutant and *pok1-1 pok2-1* double mutant plants. (E) Root meristems, stained with propidium Iodide to visualize cell walls. Whereas the *pok1-1* single mutant (left) shows a regular cell pattern of the root cell files, the *pok1-1 pok2-3* double mutant (right) cell pattern is completely disorganized. The scale bar in (B) equals 0.5 cm and 20 µm in (E).

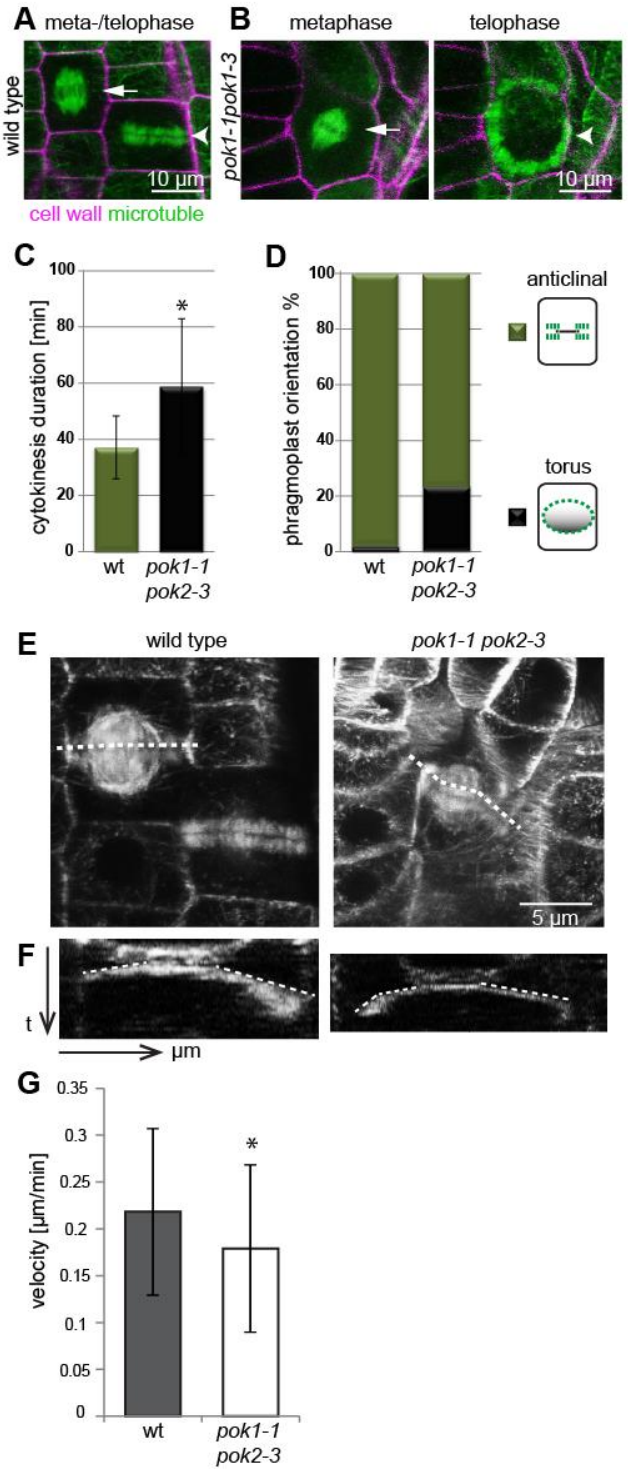

Figure 2: Duration of cytokinesis and orientation of phragmoplast expansion. Orientation of spindles (arrows) and phragmoplasts (arrowheads). (A) A wild type spindle and phragmoplast in a characteristic anticlinal orientation, with the phragmoplast expanding towards the lateral cell walls, perpendicular to the optical plane. (B) A *pok1-1pok2-3* mutant cell in metaphase (spindle) and the same cell during cytokinesis (phragmoplast). The spindle is slightly tilted. The phragmoplast expands in an oblique or periclinal orientation, thus presenting its torus. (C) The duration of phragmoplast expansion is significantly extended in *pok1-1 pok2-3* mutants (58 min ± 24, **P>0.01*, n= 17) compared to the wild type (wt, 37 min ± 11, n = 24). (D) In the wild type (wt, n = 49) 97.96% of the observed phragmoplasts displayed anticlinal orientation and only 2.04% were oriented with their torus parallel to the optical plane. In contrast, in *pok1-1 pok2-3* mutants (n = 43) the proportion of phragmoplasts presenting the torus (ring view) rises to 23.26%. (E) Projection of a time series throughout mitosis for wild type (45 min, 19 image stacks) and *pok1-1 pok2-3* mutants (60 min, 25 images). At 2.5 min intervals, image stacks were taken from mitotic cells at 1 µm z-intervals throughout the duration of mitosis. Maximum z-projections of each time point were projected for the depicted images. The white dotted lines indicate the selection for the kymograph analysis. (F) Space-time-plots (kymographs) of respective phragmoplasts depicted in (E). The x-coordinate depicts the distance in µm. The y-coordinate indicates the time t. The kymograph plugin in ImageJ was used to create kymographs and calculate the velocity of phragmoplast expansion. The slopes of the kymograph (contrast edge, selection is indicated by white dotted lines) are proportional to the velocity. In these examples, the two halves of the phragmoplasts expanded at different velocities. In addition, in one half the velocity decreased, indicated by the change in slope (2-phase expansion). (G) The average velocity of phragmoplast expansion is significantly reduced in *pok1-1 pok2-3* mutants (0.18 ± 0.09 µm/min; *P<0.02,* n = 22, Student *t*-test), compared to the expansion rate in the wild type (0.21 ± 0.09 µm/min; n = 43). Error bars indicate ± SD. Cell walls are stained with propidium iodide. Microtubules are visualized by GFP-MBD.

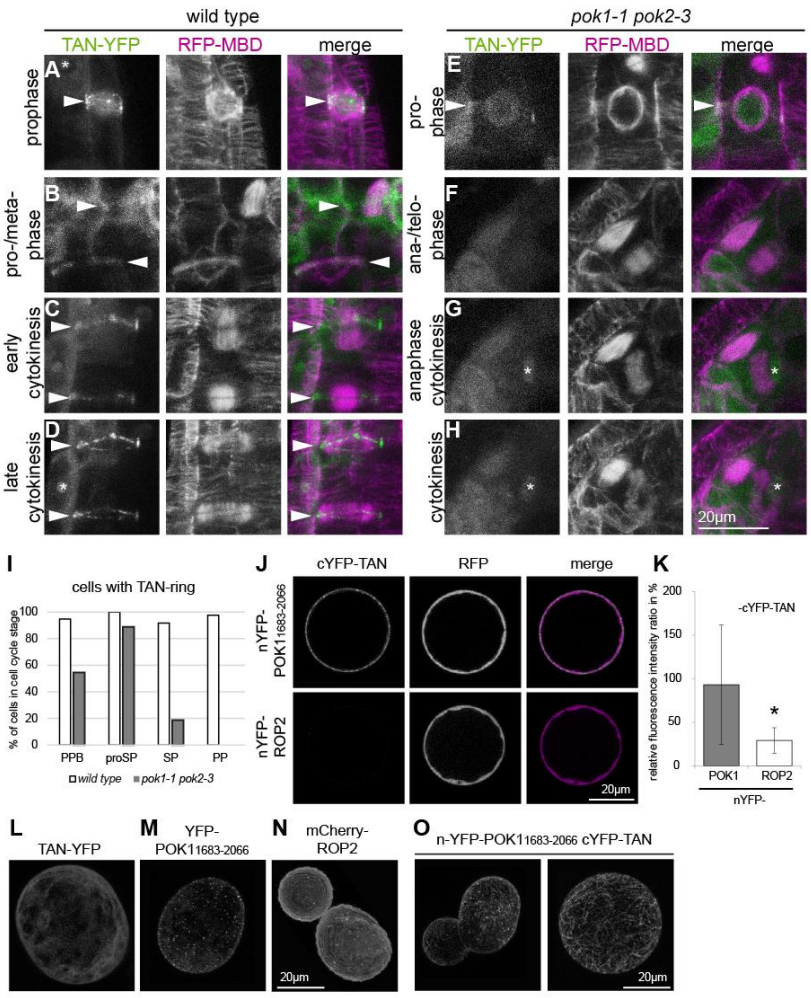

Figure 3: Loss of POK-dependent TAN localization at the cortical division zone correlates with PPB disassembly. TAN-YFP is recruited to the preprophase band in the wild type (A) and *pok1-1 pok2-3* double mutants (E). In the wild type, TAN-YFP rings co-exist with the preprophase band (A and B), pro-spindle (B), spindle (B), and early (C) and (D) late phragmoplasts. (E) Cell with pro-spindle displaying the TAN-YFP ring. (F) The spindle in the metaphase cell is not associated with cortical TAN-YFP, nor does the signal reappear during cytokinesis (F to H represent a time series). Images are z-projections of a varying number of images taken at 1 µm intervals. TAN-YFP rings are indicated by arrowheads. The nuclear localization of YFP-TAN is indicated by an asterisk. Scale bar is 10 µm. (I) Presence of TAN-YFP rings during the cell cycle in wild type and *pok1-1 pok2-3* mutants. (J to K) Interaction of TAN and the POK1 C-terminus, as determined by BiFC. (J) Confocal images of an *Arabidopsis thaliana* protoplast co-expressing nYFP-POK1$_{1683-2066}$ and cYFP-TAN, or nYFP-ROP2 and cYFP-TAN as negative controls. YFP fluorescence was specifically detected upon complementation of the fluorophore due to TAN and POK1$_{1683-2066}$ interaction in contrast to the control experiment. RFP, expressed from the same plasmid was used as an internal control. (K) Quantification of mean YFP fluorescence expressed as a ratio of mean RFP fluorescence. Data are means ± SD of 26 protoplasts per construct, each representing independent transformation events. The YFP/RFP ratio is significantly different (*P < 0.001, Student's t-test) between TAN/POK1$_{1683-2066}$ (interaction) and TAN/ROP2 (no interaction). (L to N) Localization of controls in protoplasts as indicated. Images are maximum z-projections of image stacks taken at 1 µm z-intervals. Scale bar indicates 20 µm. (L) Cytoplasmic localization upon expression of *Pro35S:TAN-YFP*. (M) Expression of *Pro35S:YFP-POK1$_{1613-2066}$* leads to punctate YFP signal in the plasma membrane similar to what is observed in *Arabidopsis thaliana* root meristem cells. (N) Expression of *pUB10:mCherry-ROP2*. (O) Examples of protoplasts co-expressing nYFP-POK1$_{1683-2066}$ and c-YFP-TAN. Images are maximum z-projections of images stacks taken at 1 µm z-intervals. Scale bar indicates 20 µm.

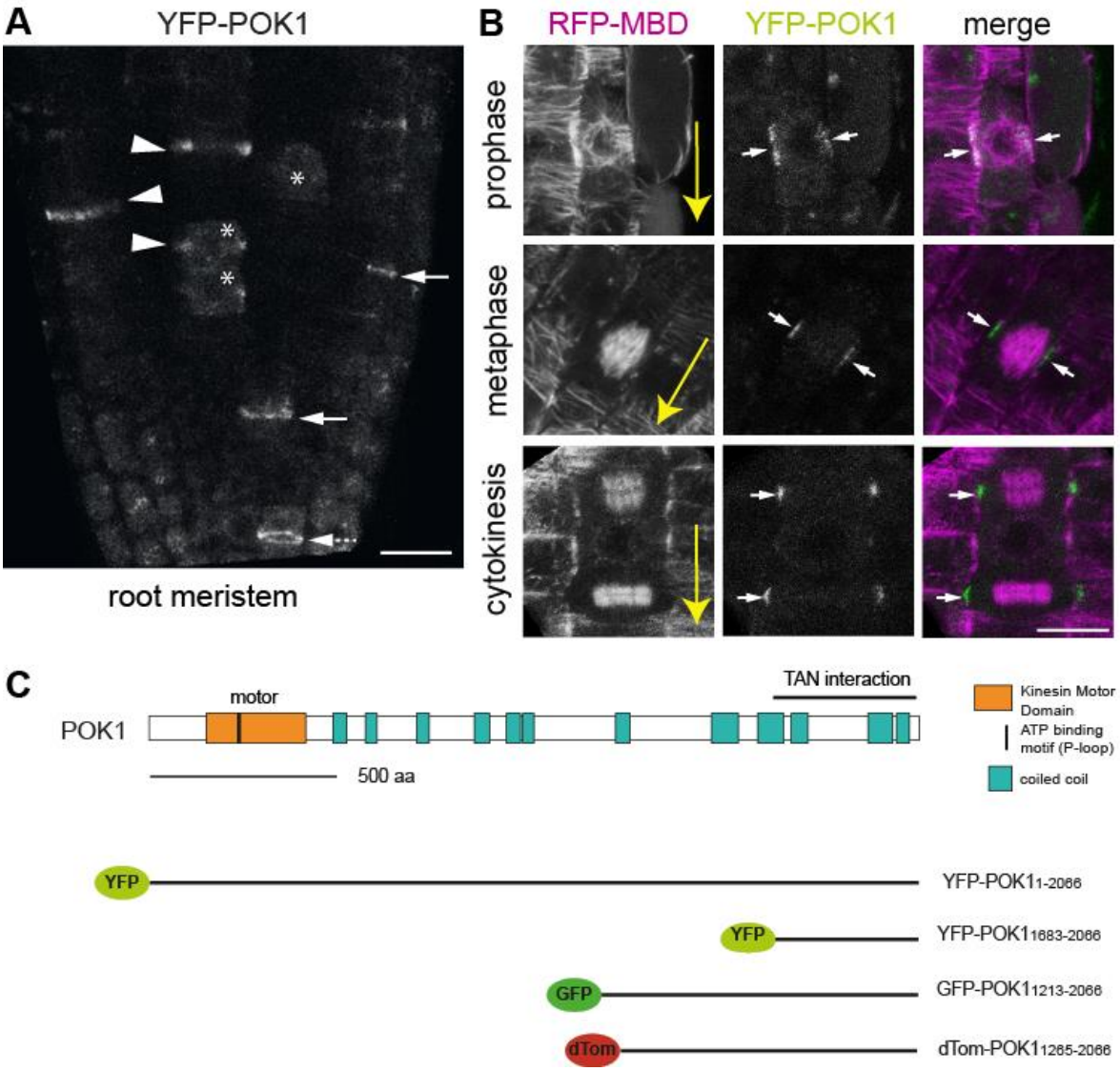

Figure 4: POK1 localizes at the cortical division zone/site. (A) Maximum z-projection of a root meristem expressing YFP-POK1. In cross sections, YFP-POK1 localizes as broad bands or dots (arrowheads) and sharp bands (arrows). Occasionally, YFP-POK1 rings are visible (arrow with dotted shaft). Some cells accumulate cytoplasmic YFP-POK1 (asterisk). (B) Co-expression of RFP-MBD and YFP-POK1 in different cell cycle stages in the root. YFP-POK1 co-localizes with the PPB in prophase and remains at the cell cortex throughout mitosis. Large yellow arrows indicate the longitudinal root axis. (C) POK1 domain organization as indicated in the legend and overview of fluorescent protein fusions used for localization studies. The POK1$_{1683-2066}$ fragment corresponds to the TAN-interacting fragment used in the BiFC experiment (Fig. 3J, 3K). Scale bar indicates 20 µm in (A) and 10 µm in (B).

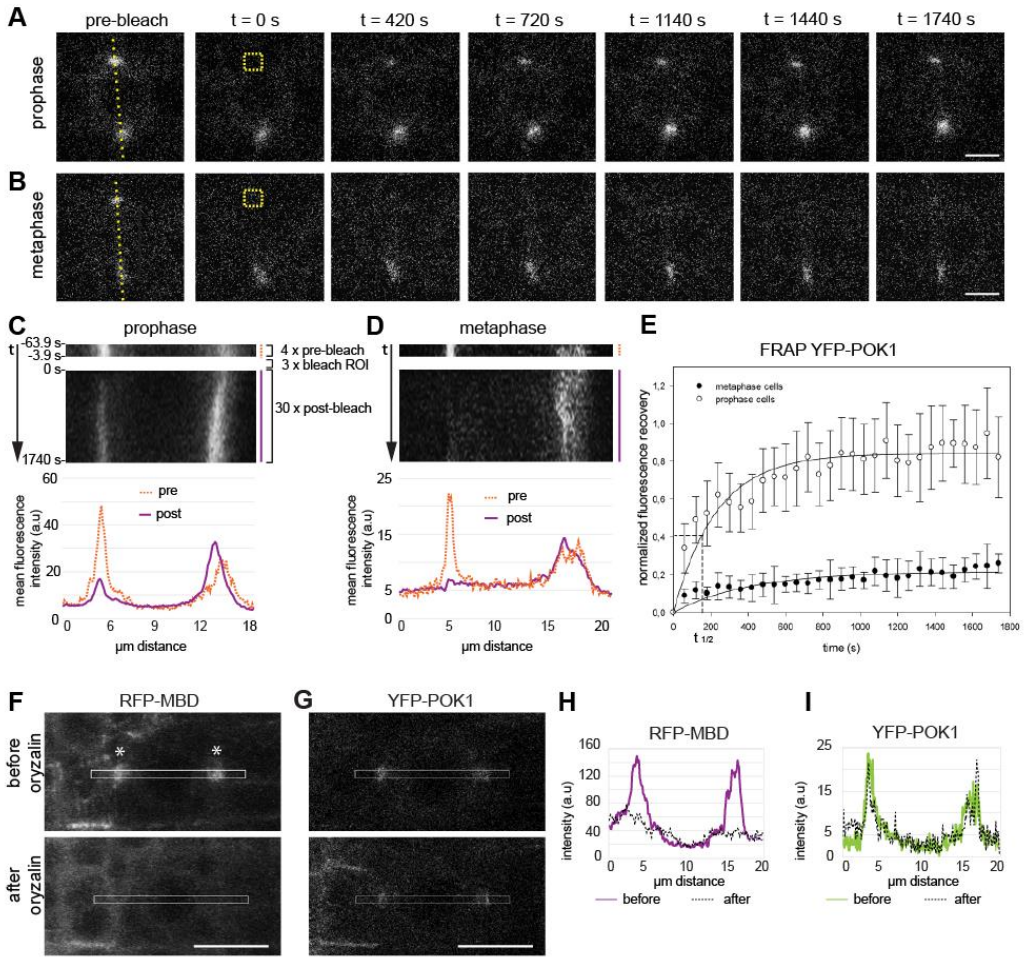

Figure 5: Differential POK1 dynamicity during mitosis. (A and B) Fluorescence Recovery After Photobleaching (FRAP) analysis of YFP-POK1. Representative time lapse of mitotic cells in the *Arabidopsis thalia*na root meristem. Transverse sections of (A) prophase and (B) metaphase cells recorded at different time points before (pre-bleach) and after photo-bleaching. Bleach regions are indicated by dashed square (region of interest, ROI) in first post-bleach images (t = 0 s). _Scale bar indicates 5µm. (C and D) Kymographs of pre-bleach and post-bleach time series corresponding to the dashed line selection as indicated in the pre-bleach images of (A) and (B). Pre-bleach kymograph (orange dashed line) of four pre-bleach images and post-bleach kymograph of 30 post-bleach images (magenta solid line) and corresponding profile plots are depicted. Profile plots show mean fluorescence intensities from the pre-bleach (orange dashed line) and post-bleach (magenta solid line) kymographs, respectively. Note the recovery of YFP signal in prophase. (E) An average of independent FRAP experiments is plotted to fit an exponential curve with rise to a maximum (y=a*(1-exp(-b*x))). In prophase cells (n=10), the YFP-POK1 signal recovers after photobleaching with a half time ($t_{1/2}$) of 154 s, while there is hardly any fluorescence recovery in metaphase cells (n=6). Error bars indicate ± SD. (F to I) POK1 localization at the cortical division zone is independent of microtubules (MT). Maximum z-projections of an *Arabidopsis thaliana* root meristem prophase cell co-expressing the microtubule (MT) reporter (F) RFP-MBD and (G) YFP-POK1 before and after treatment with 10 µM oryzalin. The PPB is indicated by asterisks. (F and G) Lower panels were recorded 15 min after oryzalin incubation and correspond to the cell in the upper panels. Due to MT de-polymerization, the RFP-MBD reporter localization becomes cytosolic, while the YFP-POK1 signal remains present at the CDZ. Scale bar indicates 10 µm. (H and I) Fluorescence intensity profile plots from a rectangular selection in (F and G) depicting (H) RFP-MBD signal distribution before oryzalin treatment (continuous, magenta line) and after oryzalin treatment (dashed, black line) and (I) YFP-POK1 signal distribution before (continuous, green line) and after (dashed, black line) oryzalin treatment. Note that the RFP-MBD peaks disappear after oryzalin treatment, while the YFP-POK1 peaks remain.

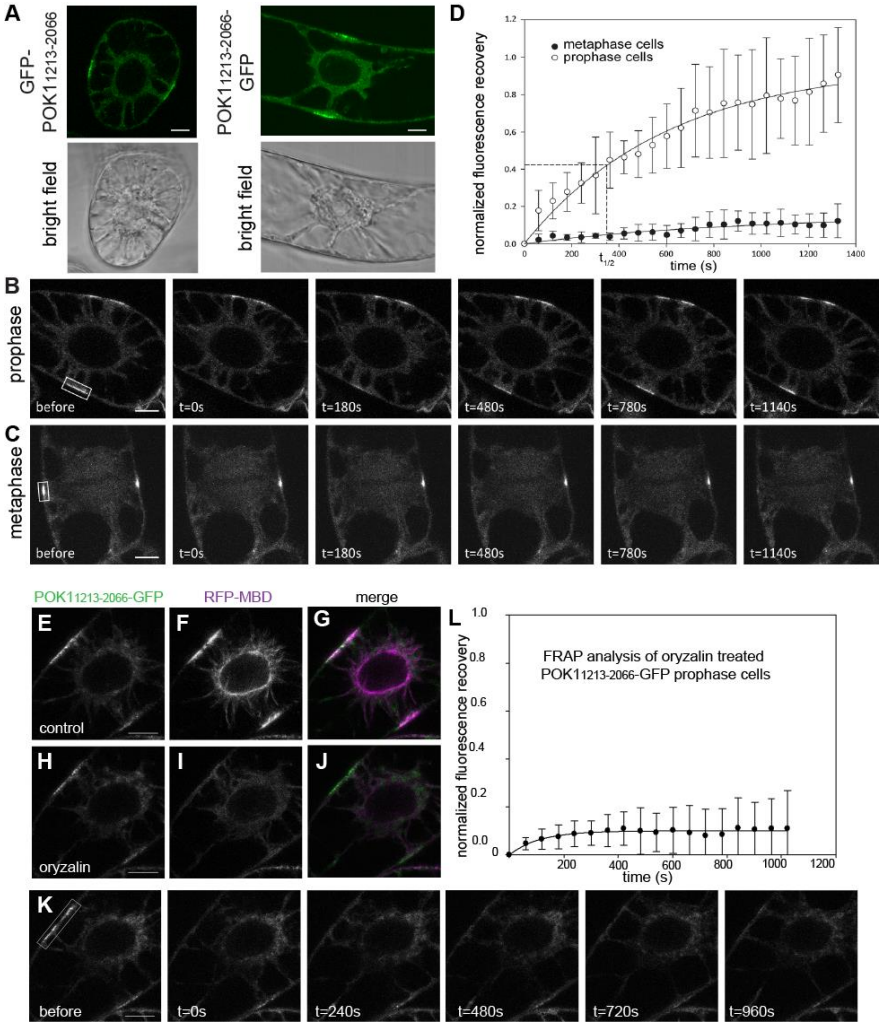

Figure 6: Changes of POK1 dynamicity during mitosis. (A) A tobacco BY-2 cell expressing *Pro35S:GFP-POK1*$_{1213-2066}$ and *Pro35S:POK1*$_{1213-2066}$-GFP) and the corresponding bright field image. Scale bar, 10 µm. (B to D) Fluorescence Recovery After Photobleaching (FRAP) analysis of GFP-POK1C. (B) Representative time lapse of a prophase BY-2 cell after photo-bleaching of GFP-POK1C at the preprophase band (PPB, white box indicates the bleached area). (C) Representative time lapse of a metaphase BY-2 cell after photobleaching the GFP-POK1 C-terminus at the cortical division zone (CDZ, indicated by white box). (D) Graph representing FRAP data for prophase and metaphase BY-2 cells overexpressing GFP-POK1$_{1213-2066}$. In prophase cells, the GFP-POK1 signal recovers slowly after photo-bleaching with a half time ($t_{1/2}$) of 362 s while there is hardly any fluorescence recovery in metaphase cells. An average of independent FRAP experiments is plotted to fit an exponential curve with rise to a maximum (y=a*(1-exp(-b*x))) (prophase cells: n=4; metaphase cells: n=7). Error bars indicate ± SD. (E to L) Recruitment of POK1C-GFP requires MTs, whereas PPB-localized POK1C-GFP statically associates with the CDZ independently of MTs in BY-2 cells. (E to J) Representative dividing BY-2 cell co-expressing the *Pro35S:RFP-MBD* MT marker and *Pro35S:POK1*$_{1213-2066}$*-GFP.* (E to G) POK1C-GFP co-localizes with the preprophase band (E, POK1C-GFP; F, RFP-MBD; G, merged image). (H to J) Upon oryzalin treatment, MTs depolymerize while POK1C-GFP remains associated with the CDZ (H, POK1C-GFP; I, RFP-MBD; J, merged image). (K) Representative time lapse of POK1C-GFP Fluorescence Recovery After Photobleaching (FRAP) performed on oryzalin-treated BY-2 cells in (E). In the absence of MTs, POK1C-GFP fluorescence did not recover at the bleached CDZ region. The bleached area is indicated by a white box. (L) Graph representing the FRAP experiments performed on oryzalin-treated prophase BY-2 cells co-expressing the *Pro35S:RFP-MBD* microtubule marker and *Pro35S:POK1*$_{1213-2066}$*-GFP* (n=6). GFP fluorescence did not recover at the CDZ upon MT depolymerization. Scale bar, 10 µm, error bars indicate ± SD.

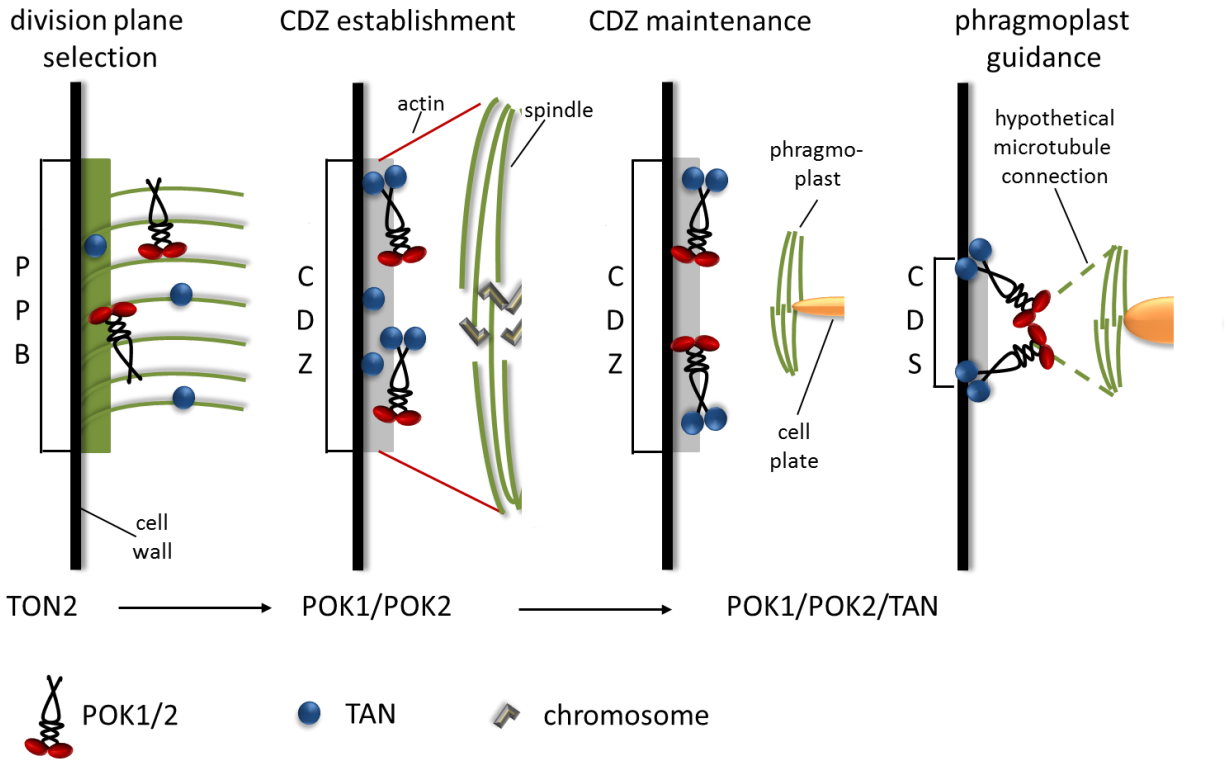

Figure 7: Schematic representation of cell cycle-dependent localization and function of POK1. In prophase cells, POK1 and TANGLED (TAN) are independently recruited to the TONNEAU (TON)2-dependent preprophase band (PPB). Upon metaphase, POK1 becomes immobilized at the cortical division zone (CDZ) and at the same time, TAN is tethered to the CDZ in a POK1/POK2-dependent manner, likely through direct binding to the C-terminus of POK1. Towards the end of cytokinesis, POK1 and TAN localization narrows to the exact site of cell plate anchoring at the parental wall, the cortical division site (CDS), via a yet unknown mechanism. Dashed line indicates hypothetical transient microtubules connecting the phragmoplast with the CDS at late cytokinesis (Supplemental Figure 6).

Table 1. Association of YFP-POK1 with the cortical division site is independent of microtubules. While microtubules disassembled, YFP-POK1 signal was not effected upon oryzalin treatment.

	RFP-MBD			YFP-POK1		
n = 8 roots	PPB	spindle	phragmoplast	PPB	spindle	phragmoplast
before oryzalin	10	5	15	8	4	20
after oryzalin	0	0	0	8	4	16

Suplemental Figures

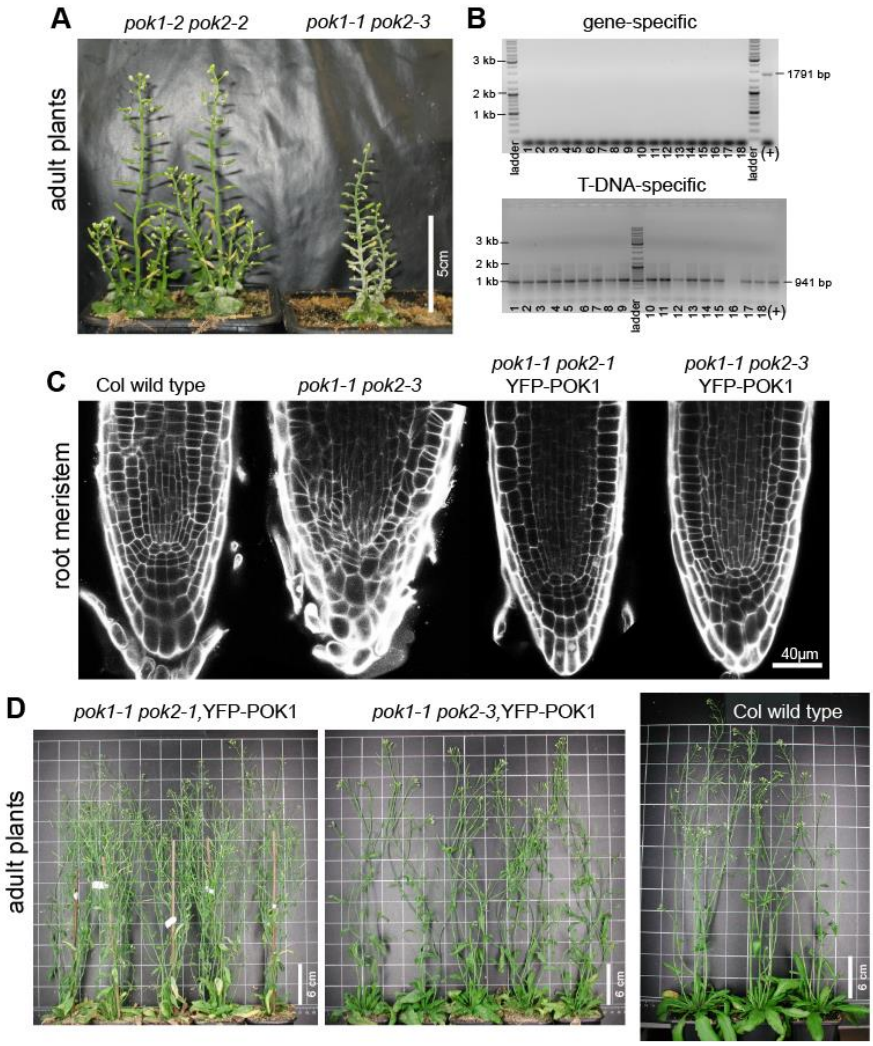

Supplementary Figure 1. Adult phenotype of *pok1 pok2* and rescue with YFP-POK1. (**A**) Comparison of 8-week-old dwarfed phenotypes of *pok1-2 pok2-2* and *pok1-1 pok2-3* double mutant plants showing the aggravated phenotype of the new allele combination. The developmental stage corresponds to the Col wild type plants in (**D**). (**B**) Gel electrophoresis of polymerase chain reaction (PCR) products. For PCR-based genotyping of a segregating F2 population (*pok1-1 pok2-3* x Col, BC1), DNA samples were prepared from phenotypically mutant plants. The presence of the 1791-bp PCR fragment using POK1-3491-F and POK1-SpeI-R (Supplemental table 1) indicates gene-specific amplification of genomic *POK1*, while the amplification of the 941-bp PCR fragment using POK1-3491-F and LBa1 (Supplemental table 1) indicates the presence of the T-DNA-specific insertion in the *POK1* locus. For all samples, except for # 16, which was of low quality, T-DNA-specific, but not gene-specific PCR fragments were amplified, indicating that the *pok1-1* T-DNA allele co-segregated with the mutant phenotype. (**C**) Confocal sections of seedling root meristems from different genotypes stained with propidium iodide. Expression of *ProPOK1:YFP-gPOK1* (YFP-POK1) in double mutants *pok1-1 pok2-1* and *pok1-1 pok2-3* restores the (wild type) phenotype indicating functional redundancy between POK1 and POK2. (**D**) Adult *pok1-1 pok2-1* and *pok1-1 pok2-3* mutants expressing YFP-POK1 show normal growth and development, comparable to adult Col wild type plants.

S

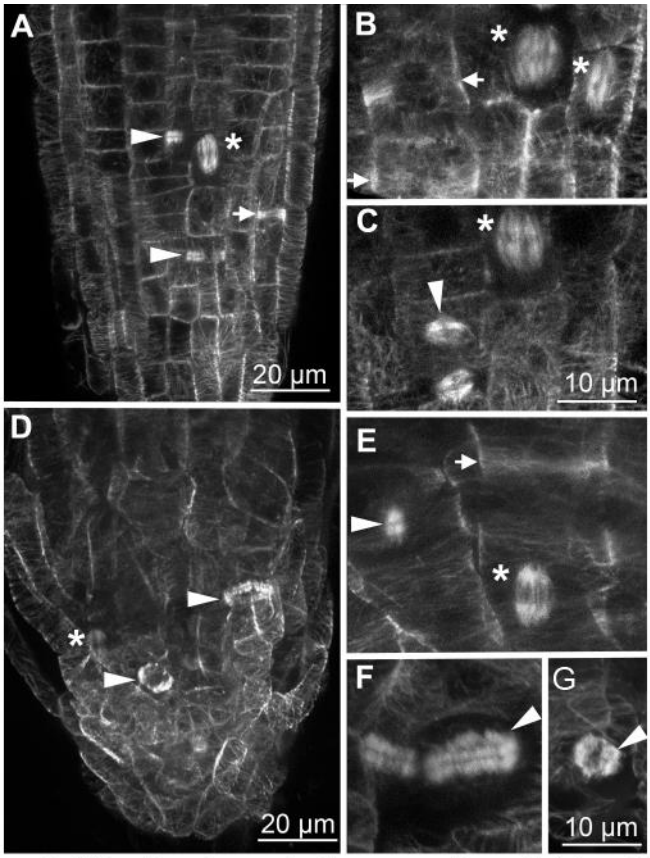

Supplementary Figure 2. Mitotic microtubule arrays in *pok1-1 pok2-3* mutants.
In vivo observations of mitotic microtubule (MT) arrays in the wild type (**A** to **C**) and *pok1-1 pok 2-3* mutants (**D** to **F**), expressing the MT reporter GFP-MBD. (**A**) Maximum Z-projection overview and (**B**, **C**) close up of mitotic cells in the wild type. (**D**) Maximum Z-projection and (**E** to **G**) close up of mitotic *pok1-1 pok2-3* cells. Arrows indicate preprophase bands (PPB). Spindles are indicated by asterisks and phragmoplasts are marked by arrowheads. Scale bars in (**A**) and (**D**) are 20 µm. Scale bars in (**B, C, E, F**) and (**G**) are 10 µm.

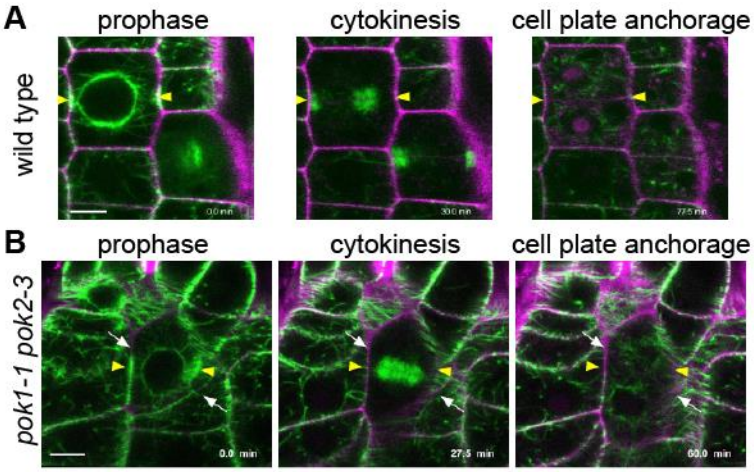

Supplementary Figure 3. Cell cycle progression. (**A**) Selected stages of cell cycle progression in the wild type. Images correspond to Supplemental movie 1 as indicated by the time stamps. Note that the position of the preprophase band and the phragmoplast/cell plate co-align (yellow arrowheads). (**B**) Selected stages of the cell cycle progression in *pok1-1 pok2-3* double mutant. Images correspond to Supplemental movie 2 as indicated by the time stamps. Note that the orientation of the preprophase band (yellow arrowheads) and the phragmoplast/cell plate (white arrows) do not match. Microtubules are visualized by GFP-MBD and indicated in green. Cell shape visualized by propidium iodide is shown in magenta. Scale bars indicate 5 µm.

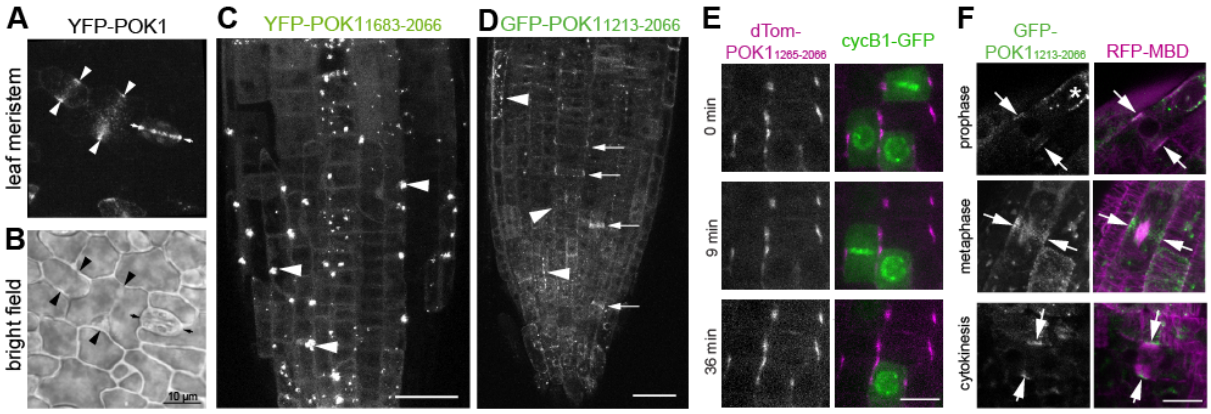

Supplementary Figure 4. Subcellular localization of different fluorescent POK1-fusions. (**A** and **B**) Expression of full length YFP-POK1 in young leaves. (**A**) Maximum z-projection of cells expressing full-length YFP-POK1. Broad bands (arrowheads) and sharp bands (arrow) are distinguishable. (**B**) bright field image corresponding to (**A**). (**C** and **D**) Overview of root meristems expressing either (**C**) *Pro35S:YFP-POK1*$_{1683-2066}$ or (**D**) *Pro35S:GFP-POK1*$_{1213-2066}$. (**C**) Arrowheads indicate YFP-POK1$_{1683-2066}$ aggregates. (**D**) Arrows indicate GFP-POK1$_{1213-2066}$ localization in mitotic cells. Note that aggregates are less prominent and smaller (arrowheads). Scale bar is 50 µm. (**E** and **F**) POK1-C terminus is sufficient for localization at the cortical division zone/site. (**E**) Time series of cells co-expressing dTom-POK1$_{1265-2066}$ (magenta) and cycB1-GFP. cycB1-GFP associates with nuclei in prophase and with chromosomes in metaphase. During the time course, transition of cycB1-GFP fluorescence indicates cell cycle progression. dTom-POK1$_{1265-2066}$ is present at the cortical division zone at prophase and remains at the site beyond metaphase. (**E**) GFP-POK1$_{1213-2066}$ localization is similar to that of YFP-POK1. Left panel: Close up of prophase, metaphase and cytokinetic cells in cross sections, exhibiting characteristic fluorescent foci on lateral cell membranes (arrows). Right panel: Color merge of cells depicted in upper panel (green) and microtubule marker RFP-MBD (magenta). Asterisk indicates small aggregates present in the *Pro35S:GFP-POK1*$_{1213-2066}$ expressing line. Scale bar indicates 10 µm in (**E** and **F**).

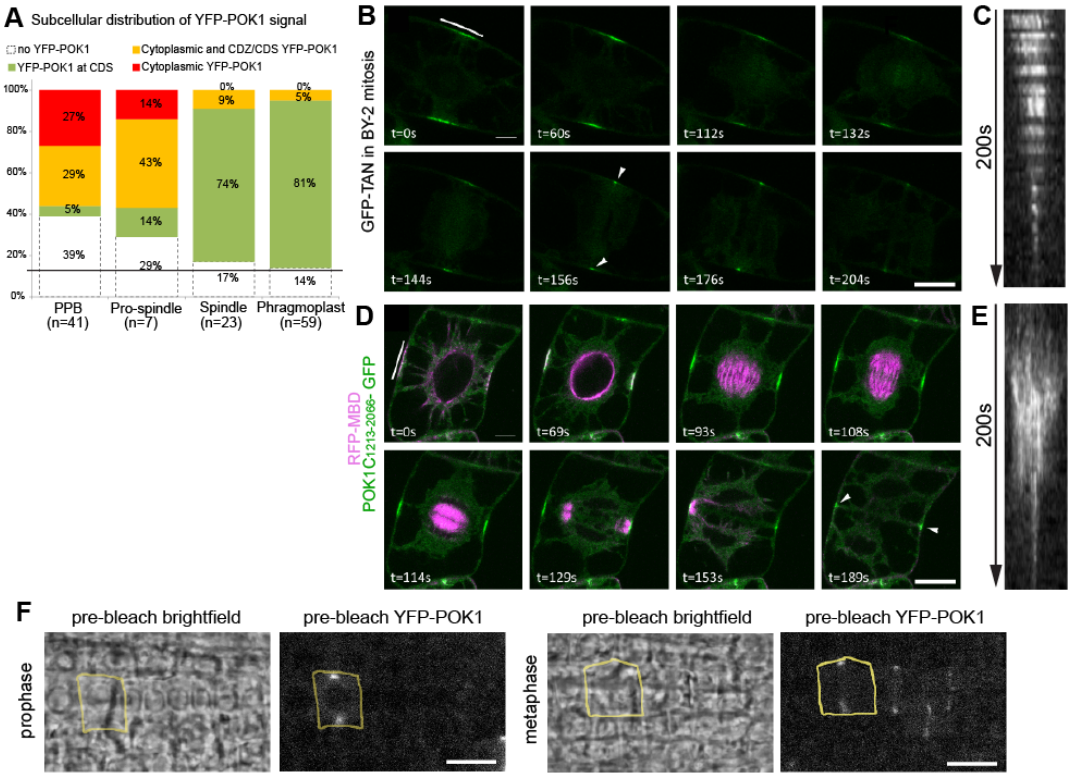

Supplementary Figure 5. Subcellular distribution of YFP-POK1 signal in *Arabidopsis* mitotic cells. (A) YFP-POK1 subcellular signal shifts from cytoplasmic to CDZ/CDS associated during the course of mitosis; (n) indicates the number of observed cells per cell cycle stage. Cells with PPBs frequently displayed both cytoplasmic and cortical YFP-POK1 in the same cell (29%), while a similar proportion (27%) of prophase cells displayed solely cytoplasmic YFP-POK1. Only a minority of prophase cells exclusively displayed YFP-POK1 at the CDS (5%) and the majority of cells with PPBs did not show any YFP-POK1 (39%). In cells with pro-spindles, the co-occurrence of both cytoplasmic and cortical YFP-POK1 rose to 43%, concurrent with the proportion of cells displaying only CDZ YFP-POK1 (14%). By contrast, fewer cells contained either cytoplasmic YFP-POK1 (14%) or no YFP-POK1 signal (29%). Cortical YFP-POK1 was prevalent in cells with spindles (74%) and in cells with phragmoplasts (81%), while in another 9% of cells with spindles and 5% of cells with phragmoplasts cytosolic YFP-POK1 and cortical YFP-POK1 signal were observed concurrently. No YFP-POK1 signal was present in 17% of cells with spindles and 14% of cells containing phragmoplasts (15.5% on average). We assume that this percentage reflects the margin of error for all cells that are expected to display YFP-POK1, but that we failed to detect due to low transgene expression or insufficient detection sensitivity. The number of cells per cell cycle stage is indicated (qualifies "number"). Narrowing of TAN band width during BY-2 mitosis. (**B**) Time lapse of a dividing BY-2 cell expressing *Pro35S:GFP-TAN.* GFP-TAN accumulates at the CDZ from (pre)prophase to cytokinesis. As mitosis progresses, GFP fluorescence gradually narrows from a broad band at the CDZ to a punctate ring corresponding to the CDS (arrowheads), which is illustrated by a kymograph (**C**) along the CDZ membrane (white line in **B**). (**D**) Time lapse of a dividing BY-2 cell co-expressing the *Pro35S:POK1*$_{1213-2066}$-GFP (green) and the microtubule marker *Pro35S:RFP-MBD* (magenta). (**D**) POK1-GFP co-localizes with the preprophase band and persists at the CDZ membrane after PPB disassembly. POK1C-GFP fluorescence also gradually narrows from the CDZ to the CDS (arrowheads) upon cell plate anchoring, as demonstrated by a kymograph (**E**) along the plasma membrane (white line in **D**). Scale bar, 10 µm. (**F**) Maximum Z-projection of the pre-bleach images (bright field and YFP-POK1) taken during the FRAP experiments depicted in Figure 5A and 5B. The respective cells are outlined as indicated by the yellow selection in the images. Note that cells in interphase or prophase show distinct nuclei in bright field. Scale bar indicates 10 µm in panels (**B**, **D** and **F**).

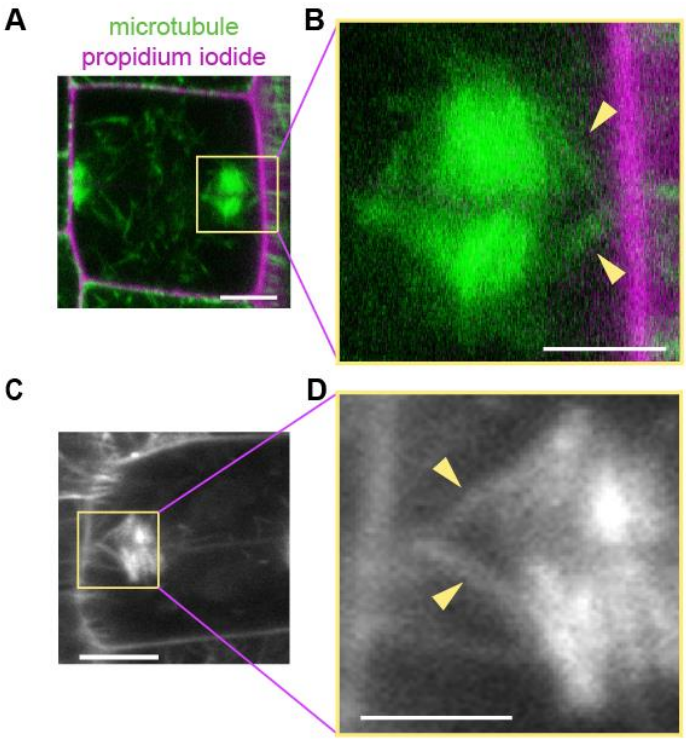

Supplementary Figure 6. Examples of transient microtubules reaching from the phragmoplast towards the putative cortical division site. (**A** and **C**) Cells in late cytokinesis with the phragmoplast approaching the parental cell wall (visualized with propidium iodide in magenta in (**A** and **B**) and in gray scale in (**B** and **D**). Microtubules originating from the phragmoplast extend towards the parental wall (indicated by arrowheads). (**B** and **D**) depict magnification of boxed areas in (**A** and **C** respectively). Scale bars indicate 5μm in (**A** and **C**) and 2.5 μm in (**B** and **D**).

Table S1 Primers used for cloning full length YFP-POK1 and genotyping of pok1-1.

POK1 homology sites are indicated in small italic font.
Oligo name *5'-3'* sequence

Venus-FgFPOK1 F
*ttattcttcccggttggtgaaagagaccacaagctacttctcgatctacc*ATGGTGAGCAAGGGCGAGGAGC
TGTTC
FgF-POK1 R
*aactcgttttcttccgattccggcatctctattctcggaacgtttcgggacat*GAAGTTCCTATTCTCTAGAAAGT
ATAGGAACTTCGCGGCCGC

p500-POK1	agttgatattattgacaccaccac
POK1-699-R	caagtgttcgttgatgctg
POK1-3491-F	gtcactgtcaggtgcataattc
POK1-SpeI-R	tcactagtgcacctctatcatag
LBa1	tggttcacgtagtgggccatcg

Table S2. List of primers used for cloning 2in1 plasmids.

The attB recombination sites present in the oligo sequence are indicated in italic.
Oligo name *5'-3'* sequence

attB1 TAN *ggggacaagtttgtacaaaaaagcaggctta*ATGGTTGCAAGAACCCCAC
AGAAGCA

attB4 TAN_r *ggggacaactttgtatagaaaagttgggtg*CTACACTTTCCTGCTCTTCATTG
GA

attB3
POK1Cshort
*ggggacaactttgtataataaagttgta*ATGGATGAAGAAGTAAAAAGGCAT
CGT

attB2 POK1C_r *ggggaccactttgtacaagaaagctgggtt*TTACCGATATCTTGTACCAGAG
CT

attB3 ROP2 *ggggacaactttgtataataaagttgta*ATGGCGTCAAGGTTTATAAAGTGT

attB2 ROP2 r *ggggaccactttgtacaagaaagctgggtt*TCACAAGAACGCGCAACGGTT
CTT

Table S3. List of primers used for cloning.

The attB recombination sites present inthe oligo sequence are indicated in italic.
Oligo name *5'-3'* sequence

minB1F-TAN *aaaaagcaggctccacc*ATGGTTGCAAGAACCCCACAGAAGC

minB2R-TAN stop *agaaagctgggtc*CTACACTTTCCTGCTCTTCATTGG

minB2R-TAN no stop *agaaagctgggtc*CACTTTCCTGCTCTTCATTGG

minB1F-POK1C *aaaaagcaggctccacc*ATGGGTCTTATGCAGAGAATGG

minB2R-POK1C stop *agaaagctgggtc*TTACCGATATCTTGTACCAGAGCT

minB2R-POK1C no stop *agaaagctgggtc*CCGATATCTTGTACCAGAGCTCTG

B1F GGGGACAAGTTTGTACAAAAAAGCAGGCTCCACC

B2R GGGGACCACTTTGTACAAGAAAGCTGGGTC

TP1-B4-SE GGGGACAACTTTGTATAGAAAAGTTGGTACCTACGTAG CCCAACACTCGAATCC

TP1-B1R-AN *ggggctgctttttgtacaaacttgcgctagcggtcg*CTTATTGATTGTTTT CTCTCTCC

B2R-POK1C-1265 *ggggacagctttcttgtacaaagtggatc*ATGAAGAGTTAATAAGTAA GG

B3-POK1C-1265 *ggggacaactttgtataataaagttga*TTACCGATATCTTGTACCAG AG

References

Azimzadeh, J., Nacry, P., Christodoulidou, A., Drevensek, S., Camilleri, C., Amiour, N., Parcy, F., Pastuglia, M., and Bouchez, D. (2008). Arabidopsis TONNEAU1 proteins are essential for preprophase band formation and interact with centrin. Plant Cell **20,** 2146-2159.

Barr, F.A., and Gruneberg, U. (2007). Cytokinesis: Placing and Making the Final Cut. Cell **131,** 847-860.

Basu, D., Le, J., Zakharova, T., Mallery, E.L., and Szymanski, D.B. (2008). A SPIKE1 signaling complex controls actin-dependent cell morphogenesis through the heteromeric WAVE and ARP2/3 complexes. Proceedings of the National Academy of Sciences of the United States of America **105,** 4044-4049.

Bement, W.M., Benink, H.A., and von Dassow, G. (2005). A microtubule-dependent zone of active RhoA during cleavage plane specification. J Cell Biol **170,** 91-101.

Benzing, T., Yaffe, M.B., Arnould, T., Sellin, L., Schermer, B., Schilling, B., Schreiber, R., Kunzelmann, K., Leparc, G.G., Kim, E., and Walz, G. (2000). 14-3-3 interacts with regulator of G protein signaling proteins and modulates their activity. Journal of Biological Chemistry.

Berry, R.W., and Shelanski, M.L. (1972). Interactions of tubulin with vinblastine and guanosine triphosphate. Journal of Molecular Biology **71,** 71-80.

Blanchoin, L., and Michelot, A. (2012). Actin Cytoskeleton: A Team Effort during Actin Assembly. Current Biology **22,** R643-R645.

Blazquez, M.A., Soowal, L.N., Lee, I., and Weigel, D. (1997). LEAFY expression and flower initiation in Arabidopsis. Development **124,** 3835-3844.

Bos, J.L., Rehmann, H., and Wittinghofer, A. (2007). GEFs and GAPs: Critical Elements in the Control of Small G Proteins. Cell **129,** 865-877.

Bourne, H.R., Sanders, D.A., and McCormick, F. (1990). The GTPase superfamily: a conserved switch for diverse cell functions. Nature **348,** 125-132.

Brembu, T., Winge, P., and Bones, A.M. (2005). The small GTPase AtRAC2/ROP7 is specifically expressed during late stages of xylem differentiation in Arabidopsis. J Exp Bot **56,** 2465-2476.

Camilleri, C., Azimzadeh, J., Pastuglia, M., Bellini, C., Grandjean, O., and Bouchez, D. (2002). The Arabidopsis TONNEAU2 gene encodes a putative novel protein phosphatase 2A regulatory subunit essential for the control of the cortical cytoskeleton. Plant Cell **14,** 833-845.

Cartwright, H.N., Humphries, J.A., and Smith, L.G. (2009). PAN1: a receptor-like protein that promotes polarization of an asymmetric cell division in maize. Science **323,** 649-651.

Chang, F., Gu, Y., Ma, H., and Yang, Z. (2013). AtPRK2 Promotes ROP1 Activation via RopGEFs in the Control of Polarized Pollen Tube Growth. Molecular Plant **6,** 1187-1201.

Cleary, A.L., Gunning, B.E.S., Wasteneys, G.O., and Hepler, P.K. (1992). Microtubule and F-actin dynamics at the division site in living Tradescantia stamen hair cells. Journal of Cell Science **103,** 977-988.

Clough, S.J., and Bent, A.F. (1998). Floral dip: a simplified method for Agrobacterium-mediated transformation of Arabidopsis thaliana. Plant J **16,** 735-743.

Craddock, C., Lavagi, I., and Yang, Z. (2012). New insights into Rho signaling from plant ROP/Rac GTPases. Trends Cell Biol **22,** 492-501.

Denison, F.C., Paul, A.-L., Zupanska, A.K., and Ferl, R.J. (2011). 14-3-3 proteins in plant physiology. Seminars in Cell & Developmental Biology **22,** 720-727.

Earley, K.W., Haag, J.R., Pontes, O., Opper, K., Juehne, T., Song, K., and Pikaard, C.S. (2006). Gateway-compatible vectors for plant functional genomics and proteomics. Plant J **45,** 616-629.

Etienne-Manneville, S., and Hall, A. (2002). Rho GTPases in cell biology. Nature **420,** 629-635.

Fu, Y., Li, H., and Yang, Z. (2002). The ROP2 GTPase controls the formation of cortical fine F-actin and the early phase of directional cell expansion during Arabidopsis organogenesis. Plant Cell **14,** 777-794.

Fu, Y., Gu, Y., Zheng, Z., Wasteneys, G., and Yang, Z. (2005). Arabidopsis Interdigitating Cell Growth Requires Two Antagonistic Pathways with Opposing Action on Cell Morphogenesis. Cell **120,** 687-700.

Fu, Y., Xu, T., Zhu, L., Wen, M., and Yang, Z. (2009). A ROP GTPase signaling pathway controls cortical microtubule ordering and cell expansion in Arabidopsis. Curr Biol **19,** 1827-1832.

Geelen, D.N., and Inze, D.G. (2001). A bright future for the bright yellow-2 cell culture. Plant Physiol **127,** 1375-1379.

Grefen, C., and Blatt, M.R. (2012). A 2in1 cloning system enables ratiometric bimolecular fluorescence complementation (rBiFC). BioTechniques **53,** 311-314.

Grefen, C., Donald, N., Hashimoto, K., Kudla, J., Schumacher, K., and Blatt, M.R. (2010). A ubiquitin-10 promoter-based vector set for fluorescent protein tagging facilitates temporal stability and native protein distribution in transient and stable expression studies. Plant J **64,** 355-365.

Gross-Hardt, R., Kagi, C., Baumann, N., Moore, J.M., Baskar, R., Gagliano, W.B., Jurgens, G., and Grossniklaus, U. (2007). LACHESIS restricts gametic cell fate in the female gametophyte of Arabidopsis. PLoS Biol **5,** e47.

Gu, Y., Fu, Y., Dowd, P., Li, S., Vernoud, V., Gilroy, S., and Yang, Z. (2005). A Rho family GTPase controls actin dynamics and tip growth via two counteracting downstream pathways in pollen tubes. J Cell Biol **169,** 127-138.

Hauser, M.-T., and Bauer, E. (2000). Histochemical analysis of root meristem activity in Arabidopsis thaliana using a cyclin:GUS (β-glucuronidase) marker line. Plant and Soil **226,** 1-10.

Heasman, S.J., and Ridley, A.J. (2008). Mammalian Rho GTPases: new insights into their functions from in vivo studies. Nat Rev Mol Cell Biol **9,** 690-701.

Heng, Y.W., and Koh, C.G. (2010). Actin cytoskeleton dynamics and the cell division cycle. The international journal of biochemistry & cell biology **42,** 1622-1633.

Hruz, T., Laule, O., Szabo, G., Wessendorp, F., Bleuler, S., Oertle, L., Widmayer, P., Gruissem, W., and Zimmermann, P. (2008). Genevestigator V3: A Reference Expression Database for the Meta-Analysis of Transcriptomes. Advances in Bioinformatics **2008,** 5.

Huang, J.B., Liu, H., Chen, M., Li, X., Wang, M., Yang, Y., Wang, C., Huang, J., Liu, G., Liu, Y., Xu, J., Cheung, A.Y., and Tao, L.Z. (2014). ROP3 GTPase contributes to polar auxin transport and auxin responses and is important for embryogenesis and seedling growth in Arabidopsis. Plant Cell **26,** 3501-3518.

Humphries, J.A., Vejlupkova, Z., Luo, A., Meeley, R.B., Sylvester, A.W., Fowler, J.E., and Smith, L.G. (2011). ROP GTPases act with the receptor-like protein PAN1 to polarize asymmetric cell division in maize. Plant Cell **23,** 2273-2284.

Hussey, P.J., Ketelaar, T., and Deeks, M.J. (2006). Control of the actin cytoskeleton in plant cell growth. Annu Rev Plant Biol **57,** 109-125.

Hwang, J.U., Jeon, B.W., Hong, D., and Lee, Y. (2011). Active ROP2 GTPase inhibits ABA- and CO2-induced stomatal closure. Plant, cell & environment **34,** 2172-2182.

Hwang, J.U., Vernoud, V., Szumlanski, A., Nielsen, E., and Yang, Z. (2008). A tip-localized RhoGAP controls cell polarity by globally inhibiting Rho GTPase at the cell apex. Curr Biol **18,** 1907-1916.

Hwang, J.U., Wu, G., Yan, A., Lee, Y.J., Grierson, C.S., and Yang, Z. (2010). Pollen-tube tip growth requires a balance of lateral propagation and global inhibition of Rho-family GTPase activity. J Cell Sci **123,** 340-350.

Inoue, S., and Salmon, E.D. (1995). Force generation by microtubule assembly/disassembly in mitosis and related movements. Mol Biol Cell **6,** 1619-1640.

Jacobs, M., Smith, H., and Taylor, E.W. (1974). Tubulin: Nucleotide binding and enzymic activity. Journal of Molecular Biology **89,** 455-468.

Jeon, B.W., Hwang, J.U., Hwang, Y., Song, W.Y., Fu, Y., Gu, Y., Bao, F., Cho, D., Kwak, J.M., Yang, Z., and Lee, Y. (2008). The Arabidopsis small G protein ROP2 is activated by light in guard cells and inhibits light-induced stomatal opening. Plant Cell **20,** 75-87.

Kawashima, T., Maruyama, D., Shagirov, M., Li, J., Hamamura, Y., Yelagandula, R., Toyama, Y., and Berger, F. (2014). Dynamic F-actin movement is essential for fertilization in Arabidopsis thaliana. eLife **3**.

Kirik, A., Ehrhardt, D.W., and Kirik, V. (2012). TONNEAU2/FASS regulates the geometry of microtubule nucleation and cortical array organization in interphase Arabidopsis cells. Plant Cell **24,** 1158-1170.

Klahre, U., and Kost, B. (2006). Tobacco RhoGTPase ACTIVATING PROTEIN1 spatially restricts signaling of RAC/Rop to the apex of pollen tubes. Plant Cell **18,** 3033-3046.

Kojo, K.H., Higaki, T., Kutsuna, N., Yoshida, Y., Yasuhara, H., and Hasezawa, S. (2013). Roles of cortical actin microfilament patterning in division plane orientation in plants. Plant Cell Physiol **54,** 1491-1503.

Korn, E.D., Carlier, M.F., and Pantaloni, D. (1987). Actin polymerization and ATP hydrolysis. Science **238,** 638-644.

Kost, B., Lemichez, E., Spielhofer, P., Hong, Y., Tolias, K., Carpenter, C., and Chua, N.H. (1999). Rac homologues and compartmentalized phosphatidylinositol 4, 5-bisphosphate act in a common pathway to regulate polar pollen tube growth. J Cell Biol **145,** 317-330.

Lauster, T. (2013). Charakterisierung von gap1gap2 und gap1gap2rop6 Mutanten und Analyse der Genexpression von GAP2 sowie der Lokalisation von ROP6 und RIC1 in Arabidopsis thaliana

Bachelorarbeit der Mathematischen-Naturwissenschaftlichen Fakultät der Eberhard Karls Universität Tübingen

Le, J., Mallery, E.L., Zhang, C., Brankle, S., and Szymanski, D.B. (2006). Arabidopsis BRICK1/HSPC300 Is an Essential WAVE-Complex Subunit that Selectively Stabilizes the Arp2/3 Activator SCAR2. Current Biology **16,** 895-901.

Lee, Y.J., Szumlanski, A., Nielsen, E., and Yang, Z. (2008). Rho-GTPase–dependent filamentous actin dynamics coordinate vesicle targeting and exocytosis during tip growth. The Journal of Cell Biology **181,** 1155-1168.

Li, H., Wu, G., Ware, D., Davis, K.R., and Yang, Z. (1998). Arabidopsis Rho-related GTPases: differential gene expression in pollen and polar localization in fission yeast. Plant Physiol **118,** 407-417.

Lin, D., Cao, L., Zhou, Z., Zhu, L., Ehrhardt, D., Yang, Z., and Fu, Y. (2013). Rho GTPase Signaling Activates Microtubule Severing to Promote Microtubule Ordering in Arabidopsis. Current Biology **23,** 290-297.

Lin, D., Nagawa, S., Chen, J., Cao, L., Chen, X., Xu, T., Li, H., Dhonukshe, P., Yamamuro, C., Friml, J., Scheres, B., Fu, Y., and Yang, Z. (2012). A ROP GTPase-dependent auxin signaling pathway regulates the subcellular distribution of PIN2 in Arabidopsis roots. Curr Biol **22,** 1319-1325.

Lin, Y., and Yang, Z. (1997). Inhibition of Pollen Tube Elongation by Microinjected Anti-Rop1Ps Antibodies Suggests a Crucial Role for Rho-Type GTPases in the Control of Tip Growth. Plant Cell **9,** 1647-1659.

Lipka, E., Herrmann, A., and Mueller, S. (2015). Mechanisms of plant cell division. Wiley interdisciplinary reviews. Developmental biology.

Lipka, E., Gadeyne, A., Stockle, D., Zimmermann, S., De Jaeger, G., Ehrhardt, D.W., Kirik, V., Van Damme, D., and Muller, S. (2014). The Phragmoplast-Orienting Kinesin-12 Class Proteins Translate the Positional Information of the Preprophase Band to Establish the Cortical Division Zone in Arabidopsis thaliana. Plant Cell **26,** 2617-2632.

Marc, J., Granger, C.L., Brincat, J., Fisher, D.D., Kao, T., McCubbin, A.G., and Cyr, R.J. (1998). A GFP-MAP4 reporter gene for visualizing cortical microtubule rearrangements in living epidermal cells. Plant Cell **10,** 1927-1940.

Mathur, J. (2005). The ARP2/3 complex: giving plant cells a leading edge. Bioessays **27,** 377-387.

Mitchison, T., and Kirschner, M. (1984). Dynamic instability of microtubule growth. Nature **312,** 237-242.

Molendijk, A.J., Bischoff, F., Rajendrakumar, C.S.V., Friml, J., Braun, M., Gilroy, S., and Palme, K. (2001). Arabidopsis thaliana Rop GTPases are localized to tips of root hairs and control polar growth. The EMBO Journal **20,** 2779-2788.

Mucha, E., Fricke, I., Schaefer, A., Wittinghofer, A., and Berken, A. (2011). Rho proteins of plants – Functional cycle and regulation of cytoskeletal dynamics. European Journal of Cell Biology **90,** 934-943.

Muller, S., Han, S., and Smith, L.G. (2006). Two kinesins are involved in the spatial control of cytokinesis in Arabidopsis thaliana. Curr Biol **16,** 888-894.

Mullins, R.D., Heuser, J.A., and Pollard, T.D. (1998). The interaction of Arp2/3 complex with actin: Nucleation, high affinity pointed end capping, and formation of branching networks of filaments. Proceedings of the National Academy of Sciences **95,** 6181-6186.

Pastuglia, M., Azimzadeh, J., Goussot, M., Camilleri, C., Belcram, K., Evrard, J.L., Schmit, A.C., Guerche, P., and Bouchez, D. (2006). Gamma-tubulin is essential for microtubule organization and development in Arabidopsis. Plant Cell **18,** 1412-1425.

Pickett-Heaps, J.D., and Northcote, D.H. (1966). Organization of microtubules and endoplasmic reticulum during mitosis and cytokinesis in wheat meristems. J Cell Sci **1,** 109-120.

Poraty-Gavra, L., Zimmermann, P., Haigis, S., Bednarek, P., Hazak, O., Stelmakh, O.R., Sadot, E., Schulze-Lefert, P., Gruissem, W., and Yalovsky, S. (2013). The Arabidopsis Rho of Plants GTPase AtROP6 Functions in Developmental and Pathogen Response Pathways. Plant Physiology **161,** 1172-1188.

Rouiller, I., Xu, X.P., Amann, K.J., Egile, C., Nickell, S., Nicastro, D., Li, R., Pollard, T.D., Volkmann, N., and Hanein, D. (2008). The structural basis of actin filament branching by the Arp2/3 complex. J Cell Biol **180,** 887-895.

Sampathkumar, A., Krupinski, P., Wightman, R., Milani, P., Berquand, A., Boudaoud, A., Hamant, O., Jonsson, H., and Meyerowitz, E.M. (2014). Subcellular and supracellular mechanical stress prescribes cytoskeleton behavior in Arabidopsis cotyledon pavement cells. eLife **3,** e01967.

Sano, T., Higaki, T., Oda, Y., Hayashi, T., and Hasezawa, S. (2005). Appearance of actin microfilament 'twin peaks' in mitosis and their function in cell plate formation, as visualized in tobacco BY-2 cells expressing GFP-fimbrin. Plant J **44,** 595-605.

Santos, B., Gutierrez, J., Calonge, T.M., and Perez, P. (2003). Novel Rho GTPase involved in cytokinesis and cell wall integrity in the fission yeast Schizosaccharomyces pombe. Eukaryot Cell **2,** 521-533.

Schutze, K., Harter, K., and Chaban, C. (2009). Bimolecular fluorescence complementation (BiFC) to study protein-protein interactions in living plant cells. Methods Mol Biol **479,** 189-202.

Sermon, B.A., Lowe, P.N., Strom, M., and Eccleston, J.F. (1998). The importance of two conserved arginine residues for catalysis by the ras GTPase-activating protein, neurofibromin. J Biol Chem **273,** 9480-9485.

Smith, L.G., Hake, S., and Sylvester, A.W. (1996). The tangled-1 mutation alters cell division orientations throughout maize leaf development without altering leaf shape. Development **122,** 481-489.

Sorek, N., Segev, O., Gutman, O., Bar, E., Richter, S., Poraty, L., Hirsch, J.A., Henis, Y.I., Lewinsohn, E., Jurgens, G., and Yalovsky, S. (2010). An S-acylation switch of conserved G domain cysteines is required for polarity signaling by ROP GTPases. Curr Biol **20,** 914-920.

Sorek, N., Gutman, O., Bar, E., Abu-Abied, M., Feng, X., Running, M.P., Lewinsohn, E., Ori, N., Sadot, E., Henis, Y.I., and Yalovsky, S. (2011).

Differential Effects of Prenylation and S-Acylation on Type I and II ROPS Membrane Interaction and Function. Plant Physiology **155,** 706-720.

Spinner, L., Pastuglia, M., Belcram, K., Pegoraro, M., Goussot, M., Bouchez, D., and Schaefer, D.G. (2010). The function of TONNEAU1 in moss reveals ancient mechanisms of division plane specification and cell elongation in land plants. Development **137,** 2733-2742.

Spinner, L., Gadeyne, A., Belcram, K., Goussot, M., Moison, M., Duroc, Y., Eeckhout, D., De Winne, N., Schaefer, E., Van De Slijke, E., Persiau, G., Witters, E., Gevaert, K., De Jaeger, G., Bouchez, D., Van Damme, D., and Pastuglia, M. (2013). A protein phosphatase 2A complex spatially controls plant cell division. Nature communications **4,** 1863.

Tolliday, N., VerPlank, L., and Li, R. (2002). Rho1 Directs Formin-Mediated Actin Ring Assembly during Budding Yeast Cytokinesis. Current Biology **12,** 1864-1870.

van Leeuwen, W., Ökrész, L., Bögre, L., and Munnik, T. (2004). Learning the lipid language of plant signalling. Trends in Plant Science **9,** 378-384.

Vernoud, V., Horton, A.C., Yang, Z., and Nielsen, E. (2003). Analysis of the small GTPase gene superfamily of Arabidopsis. Plant Physiol **131,** 1191-1208.

Walker, K.L., Muller, S., Moss, D., Ehrhardt, D.W., and Smith, L.G. (2007). Arabidopsis TANGLED identifies the division plane throughout mitosis and cytokinesis. Curr Biol **17,** 1827-1836.

Wittinghofer, A., and Pal, E.F. (1991). The structure of Ras protein: a model for a universal molecular switch. Trends in Biochemical Sciences **16,** 382-387.

Wu, S.Z., and Bezanilla, M. (2014). Myosin VIII associates with microtubule ends and together with actin plays a role in guiding plant cell division. eLife **3**.

Wu, Y., Zhao, S., Tian, H., He, Y., Xiong, W., Guo, L., and Wu, Y. (2013). CPK3-phosphorylated RhoGDI1 is essential in the development of Arabidopsis seedlings and leaf epidermal cells. Journal of Experimental Botany **64,** 3327-3338.

Xu, T., Wen, M., Nagawa, S., Fu, Y., Chen, J.-G., Wu, M.-J., Perrot-Rechenmann, C., Friml, J., Jones, A.M., and Yang, Z. (2010). Cell Surface- and Rho GTPase-Based Auxin Signaling Controls Cellular Interdigitation in Arabidopsis. Cell **143,** 99-110.

Xu, T., Dai, N., Chen, J., Nagawa, S., Cao, M., Li, H., Zhou, Z., Chen, X., De Rycke, R., Rakusova, H., Wang, W., Jones, A.M., Friml, J., Patterson, S.E., Bleecker, A.B., and Yang, Z. (2014). Cell surface ABP1-TMK auxin-sensing complex activates ROP GTPase signaling. Science **343,** 1025-1028.

Xu, X.M., Zhao, Q., Rodrigo-Peiris, T., Brkljacic, J., He, C.S., Muller, S., and Meier, I. (2008). RanGAP1 is a continuous marker of the Arabidopsis cell division plane. Proc Natl Acad Sci U S A **105,** 18637-18642.

Yaffe, M.B., and Elia, A.E.H. (2001). Phosphoserine/threonine-binding domains. Current Opinion in Cell Biology **13,** 131-138.

Yang, Z. (2008). Cell polarity signaling in Arabidopsis. Annu Rev Cell Dev Biol **24,** 551-575.

Yoshida, S., Bartolini, S., and Pellman, D. (2009). Mechanisms for concentrating Rho1 during cytokinesis. Genes Dev **23,** 810-823.